DIRECT PION-NUCLEUS INTERACTIONS IN THE RESONANCE REGION

by

GAYNOR M. FIELD

Thesis submitted in partial fulfilment for the degree of

MASTER OF SCIENCE

at the University of Cape Town

SEPTEMBER, 1983

Dedicated to the

memory of the

late Professor W.E. Frahn

ABSTRACT

The direct reactions of pions with nuclei in the energy region of the $\pi N(3,3)$ resonance are examined in the eikonal formalism. In particular, the angular and energy dependence of the elastic scattering of $\pi^{\pm}$ from the calcium isotopes $^{40,48}Ca$ is studied, using a detailed phenomenological approach. Excellent agreement is obtained with experimental data.
A closely related investigation is also made of the inelastic excitation of low-lying collective states of $^{40,48}Ca$ by pions. The resulting one-parameter fits yield deformation lengths which are compared with simple collective model predictions. The total cross-sections for neutral pion scattering from $^{40,48}Ca$ in the resonance region are investigated as well, and predictions are made.

Nuclear Reactions:

$^{40,48}Ca(\pi^{\pm}, \pi^{\pm})^{40,48}Ca$	T_{π} = 130, 180, 230 MeV
$^{40,48}Ca(\pi^{\pm}, \pi^{\pm\prime})^{40,48}Ca^{*}$	T_{π} = 180 MeV

SYNOPSIS

Following a brief discussion of pion-nucleus resonance scattering and some of its implications for pion-nucleus scattering, we review Frahn's[1] closed-form description of elastic scattering in the eikonal approximation, under strong-absorption conditions. Pion-nucleus direct reactions in the resonance region ought to be well described by such an approach, as the pion is travelling rapidly, but undergoes strong nuclear absorption near resonance. The eikonal formalism is known, however, to be a small angle approximation[2], so we slightly modify it (to make it work reasonably well also at large angles) by changing $q = 2k\sin\frac{\theta}{2}$ to $q = k\theta$ in the eikonal formulae. This modification is motivated by Frahn's strong-absorption diffuse nuclear surface work[3,4,5,6]. The eikonal amplitude is derived in analytic form involving a Fourier transform of the nuclear part of the scattering function. Coulomb effects are incorporated into the formalism to first order in the Sommerfeld parameter, a measure of the effective strength of the Coulomb interaction, which is quite weak for $\pi^{\pm}$ resonance scattering from calcium.

We examine in detail the structure of our explicit expressions for the elastic differential cross-sections. The simple Ericson form for the parameterization of the nuclear part of the scattering function[7] is inserted, and the eikonal

differential cross-section in this model is evaluated. In addition, simple asymptotic expressions are derived from which we predict the main features of fast, light charged particle scattering from nuclei under strong-absorption conditions. In particular we investigate the weak dependence of the angular distributions on the sign of the projectile charge.

As an application of these theoretical results, we consider a description of medium energy pion-nucleus scattering. In particular, we concern ourselves with charged pion scattering off nuclei in the vicinity of the πN(3,3) resonance, where the necessary strong-absorption conditions prevail for our eikonal formalism to apply. The study of π-nucleus scattering can be separated into two (overlapping) areas: (1) the details of the π-nucleon (πN) scattering mechanism and (2) the response of the whole nucleus to the interaction.

The elementary πN interaction is found to be comparatively weak at low energies, but very strong for kinetic energies between 100-250 MeV. In fact, the πN system is observed to resonate in channel $\ell = 1$, $I = \frac{3}{2}$, $J = \frac{3}{2}$ at a total centre-of-mass energy of 1232 MeV, with a decay width $\Gamma \simeq 110$ MeV[8].

We follow the approach of Kisslinger[9] in assuming that the optical potential describing π-nucleus scattering in the vicinity of the (3,3) resonance can be taken as consisting of two terms: the first term corresponding to the background

non-resonant interaction, covering the normal non-resonant nuclear scattering and absorption processes, and the second term describing the resonant scattering interaction of the pion with a nucleon embedded in the nucleus. Kisslinger takes this second term to have a resonant Breit-Wigner energy dependence, with resonance energy corresponding to that of a (3,3) resonance in the nuclear environment. This energy E_o' is shifted downward by an amount $\sim$ 30 MeV from the resonance energy for free nucleons[10], an effect which can be attributed mainly to the multiple scattering of pions from nucleons in the nucleus[11]. When the resonant and non-resonant terms of this optical potential are solved to obtain the π-nucleus cross-section, the resonance shape itself is also broadened and distorted, as well as shifted downward, relative to that of the π-nucleon cross-section. As Kisslinger points out[12], there is no π-nucleus resonance; rather, what is observed in the π-nuclear data is a reflection of the πN resonance in nuclear matter.

The non-resonant and resonant contributions to the optical potential both consist of real and imaginary parts. The background contribution to the potential is relatively small and taken as energy independent. On the other hand, the resonant term is relatively large at its resonant peak, where it is purely absorptive (negative imaginary). It only contributes with any significant magnitude at energies within about Γ of E_o', where it overshadows the non-resonant background. It is peaked at the resonance energy and falls

off to zero on either side of E_o'. In case the nucleus does not have an equal number of neutrons and protons ($N \neq Z$), this resonant term will, because of isospin considerations, be stronger for $\pi^-(\pi^+)$ scattering than for $\pi^+(\pi^-)$ scattering in the case of neutrons (protons) being in excess. A factor to model this effect[13,14] is inserted as a coefficient of the resonant part of the optical potential.

To deal with this resonant plus background optical potential in our strong-absorption eikonal approach, we choose (as an alternative to the Ericson form) Kauffmann's suggested parameterization of the nuclear part of the scattering function[15]; the parameters of which can be related directly to those of an optical potential, via eikonal integrals evaluated over the optical potential, as we indicate in detail, following Frahn[1]. We simply insert the Kisslinger non-resonant and resonant optical potentials into this framework, and then use our strong-absorption eikonal cross-section expressions to obtain a closed-form eikonal resonance model for pion-nucleus elastic scattering.

We fit this derived eikonal resonance model to the particular case of the elastic scattering of 130, 180, 230 MeV $\pi^{\pm}$ from $^{40,48}Ca$[6], after first carrying out preliminary fits with the much more elementary Black Disk and Coulomb Black Disk models to portions of these data. These latter fits are crude, but reproduce the main features of the data, lending support to the notion of strong-absorption dominance in the resonance

region. Inclusion of the weak Coulomb interaction into the Black Disk model illustrates the point that refraction causes the minima of the diffraction pattern to be partly filled in (refractive damping of diffraction), and rather improves these crude fits.

Relaxing the sharp cut-off assumption that was applied in the Black Disk analysis (that is, allowing for nuclear edge diffuseness) enables the theoretical cross-sections to decrease faster at large angles, in keeping with the experimental data. This is one of the concepts incorporated into the eikonal strong-absorption model. Another is nuclear refraction, arising from the nuclear forces between the (pion) projectile and (nucleus) target. When effects of the resonance are incorporated, both these forces and the degree of strong-absorption are seen to vary with energy, an essential result of the eikonal resonance formalism. Indeed, the pion-nucleus force actually changes from attractive to repulsive as one goes through the resonance, and the peaking of the strong-absorption at resonance causes the effective nuclear 'radius' (critical impact parameter) b_o to also peak there.

The experimental data for both π^+ and π^- elastic scattering from ^{40}Ca were fitted in our eikonal resonance model with a single set of five parameter values: $R' = 4.14$ fm, $\tilde{a} = 0.80$ fm, $v = 0.25$, $w = 0.6$ and $m_o' = 1202$ MeV - which were sufficient to describe the differential elastic scattering

cross-sections at all of the three resonance-scan energies of 130, 180 and 230 MeV. Here R' is a radius parameter, $\tilde{a}$ a diffuseness parameter, v and w measure, respectively, the relative strengths of the real and imaginary background potentials to that of the peak resonance potential, and m_0' is the displaced resonance energy. The free π-nucleon resonance width, Γ = 110 MeV, was used unchanged in the analysis; the π-nuclear resonance energy, however, is displaced from the free resonance energy by an amount $\sim$ 30 MeV, so that m_0' = 1202 MeV instead of 1232 MeV.

The corresponding six elastic differential cross-sections for ^{48}Ca were fitted with the same parameter values as for ^{40}Ca, with the exception that the diffuseness $\tilde{a}$ was slightly altered to be 0.75 fm, and the radius parameter R' for ^{48}Ca was deduced from the ^{40}Ca value by the relation $R'(48) = (48/40)^{1/3} R'(40)$, yielding $R'(48)$ = 4.40 fm.

The agreement between experiment and the eikonal resonance model is excellent for all twelve elastic differential cross-sections, a remarkable achievement, considering the few free parameters with which this considerable mass of data was fitted. This demonstrates the success of our model.

Another quantity which we have considered is the neutral pion-nucleus total cross-section. Using the optical theorem and our eikonal resonance expression for the neutral pion-nucleus forward elastic scattering amplitude, we obtained an

expression for the neutral pion-nucleus total cross-section. Using the parameter values obtained from the elastic scattering fit, we evaluated this quantity - for both ^{40}Ca and ^{48}Ca over a broad energy band around resonance. The resulting theoretical quantity displayed a resonance shape - however, as expected for the nuclear case, the total cross-section was flattened and broadened, relative to the πN case, as well as having its peak shifted downward. There are no experimental data for the $\pi^0 - ^{40,48}Ca$ total cross-sections available for direct comparison at this time. However our curves are qualitatively similar to $\pi - ^{12}C$ total cross-section data in the resonance region[17,18].

A curious feature of our resonance model is the fact that the real part of the pion-nucleus nuclear optical potential passes from being attractive below resonance to being repulsive above resonance, due to the properties of the Breit-Wigner resonant part of that potential. This feature is strongly reflected in our model plots of the real part of the neutral pion-nucleus forward elastic scattering amplitude, which passes from positive to negative values as one increases the scattering energy from below resonance to above. By making use of the 'refractive damping of diffraction' effect in conjunction with opposed Coulomb forces on the π^+ and π^-, it is possible to discern this energy dependent change in the sign of the nuclear part of the pion-nucleus force from the elastic angular distribution data. Thus, below resonance, the π^- experiences a stronger

net refractive force when scattering from ^{40}Ca than does the π^+, for the nuclear and Coulomb forces are both attractive for the π^-, while the repulsive Coulomb force opposes the attractive nuclear force for the π^+. The more strongly refracted π^- can thus be expected to have diffraction minima which are less pronounced below resonance than those of the π^+. Above resonance, however, the nuclear force is repulsive, and adds to the repulsive Coulomb force on the π^+ to make the net refractive force on the π^+ greater than that on the π^- (for which the attractive Coulomb force opposes the repulsive nuclear force). Thus, for ^{40}Ca above resonance, the more strongly refracted π^+ can be expected to show less pronounced diffraction minima than those of the more weakly refracted π^-. Due to the weakness of both the Coulomb and nuclear forces between pion and nucleus near resonance (remember that the resonant part of the nuclear optical potential is purely absorptive at resonance), these diffraction phenomena cannot be expected to be very prominent, but they do appear to be present in the ^{40}Ca data, as well as, of course, in our model fits to these data. For ^{48}Ca, for which $N > Z$, the pion isospin dependence of the nuclear part of the pion-nucleus force makes these subtle diffractive effects still more complex. It is fascinating that pion-nucleus scattering near resonance not only involves energy dependent nuclear forces which actually change sign, but because the pion comes in both charges, conveniently lends itself to a Coulombic diffractive probing of this phenomenon.

We have also extended our eikonal resonance elastic scattering model to describe inelastic scattering, following the method of Frahn[1]. The close connection between inelastic and elastic scattering is made explicit. The derived formulae describing the inelastic scattering are applied to experimental data fitting of the pion excitation of $^{40,48}Ca$ at T_π = 180 MeV to certain low lying collective states (2^+ and 3^-)[19,20]. The resulting one-parameter fits are quite good, and yield normalization constants which, where they differ from the most naive collective model predictions, are used as a motivation for reconsidering such models.

ACKNOWLEDGEMENTS

I wish to express my gratitude to:

- The late Professor W.E. Frahn, my supervisor, for initiating the project;
- Professor F.D. Brooks, for encouragement and support;
- Dr. S.K. Kauffmann, for invaluable assistance;
- Professors S.M. Perez and D.G. Aschman, for helpful discussions;
- Dr. K. Boyer, for kindly providing listings of experimental data;
- The South African Council for Scientific and Industrial Research, for a research bursary;
- The staff of the Computer Centre of the University of Cape Town, for their cooperation; and
- Lesley Jennings, for typing the manuscript.

CONTENTS

Page

1. THE πN INTERACTION

Our goal is to achieve a description of π-nucleus scattering near the πN(3,3) resonance. In this section we discuss the pion: its important properties and the mechanism involved in the resonant πN interaction. The theory is then extended to π-nucleus scattering.

1.1 Properties of the pion[8,21,22]

The pion is a strongly interacting elementary particle, recognised to be the quantum of the longest range part of the nuclear force. It possesses three charge states π^o, π^+ and π^-, is a boson with spin zero and has odd (negative) intrinsic parity.

The mass of the charged pion is measured to be

$$m_{\pi^\pm} = (273.33)m_e = 139.69 \text{ MeV}$$

while that of the neutral pion is a few MeV less

$$m_{\pi^o} = (264.20)m_e = 135.00 \text{ MeV},$$

where m_e represents the mass of the electron.

The charged pions are observed to decay spontaneously via the weak interaction into muons

$$\pi^\pm \rightarrow \mu^\pm \nu_\mu$$

with a characteristic lifetime of (2.55×10^{-8})sec; while the neutral pion decays via the electromagnetic interaction into two gamma particles with a lifetime of (2×10^{-6})sec

$$\pi^o \rightarrow 2\gamma \ .$$

The pions are described by an isospin T=1 triplet state; T_3 taking the values -1, 0, +1, which are related to the charge of the pion by

$$\frac{q}{e} = T_3 \quad .$$

T is conserved by the nuclear interaction; the properties of the nuclear state thus being dependant on T.

1.2 πN scattering:

The πN system is described in terms of combinations of isotopic spin states $T=\frac{1}{2}$ and $\frac{3}{2}$.

The quasielastic processes which occur between pions and nucleons are

$$\pi^+ + p \rightarrow \pi^+ + p \qquad \pi^- + n \rightarrow \pi^- + n$$
$$\pi^- + p \rightarrow \pi^- + p \qquad \pi^+ + n \rightarrow \pi^+ + n$$
$$\pi^- + p \rightarrow \pi^\circ + n \qquad \pi^+ + n \rightarrow \pi^\circ + p$$
$$\pi^\circ + p \rightarrow \pi^+ + n \qquad \pi^\circ + n \rightarrow \pi^- + p$$
$$\pi^\circ + p \rightarrow \pi^\circ + p \qquad \pi^\circ + n \rightarrow \pi^\circ + n$$

The observed ratio of cross-sections for the different processes: $p + \pi^+ \rightarrow p + \pi^+$, $p + \pi^- \rightarrow n + \pi^\circ$, and $p + \pi^- \rightarrow p + \pi^-$ is 9 : 2 : 1 for energies below 250 MeV. This is consistent with having the dominating scattering mechanism proceed via an intermediate $T=\frac{3}{2}$ state, which is fully effective only for π^+p and π^-n scattering. Thus the $\pi^-(\pi^+)$ interacts much more strongly with neutrons (protons) than the $\pi^+(\pi^-)$.

The πN interaction is found to be comparatively weak at low energies, but very strong for pion kinetic energies between 100 - 250 MeV. In fact, the πN system is observed to resonate in channel $\ell=1$ $I=\frac{3}{2}$ $J=\frac{3}{2}$ at a total centre of mass energy of 1232 MeV, with a decay width $\Gamma \simeq 110$ MeV[8].

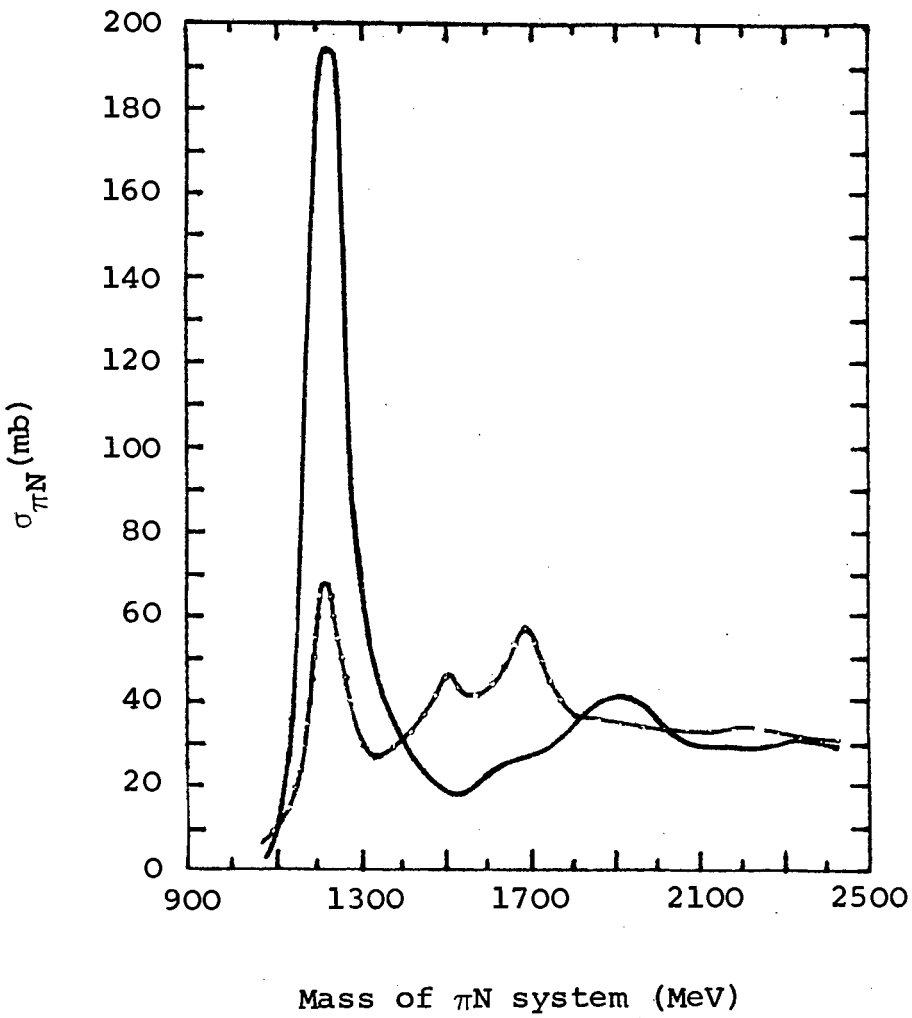

Figure (1.2-I) Total cross-section for π^+N and π^-N scattering[22]

1.3 π-nucleus scattering:

We attempt to gain insight into this complex many-body process in terms of the single particle πN interaction; in particular we investigate the effect of the $\pi N(3,3)$ resonance on the π-nucleus scattering data.

Upon examining the total cross-sections of pions on a variety of target nuclei in the vicinity of the (3,3) resonance, one observes a peak which, however, is shifted downward in energy by an amount $\simeq$ 30 MeV from the resonance energy for free nucleons, and broadened when compared with the corresponding πN cross-section. These effects can be attributed to the multiple scattering of pions from nucleons in the nucleus and nuclear size effects[11].

As Kisslinger points out[12], there is no 'π-nucleus' resonance; rather, what we are observing in the π-nuclear data is a reflection of the πN resonance in nuclear matter. Thus, if we wish to obtain an accurate description of π-nucleus scattering in the vicinity of the $\pi N(3,3)$ resonance, we must explicitly introduce the baryon resonance into our theory.

2. CLOSED-FORM EVALUATION OF THE EIKONAL AMPLITUDE FOR STRONG-ABSORPTION SCATTERING - ELASTIC SCATTERING

In this section, with reference to Frahn[1], we present analytic expressions for the eikonal amplitude for elastic scattering at intermediate and high energies, under strong-absorption conditions. Coulomb effects are incorporated into the formalism to lowest order in the Sommerfield parameter - the Coulomb strength function. We examine a variation of the approach of Frahn, in which a simple Ericson model of the scattering function is adopted to assist in a detailed study of the general formulae. In addition, simple asymptotic expressions are derived from which we predict the main features of π-nucleus scattering in the resonance region, and we investigate the pion charge dependence of the angular distributions.

2.1 The impact parameter representation of the scattering process:

Hadron nucleus scattering at intermediate and high energies is well described in the eikonal approximation[2]. The high energy, high angular momentum character of the scattering allows us to apply semi-classical, straight line trajectory methods to a description of the process.

The semi-classical representation of the collision process is made in terms of impact parameters: the colliding particles, each possessing a well-defined energy and hence momentum $\vec{p}$ are thought of as moving along trajectories, each being described by an impact parameter b. After scattering the particles are characterised by a centre-of-mass scattering angle θ_{cm}.

The scattering angle θ is related to the centre-of-mass momentum k and momentum transfer q by

$$q = 2k\sin\frac{\theta}{2} \qquad (2.1.1)$$

in the eikonal. This is the eikonal, which is an approximation known to be valid only at small θ. At small angles $2k\sin\frac{\theta}{2}$ may be replaced by $k\theta$. Moreover if we take $q = k\theta$, we know from the non-eikonal work of Frahn for diffuse, strongly absorbing potentials[3,4,5,6] that the resulting expression is also valid at intermediate angles (order 90° or more). Thus we

will take $q = k\theta$ in all our subsequent work (generalised eikonal).

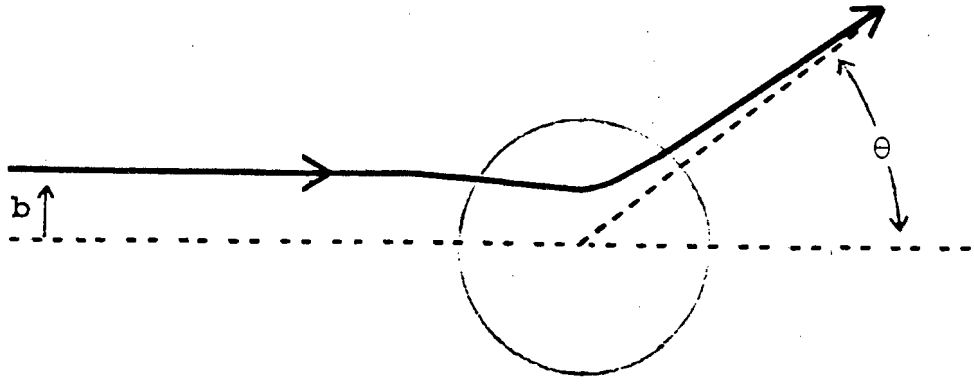

Figure (2.1-I) Semi-classical trajectory for scattering with impact parameter b and scattering angle θ [4]

2.2 The elastic eikonal amplitude:

In the eikonal approximation[2] the amplitude for the elastic scattering of a spin-zero particle by a spherically symmetric potential has the form

$$f(q) = ik\int_0^\infty db\, b\,[1-S(b)]\,J_0(bq) \qquad (2.2.1)$$

which we refer to as the eikonal amplitude in impact parameter representation.

And the differential cross-section for elastic scattering is given by

$$\frac{d\sigma}{d\Omega} = |f(q)|^2 \quad . \qquad (2.2.2)$$

We recognise $f(q)$ in (2.2.1) as the Fourier-Bessel transform of the profile function $\Gamma(b) = 1-S(b)$ in impact parameter space b to the space of momentum transfer q .

We express the scattering function $S(b)$ in terms of factored contributions from the nuclear and Coulomb interactions

$$S(b) = S_N(b)\, e^{i2\sigma_p(b)} \qquad (2.2.3)$$

where $S_N(b)$ represents the nuclear part of $S(b)$ and is of the form:

$$S_N(b) = \eta_N(b) e^{i2\delta_N(b)} . \qquad (2.2.4)$$

$\eta_N(b)$, the amplitude, describes the absorptive nature of the interaction;

$\delta_N(b)$, the nuclear phase, describes the reflective and refractive properties of the nuclear interaction;

and the quantity $\sigma_p(b)$ is representative of the Rutherford point-charge phase-shift function.

The effect of the nuclear interaction on the scattering amplitude is described by the function

$$F_N(z) = \int_{-\infty}^{\infty} db\, D_N(b)\, e^{-i\left(\frac{b-b_o}{a}\right)z} \qquad (2.2.5)$$

defined as the Fourier transform of the derivative of the nuclear part of the scattering function. We denote $\frac{dS_N(b)}{db}$ by $D_N(b)$.

We impose the condition that $S_N(b)$ possesses a strong-absorption profile in impact parameter space; the parameters b_o and a characterising the strong-absorption profile.

The quantity b_o, representative of the critical impact parameter describing the scattering, is defined as the maximum of

$$|D_N(b)| = \left|\frac{dS_N(b)}{db}\right| \qquad (2.2.6)$$

and a denotes the width of the narrow window in impact parameter space within which $|D_N(b)|$ is peaked.

We may express the elastic scattering amplitude (2.2.1) as a sum of the contributions from the nuclear and Coulomb point-charge interactions

$$f(q) = f_N(q) + f_p(q) \tag{2.2.7}$$

where

$$f_N(q) = ik\int_0^\infty db\, b\,[1-S_N(b)]e^{i2\sigma_p(b)} J_0(bq)$$

and

$$f_p(q) = ik\int_0^\infty db\, b\left[1-e^{i2\sigma_p(b)}\right]J_0(bq)\ , \tag{2.2.8}$$

and the Coulomb point-charge amplitude has the value[2]

$$f_p(q) = -\frac{2nk}{q^2}\exp\left[-i2n\left(\ln\left[\frac{q}{2k}\right]+\gamma\right)\right] \tag{2.2.9}$$

in the eikonal approximation, where $n = \frac{Z_1 Z_2 e^2}{\hbar v}$ is the Sommerfeld parameter defined in terms of the atomic numbers Z_1, Z_2 of the projectile and target nuclei and their relative velocity v, and $\gamma = 0{,}5772$ is Euler's constant.

The nuclear scattering amplitude is approximately given by

$$f_N(q) = \frac{ik}{q} e^{i2\sigma_p(b_o)} I_1(q) + \frac{2nk}{q^2} e^{i2\sigma_p(b_o)} [F_N(aq) - I_o(q)] \tag{2.2.10}$$

where we have expanded the point-charge phase shifts linearly about b_o, an approximation valid under strong-absorption conditions

$$2\sigma_p(b) \simeq 2\sigma_p(b_o) + (b-b_o)q_o \tag{2.2.11}$$

the quantity

$$q_o = \frac{2n}{b_o} \ . \tag{2.2.12}$$

The integrals $I_o(q)$ and $I_o(q)$ in (2.2.10) are of the form

$$I_o(q) = \int_o^\infty db\ D_N(b)\, e^{i(b-b_o)q_o} J_o(b_o q)$$

$$I_1(q) = \int_o^\infty db\ b\ D_N(b)\, e^{i(b-b_o)q_o} J_1(b_o q) \ . \tag{2.2.13}$$

They arise from integrations by parts in (2.2.8).

To first order in n, the total eikonal amplitude reduces to

$$f(q) = \frac{ik}{q}\left[I_1(q) + \frac{i2n}{q} I_o(q) \right] e^{i2\sigma_p(b_o)} \ . \tag{2.2.14}$$

The integrals have been approximately evaluated[6] with the result

$$I_0(q) = \frac{1}{2}\left\{F_N[a(q_0+q)]\left(J_0(b_0q) + iJ_1(b_0q)\right)\right.$$

$$\left. + F_N[a(q_0-q)]\left(J_0(b_0q) - iJ_1(b_0q)\right)\right\}$$

$$I_1(q) = \frac{b_0}{2}\left\{\tilde{F}_N[a(q_0+q)]\left(J_1(b_0q) + iJ_2(b_0q)\right)\right.$$

$$\left. + \tilde{F}_N[a(q_0-q)]\left(J_1(b_0q) - iJ_2(b_0q)\right)\right\} \qquad (2.2.15)$$

where the function $\tilde{F}_N(z)$ is related to $F_N(z)$ by

$$\tilde{F}_N(z) = F_N(z) - \frac{i2a}{b_0}F_N'(z) - \left(\frac{a}{b_0}\right)^2 F_N''(z) \qquad (2.2.16)$$

in an approximation valid for $\left(\frac{a^2q}{b_0}\right) \ll 1$.

Writing

$$F_{\pm}(q) = \frac{1}{2}\left\{F_N[a(q_0+q)] \pm F_N[a(q_0-q)]\right\}$$

and

$$\tilde{F}_{\pm}(q) = \frac{1}{2}\left\{\tilde{F}_N[a(q_0+q)] \pm \tilde{F}_N[a(q_0-q)]\right\} \qquad (2.2.17)$$

we obtain for the eikonal elastic scattering amplitude

$$f(q) = \left(\frac{ikb_0}{q}\right)\left\{\left[\tilde{F}_+(q)J_1(b_0q) + i\tilde{F}_-(q)J_2(b_0q)\right]\right.$$

$$\left. + \frac{i2n}{b_0q}\left[F_+(q)J_0(b_0q) + iF_-(q)J_1(b_0q)\right]\right\}e^{i2\sigma_p(b_0)} \qquad (2.2.18)$$

expressed to first order in n.

Expression (2.2.18) is seen to consist of combinations of Bessel functions describing the diffractive nature of the scattering process, multiplied by form factors involving Fourier transforms of the derivative of the nuclear profile function.

We consider several limiting cases and their resulting simplifications to the elastic eikonal amplitude.

limit $a \to o$

In the limit of the diffuseness of the nuclear profile vanishing, $S_N(b)$ takes on the form of a unit step function

$$S_N(b) = \Theta(b-b_o) \tag{2.2.19}$$

and its derivative is given by the delta function

$$D_N(b) = \delta(b-b_o) \ . \tag{2.2.20}$$

The Fourier transforms $\tilde{F}_N(z)$ and $F_N(z)$ reduce to

$$\tilde{F}_N(z) = F_N(z) = 1 \ . \tag{2.2.21}$$

The resulting sharp cut-off scattering amplitude is given by

$$f_{sco}(q) = \left[ikb_o^2 \frac{J_1(b_o q)}{b_o q} - \frac{2nk}{q^2} J_o(b_o q) \right] e^{i2\sigma_p(b_o)} \tag{2.2.22}$$

taking into account the Coulomb effects to lowest order in n. Taking the neutral limit, expression (2.2.22) further reduces to the Black-Disk formula

$$f_{BD}(q) = ikb_o^2 \left(\frac{J_1(b_o q)}{b_o q} \right) \ . \tag{2.2.23}$$

limit n→o

For neutral particle scattering the Fourier transforms reduce to

$$\overset{o}{\widetilde{F}}_{\pm}(q) = \frac{1}{2}\left[\widetilde{F}_N(aq) \pm \widetilde{F}_N(-aq)\right] \qquad (2.2.24)$$

and the corresponding eikonal amplitude to

$$\overset{o}{f}(q) = \frac{ikb_o}{q}\left[\overset{o}{\widetilde{F}}_+(q)J_1(b_oq) + i\overset{o}{\widetilde{F}}_-(q)J_2(b_oq)\right] . \qquad (2.2.25)$$

Evaluating the forward scattering amplitude in the neutral limit we find

$$\overset{o}{f}(o) = \frac{ikb_o^2}{2}\left[1 - i\frac{2a}{b_o}F_N'(o) - \left(\frac{a}{b_o}\right)^2 F_N''(o)\right] \qquad (2.2.26)$$

with real and imaginary parts given by

$$\mathrm{Re}\ \overset{o}{f}(o) = \frac{kb_o^2}{2}\left[\frac{2a}{b_o}\mathrm{Re}\,F_N'(o) + \left(\frac{a}{b_o}\right)^2 \mathrm{Im}\,F_N''(o)\right] \qquad (2.2.27)$$

and

$$\mathrm{Im}\ \overset{o}{f}(o) = \frac{kb_o^2}{2}\left[1 + \frac{2a}{b_o}\mathrm{Im}\,F_N'(o) - \left(\frac{a}{b_o}\right)^2 \mathrm{Re}\,F_N''(o)\right] . \qquad (2.2.28)$$

Substituting the result (2.2.28) into the optical theorem

$$\sigma_T = \frac{4\pi}{k}\mathrm{Im}\ \overset{o}{f}(o) \qquad (2.2.29)$$

we obtain for the total (neutral) cross-section

$$\sigma_T = 2\pi b_o^2 \left[1 + \frac{2a}{b_o} \operatorname{Im} F_N'(o) - \left(\frac{a}{b_o}\right)^2 \operatorname{Re} F_N''(o) \right] , \qquad (2.2.30)$$

the quantity in brackets containing the corrections to the geometric value $2\pi b_o^2$, which can be attributed to the diffuseness of the nuclear profile.

2.3 Ericson parameterization of the scattering function:

To facilitate further study and assist in interpretation of our general formulae, a suitable choice for the parameterization of the scattering function is made.

A convenient analytic form of the nuclear scattering function, as proposed by Ericson[7], is the function

$$S_N(b) = \left[1 + \exp\left[-\frac{b-b_o}{a} - i\alpha\right]\right]^{-1} \quad . \qquad (2.3.1)$$

We refer to (2.3.1) as the Ericson parameterization - in impact parameter space - of the central nuclear scattering function.

The function is characterised by a critical impact parameter b_o, a width parameter a and a real nuclear phase parameter α. Allowing for both attractive and repulsive nuclear refraction α lies in the interval $\left(-\frac{\pi}{2}, \frac{\pi}{2}\right)$.

The amplitude of the nuclear scattering function and the central nuclear phase shift function in the Ericson model have been evaluated, with the results

$$\eta_N(b) = \left[1 + 2\cos\alpha\, e^{-\mu} + e^{-2\mu}\right]^{-\frac{1}{2}} \qquad (2.3.2)$$

and

$$2\delta_N(b) = \arctan\left(\frac{\sin\alpha}{\cos\alpha + e^{-\mu}}\right) \qquad (2.3.3)$$

where

$$\mu = \left(\frac{b-b_o}{a}\right) \quad . \qquad (2.3.4)$$

2.4 The eikonal amplitude in the Ericson parametric model:

The Fourier transform $F_N(z)$ in the Ericson model has been evaluated[23]

$$F_N(z) = \frac{\pi z}{\sinh \pi z} e^{\alpha z} \quad . \tag{2.4.1}$$

Substituting the results

$$F_N'(z) = \left(\alpha - \frac{\pi^2}{3} z\right) F_N(z)$$

and

$$F_N''(z) = \left[\left(\alpha - \frac{\pi^2}{3} z\right)^2 - \frac{\pi^2}{3}\right] F_N(z) \tag{2.4.2}$$

into (2.2.16) we find

$$\tilde{F}_N(z) = \varepsilon F_N(z) \tag{2.4.3}$$

where

$$\varepsilon = \left[1 - i\left(\frac{2a}{b_o}\right)\alpha + \left(\frac{a}{b_o}\right)^2\left[\frac{\pi^2}{3} - \alpha^2\right]\right] \quad . \tag{2.4.4}$$

The quantities $F_{\pm}(q)$ and $\tilde{F}_{\pm}(q)$ given by (2.2.17) are evaluated with the results

$$F_+(q) = e^{\alpha a q_o} \left(\frac{\pi a q}{\sinh(\pi a q)}\right) \cosh(\alpha a q) \tag{2.4.5}$$

$$F_{-}(q) = e^{\alpha a q_o} \left(\frac{\pi a q}{\sinh(\pi a q)} \right) \sinh(\alpha a q) \qquad (2.4.6)$$

in which terms of order $\left(\frac{na^2q}{b_o}\right)$ have been neglected, and

$$\tilde{F}_{\pm}(q) = \varepsilon F_{\pm}(q) \ . \qquad (2.4.7)$$

We obtain for the eikonal amplitude in the Ericson model

$$f(q) = \frac{ikb_o}{q} \left\{ F_{+}(q) \left[\varepsilon J_1(b_o q) + i \frac{2n}{b_o q} J_2(b_o q) \right] + iF_{-}(q) \left[\varepsilon J_o(b_o q) + i \frac{2n}{b_o q} J_1(b_o q) \right] \right\} e^{i2\sigma_p(b_o)} \qquad (2.4.8)$$

and for the differential cross-section

$$\sigma(q) = \left(\frac{kb_o}{q} \right)^2 \left| F_{+}(q) \left[\varepsilon J_1(b_o q) + i \frac{2n}{b_o q} J_2(b_o q) \right] + iF_{-}(q) \left[\varepsilon J_o(b_o q) + i \frac{2n}{b_o q} J_1(b_o q) \right] \right|^2 \ . \qquad (2.4.9)$$

2.5 The asymptotic differential cross-section:

Replacing the Bessel functions in (2.2.9) by their asymptotic forms

$$J_m(x) \simeq \left(\frac{2}{\pi x}\right)^{\frac{1}{2}} \cos\left(x - \frac{m\pi}{2} - \frac{\pi}{4}\right) \qquad m=0,1,2,... \qquad (2.5.1)$$

we obtain the following simplified expression describing the asymptotic differential cross-section in the Ericson parametric model

$$\sigma(q) \simeq \frac{k^2 b_o}{\pi q^3} |\varepsilon|^2 \left(\frac{\pi a q}{\sinh(\pi a q)}\right)^2 \cosh(2\alpha a q)$$

$$\left\{\left[1 + \frac{4n\alpha a}{b_o}\right]\left[1 - \operatorname{sech}(2\alpha a q) \sin(2b_o q)\right]\right.$$

$$\left. - \frac{4n}{b_o q} \frac{\mathrm{Re}\,\varepsilon}{|\varepsilon|^2} \tanh(2\alpha a q)\right\} \qquad (2.5.2)$$

correct to first order in n.

The cross-sections describing charged particle scattering can be expressed as

$$\sigma^o(q) \simeq \overline{\sigma^o}(q)\,\Omega^o(q)$$

$$\sigma^{\pm}(q) \simeq \overline{\sigma^o}(q)\left\{\Omega^{\pm}(q) - \frac{n}{kb_o}\left[(1 - 4\alpha k a)\,\Omega^{\pm}(q)\right.\right.$$

$$\left.\left. + \frac{4k}{q} \frac{\mathrm{Re}\,\varepsilon}{|\varepsilon|^2} \tanh(2\alpha a q)\right]\right\} \qquad (2.5.3)$$

where

$$\overline{\sigma^{o}}(q) = \left(\frac{k^2 b_o}{\pi q^3}\right) |\varepsilon|^2 \left(\frac{\pi a q}{\sinh(\pi a q)}\right)^2 \cosh(2\alpha a q) \qquad (2.5.4)$$

denotes the mean cross-section, and the factors $\Omega^{o}(q)$ and $\Omega^{\pm}(q)$ are representative of the diffraction oscillations characteristic of neutral and charged particle scattering respectively and are given by

$$\Omega^{o}(q) = 1 - \operatorname{sech}(2\alpha a q) \sin(2b_o q)$$

$$\Omega^{\pm}(q) = 1 - \operatorname{sech}(2\alpha a q) \sin\left[2\left(b_o - \frac{n}{k}\right)q\right] . \qquad (2.5.5)$$

The features of the asymptotic angular distributions given by (2.5.3) are applicable to a description of π-nucleus scattering near the (3,3) resonance, where the necessary strong-absorption condition is satisfied.

The cross-sections for π°, π^{+}, π^{-} scattering are denoted by $\sigma^{\circ}(q)$, $\sigma^{+}(q)$ and $\sigma^{-}(q)$ respectively.

Firstly, we make the observation that the mean cross-section given by (2.5.4) falls off rapidly with increasing q as

$$\overline{\sigma^{\circ}}(q) \simeq \frac{2k^2a^2\pi b_o}{q} |\varepsilon|^2 \exp[-2(\pi-\alpha)aq] \qquad (2.5.6)$$

the exponential fall-off getting steeper with increasing diffuseness a, but its rate is lessened by the nuclear phase parameter α.

Secondly, the diffraction oscillations of (2.5.5) are observed to possess constant periods given by

$$\delta q^{\circ} = \frac{\pi}{b_o}$$

and

$$\delta q^{\pm} = \frac{\pi}{\left(b_o - \frac{n}{k}\right)} \qquad (2.5.7)$$

for neutral and charged particle scattering respectively.

The minima of the diffraction oscillations for neutral particle scattering occur at q values defined by

$$q^{\circ}_{min} = \frac{\pi}{b_{\circ}}\left(m+\frac{1}{4}\right) \qquad m=0,1,2,\ldots$$

and for charged particle scattering at values

$$q^{\pm}_{min} = \left[\frac{\pi}{b_{\circ}}\left(m+\frac{1}{4}\right)\right]\left[1+\frac{n}{kb_{\circ}}\right] = \left[1+\frac{n}{kb_{\circ}}\right]q^{\circ}_{min} \qquad (2.5.8)$$

(2.5.8) displays the interesting feature that the positions of the minima are shifted towards larger q values for positive particle and towards smaller q for negative particle scattering.

The corresponding diffraction minima are

$$\sigma^{\circ}(q^{\circ}_{min}) = \overline{\sigma^{\circ}}(q^{\circ}_{min})\,\Omega^{\circ}(q^{\circ}_{min})$$

$$= \overline{\sigma^{\circ}}(q^{\circ}_{min})\left[1-\operatorname{sech}(2\alpha a q^{\circ}_{min})\right]$$

and

$$\sigma^{\pm}(q^{\pm}_{min}) = \overline{\sigma^{\circ}}(q^{\pm}_{min})\left\{\Omega^{\pm}(q^{\pm}_{min}) - \frac{n}{kb_{\circ}}\left[(1-4\alpha ka)\,\Omega^{\pm}(q^{\pm}_{min}) + \frac{4k}{q^{\pm}_{min}}\,\frac{Re\,\varepsilon}{|\varepsilon|^{2}}\tanh(2\alpha a q^{\pm}_{min})\right]\right\}$$

$$\simeq \overline{\sigma^{\circ}}(q^{\pm}_{min})\left\{\left[1-\operatorname{sech}(2\alpha a q^{\pm}_{min})\right]\left[1-\frac{n}{kb_{\circ}}\right]\right\}$$

$$= \left[1-\frac{n}{kb_{\circ}}\right]\sigma^{\circ}(q^{\pm}_{min}) \qquad (2.5.9)$$

In the case of neutral particle scattering the diffraction minima are filled in by the nuclear interaction; the Coulomb interaction, present in charged particle scattering, has the effect of lowering the minima for positive particles and raising them for negative particles.

Ideally, what we require is a single critical impact parameter that will describe both neutral and charged particle scattering. With this in mind, we redefine our quantity b_o as

$$b_o \triangleq \overset{o}{b}_o - \frac{n}{k} \tag{2.5.10}$$

where $\overset{o}{b}_o$ represents the critical impact parameter describing neutral particle scattering, and the Coulomb-energy correction term $-\frac{n}{k}$, the effect of the Coulomb interaction on the value $\overset{o}{b}_o$.

We associate $\overset{o}{b}_o$ with an energy-independent strong-absorption radius R_{SA}; and observe that the critical impact parameter describing negative particle scattering is larger than the corresponding one for positive particle scattering. This has to do with the long range Coulomb change in the effective impact parameter, due to the Coulomb trajectory.

Use of (2.5.10) allows us to express the asymptotic elastic cross-sections (2.5.3) - (2.5.5) in a more concise form

$$\sigma^o(q) \simeq \overline{\sigma^o}(q)\Omega(q)$$

$$\sigma^{\pm}(q) \simeq \overline{\sigma^o}(q)\left\{\Omega(q) - \frac{n}{\overset{o}{k}b_o}\left[(1-4k\alpha a)\Omega(q) + \frac{4k}{q}\frac{Re\varepsilon}{|\varepsilon|^2}\tanh(2\alpha aq)\right]\right\}$$

with

$$\overline{\sigma^{o}}(q) = \frac{k^2 \overset{o}{b}_o}{\pi q^3} |\varepsilon|^2 \left(\frac{\pi aq}{\sinh(\pi aq)}\right)^2 \cosh(2\alpha aq)$$

$$\Omega(q) = 1 - \operatorname{sech}(2\alpha aq) \sin(2b_o q) \qquad (2.5.11)$$

correct to first order in n.

3. TREATMENT OF π-NUCLEUS RESONANCE SCATTERING

In this section we adopt a method of treating the phenomenon of resonance scattering which explicitly incorporates the resonance into the eikonal formalism.

3.1 The resonant optical potential:

We follow the approach of Kisslinger[9] in assuming that the optical potential describing pion-nucleus scattering in the vicinity of the (3,3) resonance can be taken as consisting of two terms: the first term corresponding to the background non-resonant interaction, covering the normal non-resonant nuclear scattering and absorption processes, and the second term describing the resonant scattering interaction of the pion with a nucleon embedded in the nucleus. Kisslinger takes this second term to have a resonant Breit-Wigner energy dependence, with resonance energy corresponding to that of a (3,3) resonance in the nuclear environment.

Our analysis of the scattering carried out in the previous sections has incorporated a phenomenological Ericson parameterization of the nuclear S-matrix. However, to utilize the resonant optical potential, we require a relationship between the S-matrix and optical potential parameters.

We thus choose (as an alternative to the Ericson form) Kauffmann's suggested parameterization of the nuclear part of the scattering function[15], the parameters of which can be related to those of an optical potential. In his work, Kauffmann considered a phenomenological complex optical potential describing the elastic scattering of spin-zero particles, with nuclear part of the form

$$U(r) = -(V+iW)\, f(r,R,a) \qquad (3.1.1)$$

where V and W denote the strengths of the real and imaginary potential well depths; the common form-factor f(r,R,a) is characterised by radius and surface diffuseness parameters and taken to be of the Saxon-Woods form

$$f(r,R,a) = \frac{1}{\left[1+\exp\left(\frac{r-R}{a}\right)\right]} \quad . \qquad (3.1.2)$$

We shall be discussing in detail the eikonal treatment of such an optical potential to obtain Kauffmann's form for the nuclear scattering matrix in a later section.

We now insert the Kisslinger non-resonant and resonant optical potentials into this framework, writing our optical model nuclear potential in the form

$$\begin{aligned} U(r,E) &= U_{NR}(r) + U_R(r,E) \\ &= \left[-(V_{NR} + iW_{NR}) + U_R T_R(E)\right] f(r,R,a) \end{aligned} \qquad (3.1.3)$$

where $T_R(E)$ is the t-matrix for the π-nucleon (3,3) resonance in the nuclear environment. It has a Breit-Wigner resonance shape and is given by

$$T_R(E) = -\frac{1}{2i}\left(\frac{i\Gamma}{E_o' - E - \frac{i\Gamma}{2}}\right) = \frac{\frac{\Gamma}{2}}{(E-E_o') + \frac{i\Gamma}{2}} \quad , \qquad (3.1.4)$$

i.e. we take $T_R(E)$ to be a modified elementary resonant

t-matrix for π-nucleon scattering in free space

$$t_R(E) = \frac{\frac{\Gamma}{2}}{(E - E_O) + \frac{i\Gamma}{2}} \quad . \tag{3.1.5}$$

We expect $E_O' \simeq E_O$, because nucleons bound in the nucleus scatter pions very similarly to free nucleons. The resonant contribution to the π-nucleus interaction is thus described in terms of a slightly modified resonant πN free space scattering amplitude, which incorporates a small shift in the resonance energy parameter to deal with the effects of multiple scattering and binding in nuclear matter.

If we were to use only the unmodified resonant elementary t-matrix in our theory, we would be applying what is essentially a resonant Impulse Approximation to a nucleonic structure whose spatial distribution conforms to the form factor f(r,R,a).

Our procedure consists of modifying the resonant Impulse Approximation by including non-resonant scattering from the nucleus and introducing a modified resonance energy to take account of nuclear binding and multiple scattering corrections.

This method of dealing with this problem is suggested both by Kisslinger's work[9] and by research carried out by Cottingame and Holtkamp[10].

Thus our general optical model potential describing resonance

scattering is expressed as

$$U(r,E) = -\left[\left[V_{NR} + iW_{NR}\right] - U_R\left(\frac{\frac{\Gamma}{2}}{(E - E_o') + \frac{i\Gamma}{2}}\right)\right] f(r,R,a)$$

$$= -U_R\left[\left[v + iw\right] - \left(\frac{\frac{\Gamma}{2}}{(E - E_o') + \frac{i\Gamma}{2}}\right)\right] f(r,R,a) \qquad (3.1.6)$$

where we have assumed the same nuclear form-factor f(r,R,a) for both the resonant and non-resonant potentials. U_R, expressed in MeV, represents the strength of the resonant potential; v and w the relative strengths of the non-resonant real and imaginary potentials respectively. v and w are dimensionless quantities

$$v = \frac{V_{NR}}{U_R} \quad \text{and} \quad w = \frac{W_{NR}}{U_R} .$$

The non-resonant and resonant contributions above both consist of real and imaginary parts. The presence of the non-resonant background term is logical. At energies far from resonance, i.e. too far away for there to be any effect of the resonance on the scattering, the presence of a background interaction is necessary to describe the other processes observed to be occurring. However, at energies close to resonance, we naturally expect the resonance to dominate the scattering, partially 'masking' the background. We expect the background contribution to the potential to be relatively small and almost energy independent, and representative of all the processes not proceeding through the resonance. We further expect to find $w > v$, as

non-resonant absorption is more important than non-resonant refraction, where both w and v are less than unity - the resonance scattering itself being the most important process occurring at the energies of interest to us.

On the other hand, we expect the resonant term to be relatively large and strongly energy dependent. It is peaked at the resonance energy and falls off to zero on either side of E_o'. It only contributes with significant magnitude at energies within about Γ of E_o', where it overshadows the non-resonant background. At resonance we have that $\mathrm{Re}(U_R(r,E))$ vanishes, so that the resonant contribution to the potential is pure negative imaginary at $E = E_o'$, i.e. purely absorptive there.

3.2 The isospin dependence of the resonant term:

The resonant optical potential (3.1.6) is only strictly proper for N=Z nuclei. When N≠Z, further isospin effects would be expected[13,14], which we discuss here.

The π^+ and π^- interaction with neutrons differs at the energies in question. Since the dominant interaction is via the resonant isospin $\frac{3}{2}$ state, the π^-'s interact much more strongly with neutrons than do the π^+'s. We observe this at the (3,3) resonance, where the resonant π^-n (π^+p) elastic amplitude is three times larger than the π^+n (π^-p) one. This dependence on isospin must be taken into account in evaluating the resonant contribution to the scattering amplitude for N≠Z target nuclei, for example, those having a neutron excess; and is done in the following way:

For scattering of the π^+ projectile: each of the Z protons in the target nucleus is observed to contribute fully to the resonance - the $|\pi^+p\rangle$ state has $I_z = \frac{3}{2}$ - and is thus pure isospin $I = \frac{3}{2}$. However, the contribution of the N neutrons to the $I = \frac{3}{2}$ resonant amplitude is with a Clebsch-Gordon coefficient which is smaller than unity, namely

$$\langle \pi^+ n | I = \tfrac{3}{2}, I_z = \tfrac{1}{2} \rangle = \sqrt{\tfrac{1}{3}} \qquad \text{compared with}$$

$$\langle \pi^+ p | I = \tfrac{3}{2}, I_z = \tfrac{3}{2} \rangle = 1 .$$

Similarly, considering the scattering of π^-: each of the N neutrons contributes fully to the resonance

$$< \pi^- n | I = \frac{3}{2} , I_z = \frac{3}{2} > = 1$$

whereas each of the Z protons contributes with a Clebsch-Gordon coefficient less than 1

$$< \pi^- p | I = \frac{3}{2} , I_z = -\frac{1}{2} > = \sqrt{\frac{1}{3}} .$$

The expression for the elastic scattering amplitude describing πN scattering in the resonance region is dominated by the term

$$< \pi N | T | I_{3/2} > < I_{3/2} | \pi N >$$

which describes the scattering process proceeding from an initial state $|\pi N>$ into the resonant $I = \frac{3}{2}$ state, whose overlap with the final state $<\pi N|$ must then enter as a factor. A second such Clebsch-Gordon factor is then extracted from $<\pi N|T|I_{\frac{3}{2}}>$ by use of the Wigner-Eckhart Theorem.

Thus, for $\pi^{\pm}$ projectiles incident on a target nucleus (A = N+Z), the resonant part of the optical potential describing the scattering is modified by a factor $\gamma(\pi^{\pm},N,Z)$, which takes the isospin dependence of the resonant contribution into account, where

$$\gamma(\pi^+,N,Z) = \left[\frac{Z + \frac{1}{3} N}{\frac{2A}{3}}\right] = \frac{(3Z + N)}{2A}$$

and

$$\gamma(\pi^-,N,Z) = \left[\frac{N + \frac{1}{3} Z}{\frac{2A}{3}}\right] = \frac{(3N + Z)}{2A} \quad , \qquad (3.2.1)$$

being normalized, such that for a $N = Z = \frac{A}{2}$ nucleus, $\gamma(\pi^{\pm},N,Z) = 1$.

Thus, our expression for the resonant contribution to the nuclear optical potential is

$$U_R(r,E) = \gamma(\pi^{\pm},N,Z)U_R\left(\frac{\frac{\Gamma}{2}}{(E-E_o') + \frac{i\Gamma}{2}}\right) f(r,R,a) \qquad (3.2.2)$$

which incorporates both the energy and isospin dependence of the pure resonance scattering.

Correcting expression (3.1.6) to read

$$U(r,E) = -U_R\left[[v + iw] - \gamma\left(\frac{\frac{\Gamma}{2}}{(E-E_o') + \frac{i\Gamma}{2}}\right)\right] f(r,R,a) \qquad (3.2.3)$$

we derive the real and imaginary potentials

$$V(r,E) \equiv \text{Re } U(r,E) = V_{NR}(r) + V_R(r,E)$$

$$= -U_R\left[v - \gamma \frac{\frac{\Gamma}{2}(E-E_o')}{(E-E_o')^2 + \frac{\Gamma^2}{4}}\right] f(r,R,a)$$

$$= -U_R\left[\frac{v\left[(E-E_o')^2 + \frac{\Gamma^2}{4}\right] - \gamma\frac{\Gamma}{2}(E-E_o')}{(E-E_o')^2 + \frac{\Gamma^2}{4}}\right] f(r,R,a)$$

$$\equiv -V(E)\, f(r,R,a) \qquad (3.2.4)$$

and

$$W(r,E) \equiv \text{Im}\, U(r,E) = W_{NR}(r) + W_R(r,E)$$

$$= -U_R\left[w + \gamma \frac{\frac{\Gamma^2}{4}}{(E-E_o')^2 + \frac{\Gamma^2}{4}}\right] f(r,R,a)$$

$$= -U_R\left[\frac{(\gamma+w)\frac{\Gamma^2}{4} + w(E-E_o')^2}{(E-E_o')^2 + \frac{\Gamma^2}{4}}\right] f(r,R,a)$$

$$\equiv -W(E)\, f(r,R,a) \qquad (3.2.5)$$

describing the background plus resonant interactions.

From (3.2.4) and (3.2.5) we obtain an expression for the relative strength of the real and imaginary potential

$$\frac{V(E)}{W(E)} = \frac{v\left[(E-E_o')^2 + \frac{\Gamma^2}{4}\right] - \gamma\frac{\Gamma}{2}(E-E_o')}{w\left[(E-E_o')^2 + \frac{\Gamma^2}{4}\right] + \gamma\frac{\Gamma^2}{4}} \quad . \qquad (3.2.6)$$

3.3 Eikonal parameterization of the scattering function:

Strongly absorbing potentials of the type (3.1.1) with an exponential tail can be approximated by

$$U(r) \simeq -(V + iW) \exp\left[-\frac{r-R}{a}\right] . \qquad (3.3.1)$$

The potentials (3.1.1) and (3.3.1) only differ significantly when $r \ll R$, where, however, they are both strongly absorptive. Thus they may be expected to yield virtually the same physics.

The form (3.3.1) can be used in an evaluation of the eikonal nuclear phase shift function, given by

$$\delta_N(b) = -\frac{1}{(2\hbar v)} \int_b^\infty dr \, \frac{rU(r)}{(r^2 - b^2)^{\frac{1}{2}}} , \qquad (3.3.2)$$

with the approximate result[1]

$$2\delta_N(b) \simeq \frac{1}{(\hbar v)} \left(\frac{\pi a R}{2}\right)^{\frac{1}{2}} (V + iW) \exp\left[-\frac{b-R}{a}\right] . \qquad (3.3.3)$$

Recalling that the scattering function in the eikonal approximation is given in exponential form

$$S_N(b) = e^{i2\delta_N(b)} , \qquad (3.3.4)$$

substitution of (3.3.3) into (3.3.4) then yields the following parametric form for the nuclear scattering function

$$S_N(b) = \exp\left[-(1 - iA)e^{-\tilde{\mu}}\right] \qquad \tilde{\mu} = \left(\frac{b-\tilde{b}_o}{\tilde{a}}\right) \qquad (3.3.5)$$

which is the impact parameter analog of the form proposed by Kauffmann.

We refer to (3.3.5) as the eikonal parametric model of the nuclear scattering function. The amplitude of the nuclear scattering function and the nuclear phase shift function in the eikonal model are given by

$$\eta_N(b) = \exp\left[-e^{-\tilde{\mu}}\right] \qquad (3.3.6)$$

and

$$2\delta_N(b) = (A + i)e^{-\tilde{\mu}} \ . \qquad (3.3.7)$$

The three quantities $\tilde{b}_o$ - the critical impact parameter, $\tilde{a}$ - the diffuseness, and A - the nuclear phase parameter, in expression (3.3.5) are now related to the potential parameters in (3.1.1), as we require.

We find, correct to first order in n, that

$$\tilde{b}_o = R - \frac{n}{k} + \tilde{a} \ln\left[\frac{W}{E} k \left(\frac{\pi \tilde{a} R}{2}\right)^{\frac{1}{2}}\right] , \qquad (3.3.8)$$

the $-\frac{n}{k}$ term resulting from consideration of the Coulomb contribution via (2.2.3), and

$$A = \frac{V}{W} \ . \qquad (3.3.9)$$

In the case of the resonant optical potential (3.2.3), V and W are actually functions of the energy E, as set forth in (3.2.4) and (3.2.5), and A is explicitly given by (3.2.6).

The explicitly energy-dependent part $\frac{W(E)}{E}k$ in (3.3.8) we write as

$$W(E)\left(\frac{mv_{\pi,lab}}{\hbar}\right)\Big/T_{\pi,lab} = \left(\frac{1}{v}\right)\left(\frac{2W(E)}{\hbar}\right) , \qquad (3.3.10)$$

a consequence of equating the π-nucleus centre-of-mass and laboratory systems. For the resonant optical potential we have

$$W(E) = U_R \left[\frac{(\gamma+w)\frac{\Gamma^2}{4} + w(E-E_o')^2}{(E-E_o')^2 + \frac{\Gamma^2}{4}}\right]. \qquad (3.3.11)$$

Our expression for the critical impact parameter then reads

$$\tilde{b}_o = R - \frac{n}{k} + \tilde{a}\ln\left[\left[\frac{v_o'}{v}\frac{1}{(\gamma+w)}\frac{(\gamma+w)\frac{\Gamma^2}{4} + w(E-E_o')^2}{(E-E_o')^2 + \frac{\Gamma^2}{4}}\right]\right.$$

$$\left.\left[\frac{1}{v_o'}(\gamma+w)U_R\left(\frac{2}{\hbar}\right)\left(\frac{\pi\tilde{a}R}{2}\right)^{\frac{1}{2}}\right]\right] , \qquad (3.3.12)$$

where v_o' is the pion lab velocity at the displaced resonance energy E_o'. The argument of the ln is written as a product of two factors, the first of which reduces to unity at $E = E_o'$, and the second of which is independent of the energy E.

Using this decomposition, we obtain

$$\tilde{b}_o = R' - \frac{n}{k} + \tilde{a} \ln \left[\frac{v_o'}{v} \frac{1}{(\gamma+w)} \frac{(\gamma+w)\frac{\Gamma^2}{4} + w(E-E_o')^2}{(E-E_o')^2 + \frac{\Gamma^2}{4}} \right] \quad (3.3.13)$$

where we have redefined our effective strong-absorption radius R′ so as to absorb the energy-independent ln term

$$R' = R + \tilde{a} \ln \left[\frac{1}{v_o'} (\gamma+w) U_R \left(\frac{2}{\hbar}\right)\left(\frac{\pi\tilde{a}R}{2}\right)^{\frac{1}{2}} \right] . \quad (3.3.14)$$

The other two terms of (3.3.13) are both energy-dependent quantities: $-\frac{n}{k}$ describes the charge dependence and the resonant ln term the effect of resonance and isospin - for N≠Z nuclei - on the scattering.

We note that the resonant ln term varies significantly with energy near resonance, where it causes b_o to have a peak. At the displaced resonance energy E_o' (3.3.13) reduces to

$$\tilde{b}_o = R' - \frac{n}{k} , \quad (3.3.15)$$

i.e., no contribution from this term. At other nearby energies $E \neq E_o'$ its contribution to the value of b_o is negative; its magnitude increasing with increasing displacement of E from E_o'. Hence we may consider the resonant ln term as a correction term to strong-absorption scattering: at E_o', the resonance peak, the scattering is quite strongly absorptive in nature, described by the strong-absorption critical impact parameter (3.3.15); while at

energies on either side of E_o' the effect of resonance diminishes, and with it the degree of strong absorption. This is reflected in the energy dependence of the critical impact parameter given by (3.3.13), which has its peak at resonance.

3.4 The eikonal amplitude in the eikonal parametric model:

We present the corresponding expressions to (2.4.1) - (2.4.9) which were evaluated in the Ericson model. The results of Frahn[1] are summarized.

The Fourier transform $F_N(z)$ given by (2.2.5) in the eikonal model is[15]

$$F_N(z) = \exp[iz \ln(1-iA)]\, \Gamma(1-iA) \tag{3.4.1}$$

which is approximated by the function

$$F_N(z) \simeq e^{(\alpha+i\beta)z} \left(\frac{\pi z}{\sinh(\pi z)}\right)^{\frac{1}{2}} \tag{3.4.2}$$

where

$$\alpha = \arctan A$$

and

$$\beta = \gamma + \frac{1}{2}\ln(1+A^2)$$

where γ is Euler's constant.

Into (2.2.16) we substitute the results

$$F_N'(z) = \left[(\alpha+i\beta) - \frac{\pi^2}{6} z\right] F_N(z)$$

and

$$F_N''(z) = \left[\left[(\alpha+i\beta) - \frac{\pi^2}{6} z\right]^2 - \frac{\pi^2}{6}\right] F_N(z) \qquad (3.4.3)$$

to obtain

$$\tilde{F}_N(z) = \tilde{\varepsilon} F_N(z) \qquad (3.4.4)$$

where

$$\tilde{\varepsilon} = \left[1 - i2(\alpha+i\beta)\left(\frac{\tilde{a}}{\tilde{b}_o}\right) + \left[\frac{\pi^2}{6} - (\alpha+i\beta)^2\right]\left(\frac{\tilde{a}}{\tilde{b}_o}\right)^2\right] . \qquad (3.4.5)$$

Neglecting terms of order $\frac{n\tilde{a}^2 q}{\tilde{b}_o}$ as done previously, the functions $F_{\pm}(q)$ and related quantities $\tilde{F}_{\pm}(q)$ of (2.2.17) are given by

$$F_+(q) = e^{(\alpha+i\beta)\tilde{a}q_o}\left(\frac{\pi\tilde{a}q}{\sinh(\pi\tilde{a}q)}\right)^{\frac{1}{2}} \cosh\left[(\alpha+i\beta)\tilde{a}q\right] \qquad (3.4.6)$$

$$F_-(q) = e^{(\alpha+i\beta)\tilde{a}q_o}\left(\frac{\pi\tilde{a}q}{\sinh(\pi\tilde{a}q)}\right)^{\frac{1}{2}} \sinh\left[(\alpha+i\beta)\tilde{a}q\right] \qquad (3.4.7)$$

and

$$\tilde{F}_{\pm}(q) = \tilde{\varepsilon} F_{\pm}(q) . \qquad (3.4.8)$$

The eikonal elastic amplitude of (2.2.18) in the eikonal model is then given by

$$f(q) = \frac{ik\tilde{b}_o}{q}\left\{F_+(q)\left[\tilde{\varepsilon}J_1(\tilde{b}_o q) + i\frac{2n}{\tilde{b}_o q}J_2(\tilde{b}_o q)\right]\right.$$

$$\left. + iF_-(q)\left[\tilde{\varepsilon}J_o(\tilde{b}_o q) + \frac{i2n}{\tilde{b}_o q}J_1(\tilde{b}_o q)\right]\right\} e^{i2\sigma_p(\tilde{b}_o)} \qquad (3.4.9)$$

and the differential cross-section by

$$\sigma(q) = \left(\frac{k\tilde{b}_o}{q}\right)^2 \left|F_+(q)\left[\tilde{\varepsilon}J_1(\tilde{b}_o q) + i\frac{2n}{\tilde{b}_o q}J_2(\tilde{b}_o q)\right]\right.$$

$$\left. + iF_-(q)\left[\tilde{\varepsilon}J_o(\tilde{b}_o q) + i\frac{2n}{\tilde{b}_o q}J_1(\tilde{b}_o q)\right]\right|^2 \qquad (3.4.10)$$

with the quantities as defined above.

The real and imaginary parts of the neutral forward scattering amplitude, given by (2.2.27) and (2.2.28) respectively, are evaluated in this model using

$$F_N'(0) = \alpha + i\beta \qquad \text{and}$$

$$F_N''(0) = (\alpha + i\beta)^2 - \frac{\pi^2}{6} \qquad (3.4.11)$$

with the results

$$\text{Re } \overset{o}{f}(o) = \frac{k\tilde{b}_o^2}{2} 2\alpha\left(\frac{\tilde{a}}{\tilde{b}_o}\right)\left[1 + \beta\left(\frac{\tilde{a}}{\tilde{b}_o}\right)\right] \qquad (3.4.12)$$

and

$$\text{Im } \overset{o}{f}(o) = \frac{k\tilde{b}_o^2}{2}\left[1 + 2\beta\left(\frac{\tilde{a}}{\tilde{b}_o}\right) + \left[\frac{\pi^2}{6} - \alpha^2 + \beta^2\right]\left(\frac{\tilde{a}}{\tilde{b}_o}\right)^2\right] \qquad (3.4.13)$$

Finally, for the total neutral cross-section in the eikonal model, we substitute the result (3.4.13) into (2.2.29) to obtain

$$\sigma_T = 2\pi\tilde{b}_o^2 \left[1 + 2\beta\left(\frac{\tilde{a}}{\tilde{b}_o}\right) + \left[\frac{\pi^2}{6} - \alpha^2 + \beta^2\right]\left(\frac{\tilde{a}}{\tilde{b}_o}\right)^2\right] . \qquad (3.4.14)$$

4. ANALYSIS OF EXPERIMENTAL DATA

π-nucleus scattering at intermediate energies and under strong-absorption conditions is one of the domains where the eikonal formalism can be successfully applied. Here we apply the eikonal resonance model derived in the previous sections to the particular case of 130, 180, 230 MeV pion - ^{40,48}Ca scattering.

To illustrate the extent to which π-nucleus scattering near the (3,3) resonance is dominated by strong-absorption, we first carry out a Black Disk analysis of the scattering data. Inclusion of the weak Coulomb interaction causes the minima of the diffraction pattern in the Black Disk model to be filled in. We then carry out the full eikonal resonance analysis of the scattering problem.

Comparison with experimental data is made in all cases. Discrepancies encountered in these comparisons are discussed with respect to deficiencies in the models.

The method formulated in the previous section is applied to a study of the elastic scattering of charged pions from the calcium isotopes $^{40,48}Ca$. The experimental differential cross-sections of Gretillet et al.[16], measured at incident pion kinetic energies of 130, 180 and 230 MeV - in the energy region of the $\pi N(3,3)$ resonance - are analysed.

All kinematics calculations are carried out using relativistic formulae. Because the target nuclei are very massive relative to the total energies of the incident pion projectiles, we may equate the π-nucleus centre-of-mass and laboratory systems.

Table (4.1-I)

Relativistic kinematic quantities evaluated for the $\pi^{\pm} - ^{40,48}Ca$ systems.

system	T_{lab}(MeV)	$p_{lab}\left(\frac{MeV}{c}\right)$	$k_{lab} \propto k_{cm}(fm^{-1})$	$\frac{v}{c}$	n
$\pi^{\pm} - ^{40,48}Ca$	130	230.6	1.169	0.8555	$\pm$0.1706
	180	287.5	1.457	0.8996	$\pm$0.1623
	230	342.2	1.735	0.9259	$\pm$0.1577

4.1 Black Disk analysis

In the Black Disk strong absorption model the nuclear interaction region is represented by a completely opaque spherical region of radius R possessing a sharp, well-defined boundary. In a semiclassical picture, particle trajectories having impact parameters $b \lesssim R$ are completely absorbed, while those with $b > R$ are completely transmitted.

We thus parameterise the S-matrix elements S(b) of the eikonal elastic scattering amplitude

$$f(q) = ik \int_0^\infty db\, b\,[1-S(b)]\, J_0(bq) \qquad (4.1.1)$$

as

$$S_{BD}(b) = \begin{cases} 0 & b \lesssim R \\ 1 & b > R \end{cases} . \qquad (4.1.2)$$

This results in the differential cross-section for elastic scattering having the form

$$\sigma_{BD}(q) = |f_{BD}(q)|^2 = (kR^2)^2 \left(\frac{J_1(Rq)}{Rq}\right)^2 \qquad (4.1.3)$$

where the oscillation pattern is given by the Bessel function $J_1^2(Rq)$.

This Black Disk model corresponds to the sharp cut-off limit

(limit $a \rightarrow o$) of the diffuse elastic eikonal amplitude, evaluated in the neutral limit - as given by expression (2.2.23).

In order to test the concept of 'strong-absorption' against experimental data in the resonance region, Black Disk fits were carried out for the $\pi^{\pm}$ - ^{40,48}Ca elastic scattering data.

Values for the Black Disk radii were taken from reference[16] and are given in Table (4.1-II). The calculated theoretical curves based on these parameters are presented in Figure (4.1-I). On comparing the theoretical curves and experimental data we note that, although the Black Disk model is a very crude method to apply to analysing this data, it is seen to be reasonably successful in describing the scattering in the region around the first diffraction minimum. The position of the minima and the general order of magnitude of the cross-sections are fairly well reproduced. The success of this model can be attributed to the strong πN interaction in the region of the (3,3) resonance. Close to resonance the interaction is very strong and absorptive, so that it is not very surprising that the π - ^{40,48}Ca elastic scattering data can in a first approximation be treated as Black Disk scattering.

Table (4.1-II)

Black Disk radii for π^+ and π^- scattering off $^{40,48}Ca$ at incident pion energies 130, 180 and 230 MeV [16].

	^{40}Ca		^{48}Ca	
T_π(MeV)	R_π+(fm)	R_π-(fm)	R_π+(fm)	R_π-(fm)
130	4.72	5.00	4.75	5.25
180	4.68	4.80	4.75	5.08
230	4.54	4.54	4.63	4.82

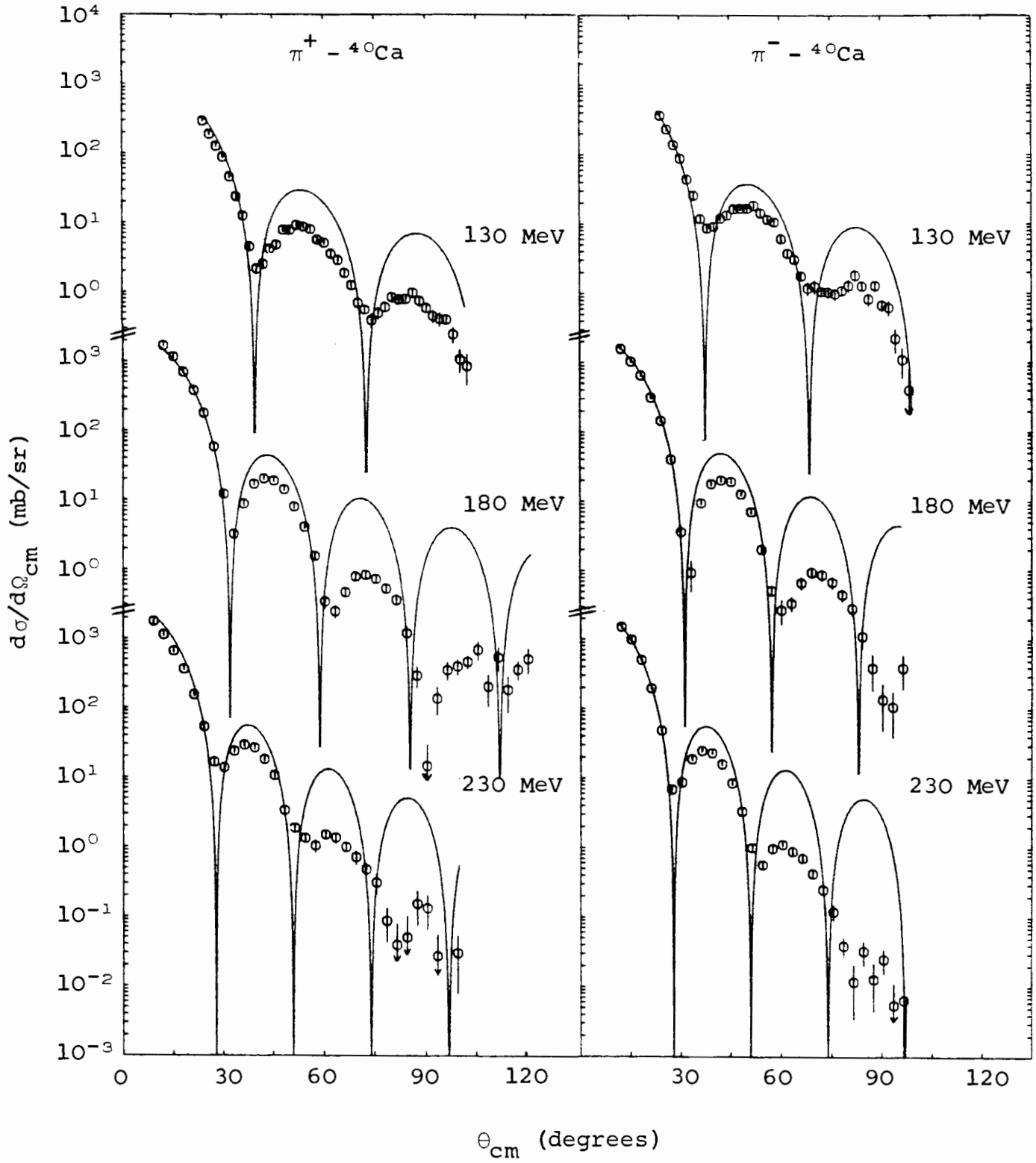

Figure (4.1-I) Black Disk $\pi^{\pm} - {}^{40}Ca$ elastic scattering differential cross-sections at T_π = 130, 180 230 MeV. The data are from reference[16].

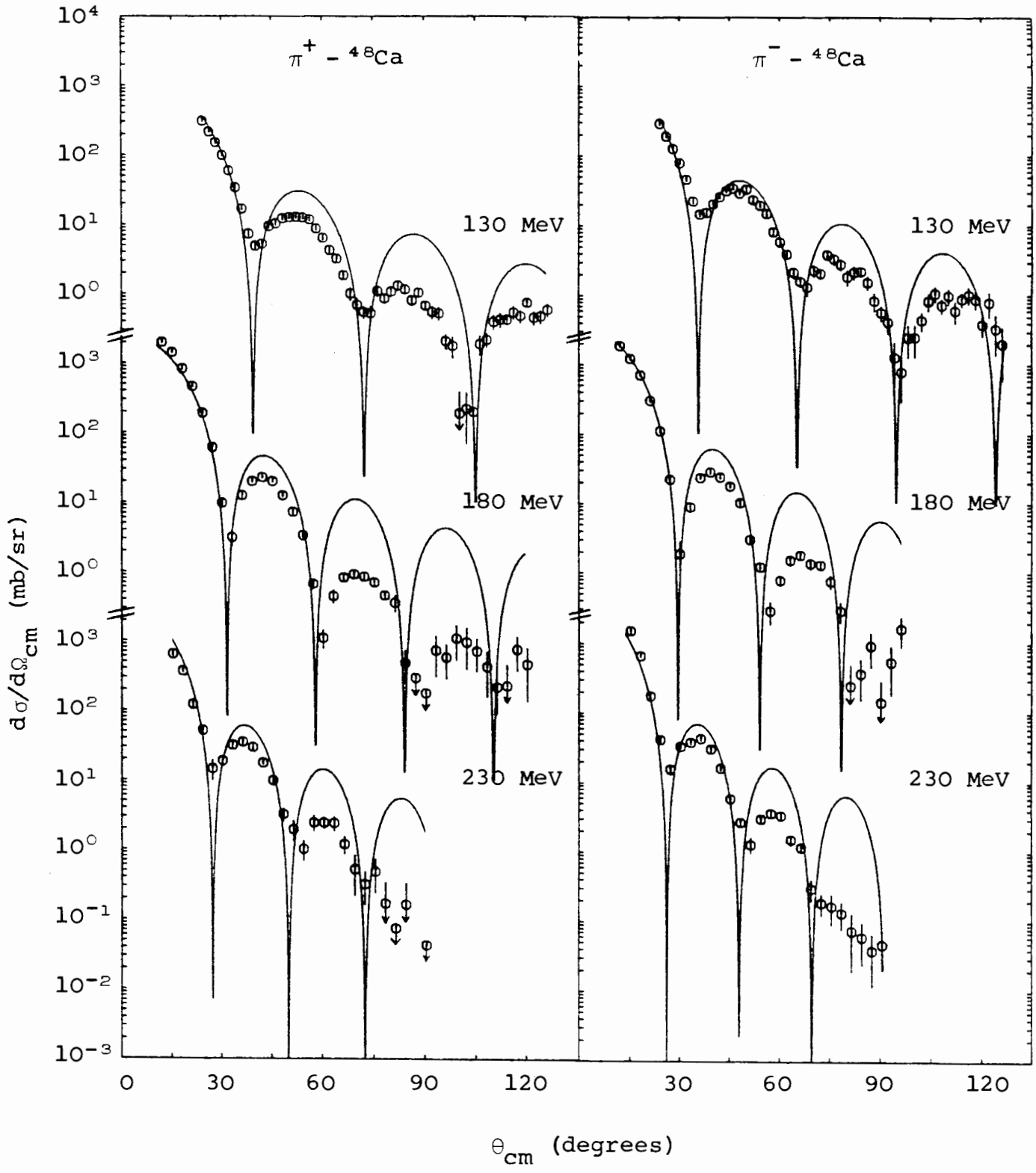

Figure (4.1-II) Black Disk $\pi^{\pm}$ - ^{48}Ca elastic scattering differential cross-sections at T_π = 130, 180 and 230 MeV. The data are from reference[16].

4.2 The sharp cut-off approximation: Black Disk model incorporating the Coulomb effects

Referring to expression (2.2.22) for the sharp cut-off amplitude, we evaluate the differential cross-section in the sharp cut-off model

$$\sigma_{sco}(q) = |f_{sco}(q)|^2$$

$$= \left(\frac{kb_o}{q}\right)^2 \left| J_1(b_o q) + \frac{i2n}{b_o q} J_o(b_o q) \right|^2 \qquad (4.2.1)$$

where we have taken the Coulomb effects into account to first order in n.

We now compute $\sigma_{sco}(q)$, using for b_o the R values from the previous given table, and compare our fits with those obtained in the neutral Black Disk analysis. Including the Coulomb effects has the consequence of improving the fits to the data; the Coulomb interaction causes a filling in of the diffraction minima.

The not unreasonable fits obtained from this preliminary Black Disk analysis indicate that pion scattering near resonance is dominated by strong-absorption.

The obvious cause for the observed discrepancies between the calculated differential cross-sections and the experimental data is the sharp cut-off assumption which we have applied in

our analysis up to now. Relaxing the sharp cut-off condition enables the theoretical cross-sections to decrease faster at large angles, in keeping with the experimental data. The nuclear interaction region is not so sharply defined as we have been assuming; rather there is a finite surface thickness a over which the nuclear density decreases from an approximately constant value inside the nucleus to a value of zero. In a semi-classical picture, partial absorption will be experienced by particles travelling along trajectories which penetrate this diffuse surface region. Such a 'smoothly grazing' edge cuts down the diffraction illumination of the large angle 'shadow' region.

This would suggest that we modify our sharp cut-off assumption to one describing a gradual transition from total absorption to no absorption over a region (window) a in impact parameter space describing the diffuseness of the nuclear profile around the critical impact parameter b_o.

Thus we would expect our eikonal model, which incorporates the Coulomb interaction as well as the idea of surface diffuseness, to provide us with a good description of the scattering.

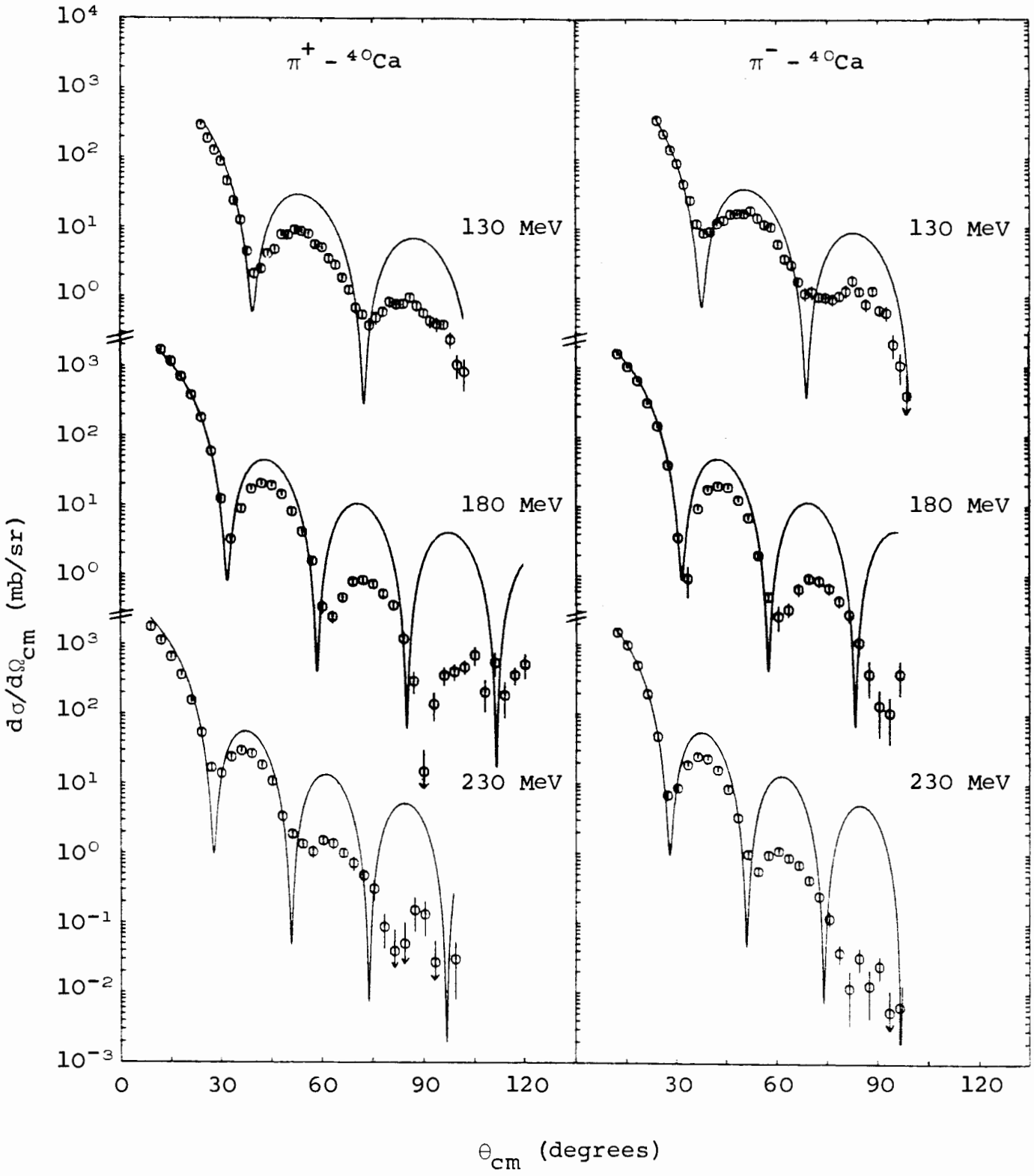

Figure (4.2-I) Black Disk $\pi^{\pm}$ - ^{40}Ca elastic scattering differential cross-sections at T_π = 130, 180 and 230 MeV. Coulomb scattering is included to first order in n. The data are from reference[16].

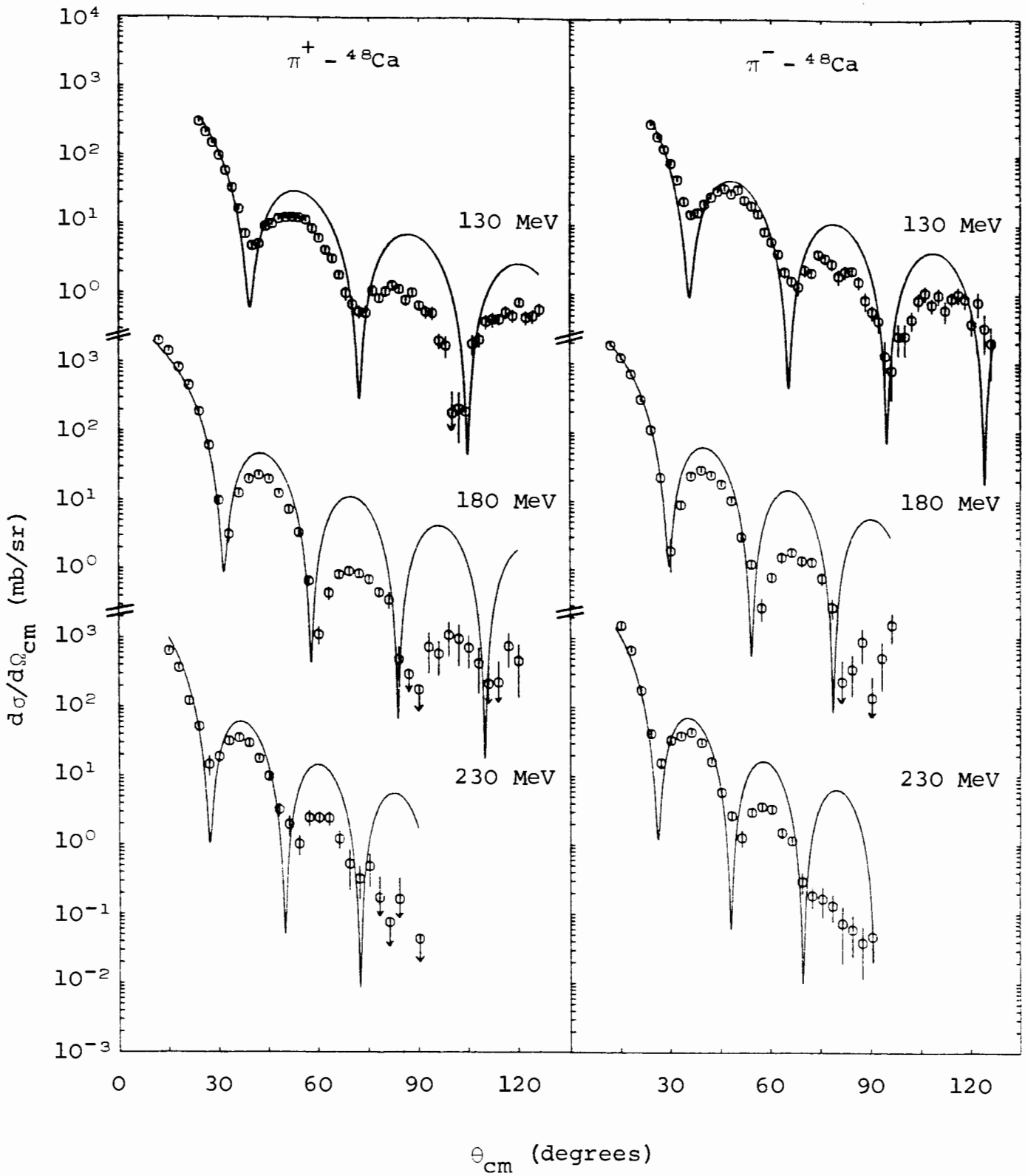

Figure (4.2-II) Black Disk $\pi^{\pm}$ - ^{48}Ca elastic scattering differential cross-sections at T_π = 130, 180 and 230 MeV. Coulomb scattering is included to first order in n. The data are from reference[16].

4.3 Eikonal resonance analysis

We extend our non-relativistic formalism of section 3.3 by applying relativistic kinematics to our calculation of the differential cross-section.

We also replace the non-relativistic Breit-Wigner form with its relativistic equivalent, that is, replace

$$\frac{\frac{\Gamma}{2}}{(E-E'_o)+\frac{i\Gamma}{2}} \quad \text{by} \quad \frac{m'_o\Gamma}{(s-m'^2_o)+im'_o\Gamma} \tag{4.3.1}$$

where s is the square of the total centre-of-mass energy

$$s = \left[\sqrt{p^2_{\pi,lab}+m^2_\pi}+m_N\right]^2 - p^2_{\pi,lab} \tag{4.3.2}$$

expressed in terms of the pion momentum in the laboratory frame, $p_{\pi,lab}$, and the nucleon mass, m_N. The quantity m'_o represents the displaced resonance energy as measured in the πN centre-of-mass system.

We thus obtain the relativistic generalisation of expression (3.4.10) for the differential cross-section in the eikonal parametric model, with parameters now defined as

$$\tilde{b}_o = R' - \frac{n}{k} + \tilde{a}\ln\left[\left(\frac{v'_o}{v}\right)\frac{1}{(\gamma+w)}\ \frac{(\gamma+w)(m'_o\Gamma)^2+w(s-m'^2_o)^2}{(s-m'^2_o)^2+(m'_o\Gamma)^2}\right] \tag{4.3.3}$$

and

$$A = \frac{V(s)}{W(s)} = \frac{\gamma(m_o'\Gamma)(m_o'^2-s) + v[(s-m_o'^2)^2 + (m_o'\Gamma)^2]}{\gamma(m_o'\Gamma)^2 + w[(s-m_o'^2)^2 + (m_o'\Gamma)^2]} \qquad (4.3.4)$$

where the quantity v in (4.3.3) is the relativistic pion velocity in the lab frame (which is virtually the same as the π-nucleus centre-of-mass frame).

$$v = \frac{p_{\pi,lab}}{\sqrt{m_\pi^2 + p_{\pi,lab}^2}} \qquad (4.3.5)$$

and v_o' is the value of v when $s = m_o'^2$, i.e. v_o' is the pion's lab velocity at the displaced resonance energy

$$v_o' = \frac{(m_o'^2 - (m_N+m_\pi)^2)^{\frac{1}{2}}(m_o'^2 - (m_N-m_\pi)^2)^{\frac{1}{2}}}{(m_o'^2 - m_N^2 - m_\pi^2)} \quad . \qquad (4.3.6)$$

We fitted the experimental elastic scattering[16] of both π^+ and π^- from ^{40}Ca at the three 'resonance scan' lab kinetic energies of 130, 180 and 230 MeV using (3.4.10) with the <u>single</u> set of parameter values

R' = 4.14 fm, $\tilde{a}$ = 0.80 fm, v = 0.25, w = 0.6, and m_o' = 1202 MeV.

The fit to all six experimental cross-sections shown in Figure (4.3-I) is very good. We used the free space value of the resonance width Γ = 110 MeV[8], but our displaced resonance energy m_o' = 1202 MeV is 30 MeV below the free space resonance energy m_o = 1232 MeV. The same value of m_o' was obtained by Cottingame and Holtkamp[10] for elastic pion scattering from ^{40}Ca. The pion lab kinetic energy

corresponding to m_0' is E_0' = 150 MeV.

We have also fitted the six corresponding pion on ^{48}Ca experimental elastic cross-sections[16] with the same parameter values as for ^{40}Ca, with the exception that $\tilde{a}$ was slightly changed to be 0.75 fm, and, of course, $R' = 4.14\ (48/40)^{1/3}$ fm = 4.40 fm, was appropriately enhanced for the additional nucleon number. Again the fit to the six experimental cross-sections, shown in Figure (4.3-II), is good.

These twelve excellent cross-section fits, using essentially a single set of parameter values, are an impressive success for the eikonal resonance model.

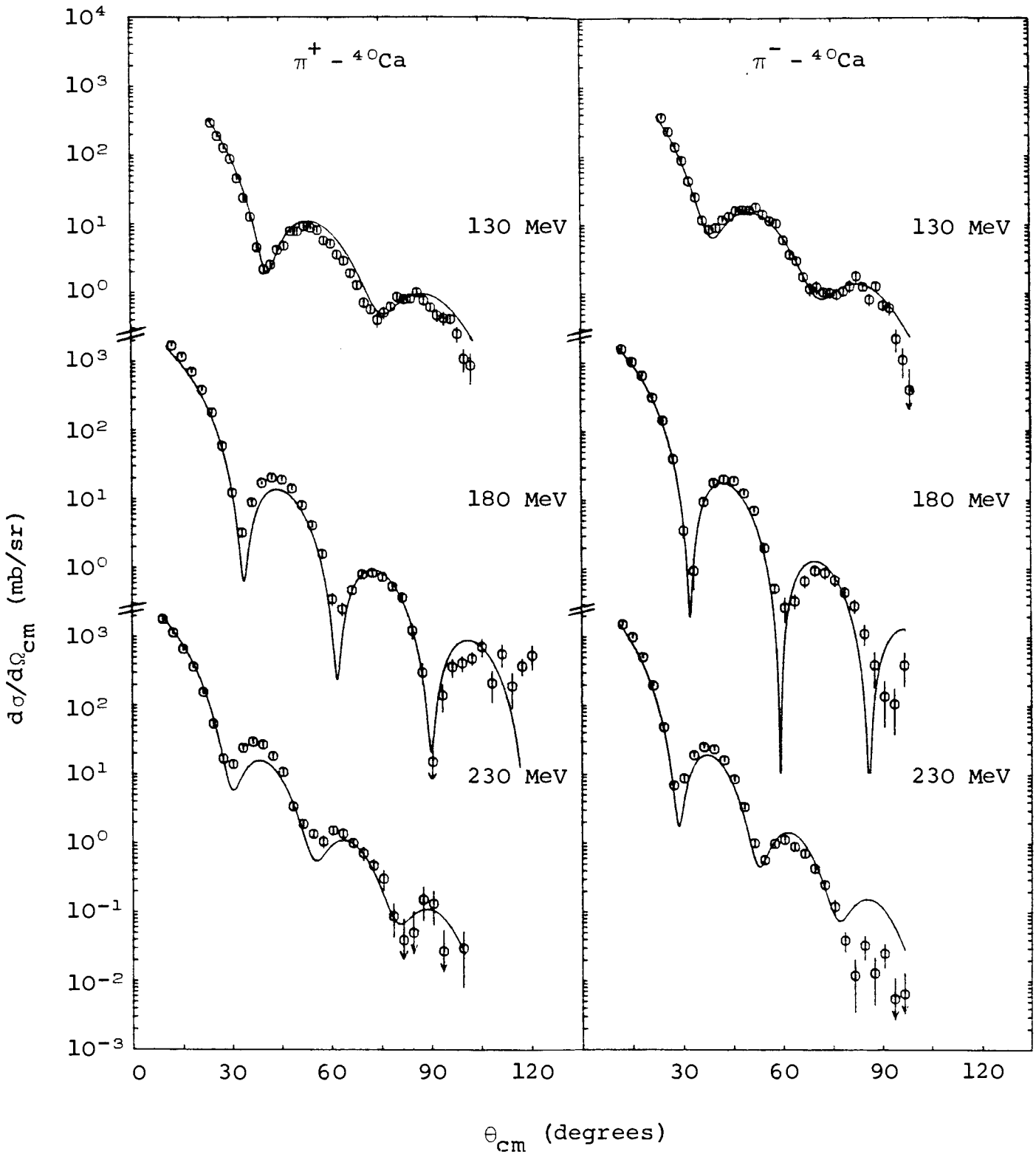

Figure (4.3-I) Eikonal resonance $\pi^{\pm} - {}^{40}Ca$ elastic scattering differential cross-sections at T_π = 130, 180 and 230 MeV. The data are from reference[16]. All six cross-sections are fitted with the single set of parameter values R' = 4.14 fm, $\tilde{a}$ = 0.80 fm, v = 0.25, w = 0.60, m'_o = 1202 MeV.

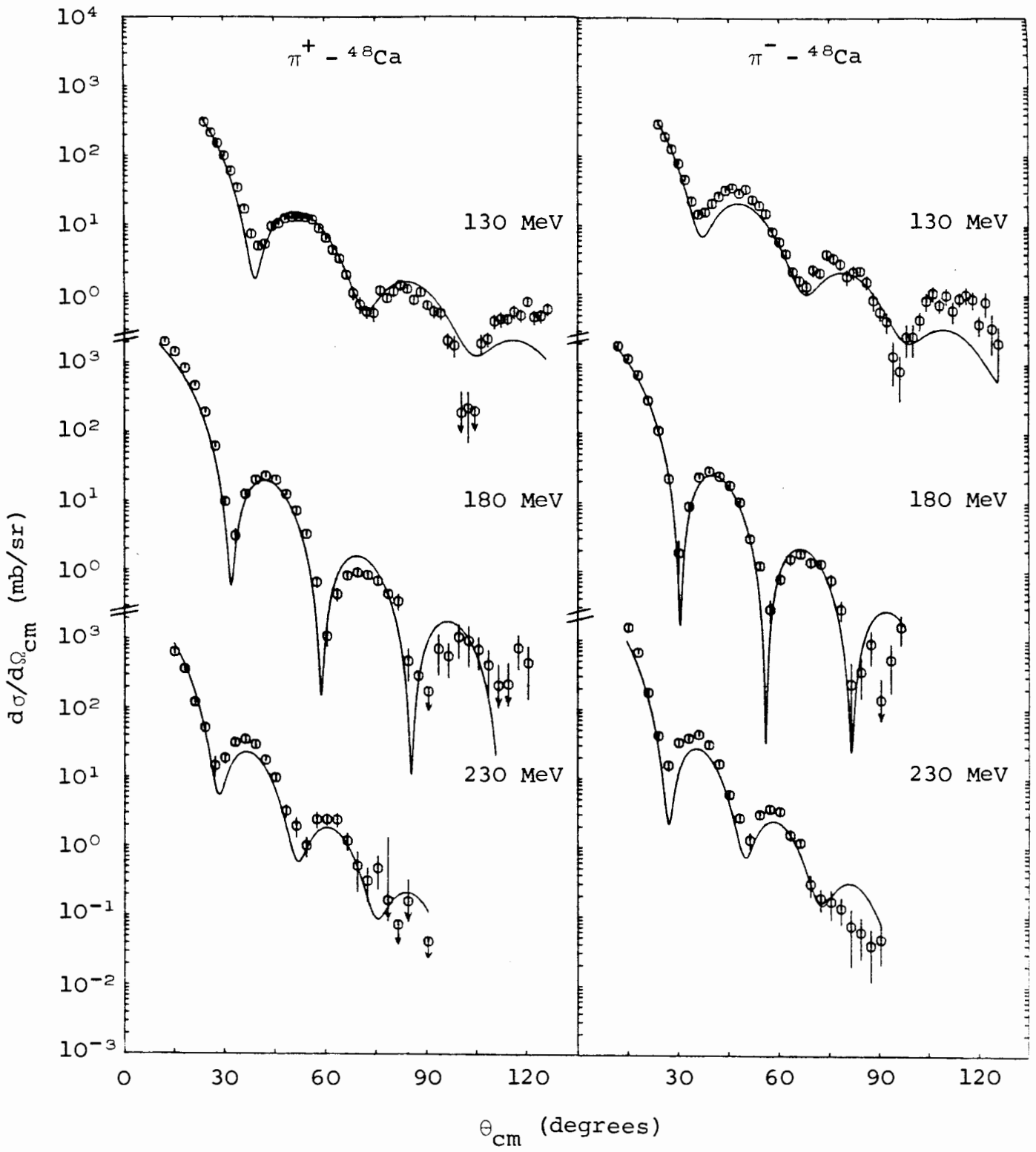

Figure (4.3-II) Eikonal resonance $\pi^{\pm} - {}^{48}Ca$ elastic scattering differential cross-sections at T_π = 130, 180 and 230 MeV. The data are from reference[16]. The six cross-sections are fitted with the single set of parameter values R′ = 4.40 fm, $\tilde{a}$ = 0.75 fm, v = 0.25, w = 0.60, m_0' = 1202 MeV.

Table (4.3-I)

Energy-dependent parameters $\tilde{b}_o$ and α of the eikonal resonance model.

T_π(lab)	system	$\tilde{b}_o$(fm)	α
130	$\pi^+ - {}^{40}Ca$	3.97	0.33
	$\pi^- - {}^{40}Ca$	4.26	0.33
	$\pi^+ - {}^{48}Ca$	4.25	0.30
	$\pi^- - {}^{48}Ca$	4.54	0.35
180	$\pi^+ - {}^{40}Ca$	3.92	-0.03
	$\pi^- - {}^{40}Ca$	4.14	-0.03
	$\pi^+ - {}^{48}Ca$	4.20	-0.01
	$\pi^- - {}^{48}Ca$	4.42	-0.05
230	$\pi^+ - {}^{40}Ca$	3.65	-0.24
	$\pi^- - {}^{40}Ca$	3.83	-0.24
	$\pi^+ - {}^{48}Ca$	3.96	-0.21
	$\pi^- - {}^{48}Ca$	4.11	-0.27

critical impact parameter $\tilde{b}_o$:

The resonant ln term contribution to the value of $\tilde{b}_o$ for ^{40}Ca is independent of the charge of the pion. Superimposed plots of $\tilde{b}_o$ for π^+ and π^- as a function of energy thus reflect its charge dependent contribution, $-\frac{n}{k}$, and are given in Figure (4.3-III). As expected, due to the repulsive Coulomb interaction, $\tilde{b}_o(\pi^+)$ is found to be smaller than the corresponding $\tilde{b}_o(\pi^-)$ at each energy, as is also shown in Table (4.3-I). This can be illustrated semi-classically by the following trajectory diagram

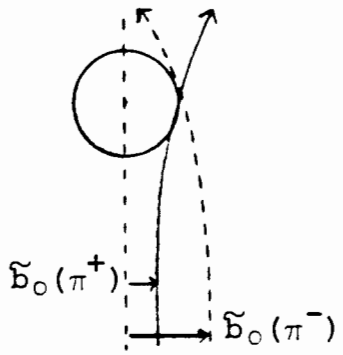

Inspection of Figure (4.3-III) shows that the effect of the $-\frac{n}{k}$ term diminishes as the energy increases: the difference $\Delta\tilde{b}_o = \tilde{b}_o(\pi^-) - \tilde{b}_o(\pi^+)$ gets less as the incident pion kinetic energy increases.

Superimposed plots of $\tilde{b}_o$ versus energy for π^+ and π^- scattering off ^{48}Ca are also affected in principle by isospin. The isospin effect on $\tilde{b}_o$ is small, however, and not really discernible on the plot.

Figure (4.4-IV) shows the variation of the resonant ln term

with energy across the resonance. This illustrates the point made previously: it becomes increasingly negative as one moves away from $E = E'_0 = 150$ MeV, to compensate for reduced absorption (which peaks at the resonance, as pointed out in section 3.3).

Figure (4.4-V) displays the effect which varying our fitted parameters has on the shape of the critical impact parameter $\tilde{b}_0$, plotted as a function of the pion kinetic energy. From (a) we see that inclusion of the energy shift Δ in our formalism causes the peak in $\tilde{b}_0$ to be shifted down from the free space resonance energy E_0 to the displaced resonance energy E'_0. The effect of increasing w, as illustrated in (b), is to broaden the peak in $\tilde{b}_0$ (particularly raising the 'tails'). For zero background imaginary potential the peaked shape of $\tilde{b}_0$ is at its most narrow, whereas for equal background and resonant imaginary potentials, its shape is flattened and broader. Increasing the value of the strong-absorption radius R' results in shifting the entire $\tilde{b}_0$ curve vertically, as seen in (c).

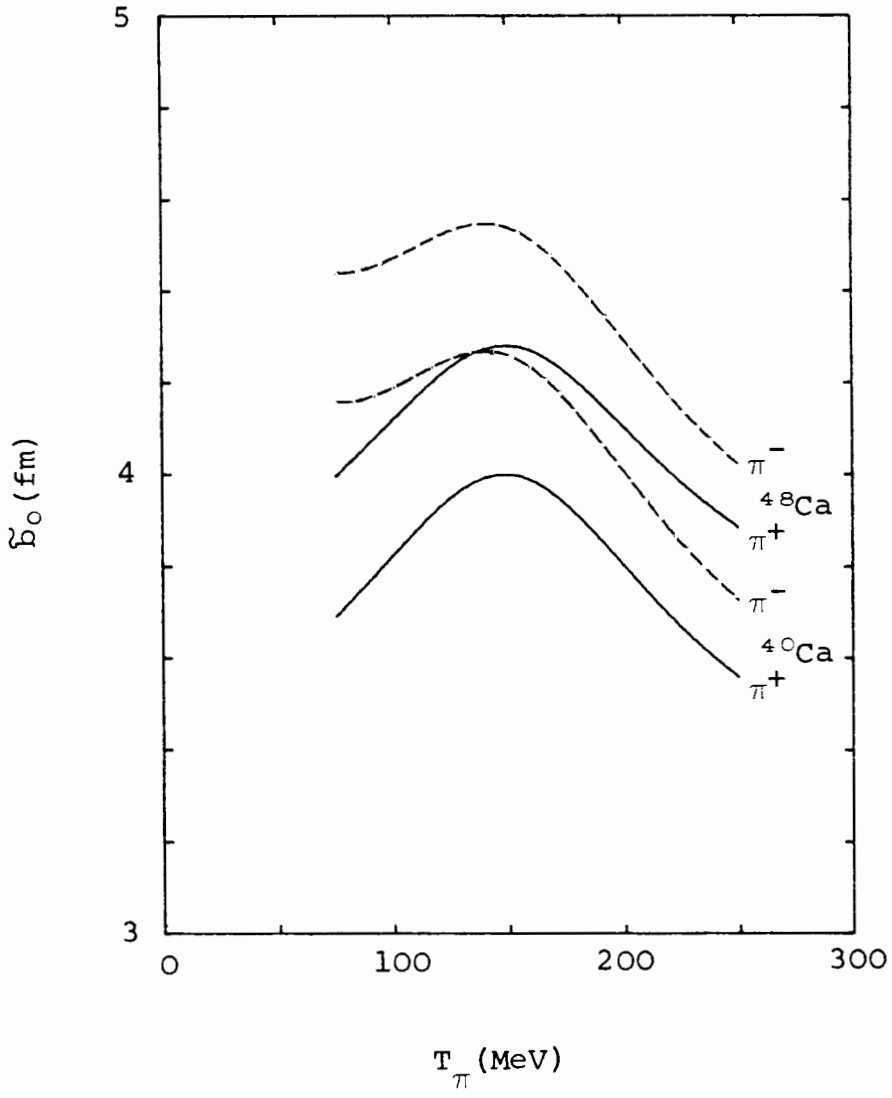

Figure (4.3-III) Critical impact parameter $\tilde{b}_o$ as a function of the pion kinetic energy.

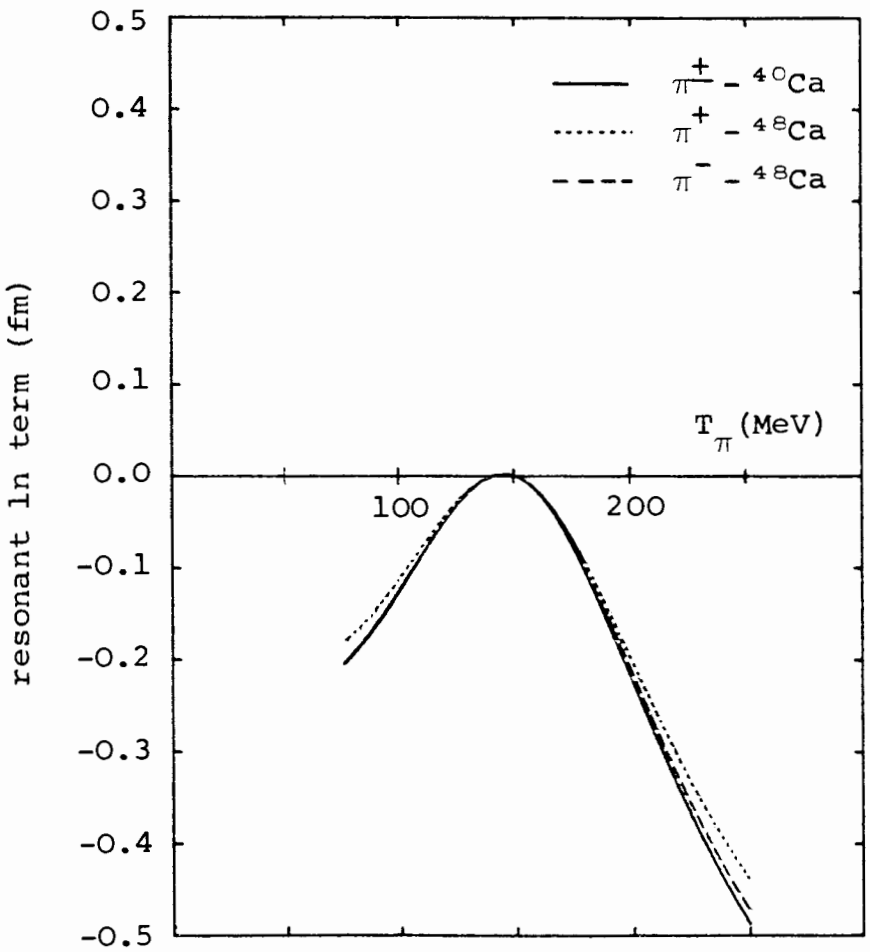

Figure (4.3 - IV) showing the variation of the resonant ln term with energy across the resonance.

Figure (4.3 - V)

Critical impact parameter for π^- - ^{40}Ca scattering as a function of the pion kinetic energy, illustrating the effect of (a) varying the energy shift Δ in E'_0, (b) varying w, the relative background imaginary potential, from its fitted value 0.6, and (c) varying the value of the strong-absorption radius R'.

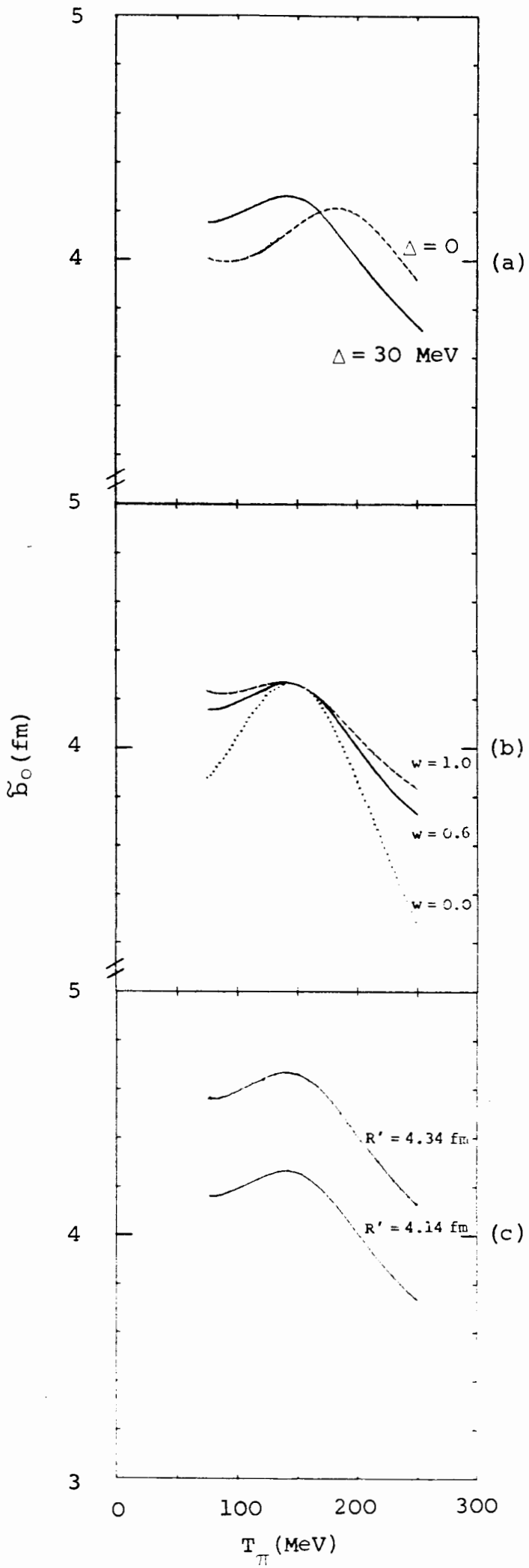

the nuclear phase shift parameter α:

This is seen to vanish for $\frac{V(E)}{W(E)} = 0$, that is, for

$$(E-E_o')^2 - \frac{\gamma}{v}\left(\frac{\Gamma}{2}\right)(E-E_o') + \frac{\Gamma^2}{4} = 0 \qquad (4.3.7)$$

with two solutions

$$E_1 = E_o' + \left(\frac{\Gamma}{2}\right)\left(\frac{\gamma}{2v}\right)\left[1 - \left(1 - \left(\frac{2v}{\gamma}\right)^2\right)^{\frac{1}{2}}\right] \qquad (4.3.8)$$

and

$$E_2 = E_o' + \left(\frac{\Gamma}{2}\right)\left(\frac{\gamma}{2v}\right)\left[1 + \left(1 - \left(\frac{2v}{\gamma}\right)^2\right)^{\frac{1}{2}}\right] \quad . \qquad (4.3.9)$$

For $v \ll \frac{\gamma}{2}$ these can be simplified to read

$$E_1 \approx E_o' + \left(\frac{\Gamma}{2}\right)\left(\frac{v}{\gamma}\right) \qquad (4.3.10)$$

$$E_2 \approx E_o' + \left(\frac{\Gamma}{2}\right)\left(\frac{\gamma}{v}\right) \quad . \qquad (4.3.11)$$

The quantity $\frac{V(E)}{W(E)}$ and hence α is positive for energies $E < E_1$, vanishes at E_1, and then becomes negative for $E_1 < E < E_2$; regaining positive values for energies $E > E_2$. In our case, for $\pi^{\pm}$ - ^{40}Ca scattering, E_1 is calculated to be 168 MeV. Plotting α versus the pion kinetic energy, as is done in Figure (4.3-VI) for ^{40}Ca, highlights its change in sign at E_1. As expected, α is affected by isospin. It has already been pointed out that the isospin effect on $\tilde{b}_o$ is small and hardly

noticeable; the main influence of isospin is on the refractive parameter α, as shown in Table (4.3-I), where one may compare the values of α for ^{48}Ca and ^{40}Ca.

The behaviour of α as a function of energy depends on the values of the fitted parameters w and v. We illustrate the systematics of these dependences: The presence of the background imaginary term w in the potential is seen, in Figure (4.3-VII)(a), to slow the departure of the function α from zero as energy increases from E_1; in particular, increasing w decreases the magnitude of the slope of α at E_1. From Figure (4.3-VII)(b) we observe that an increase in v causes the zero E_1 of α to move further above E_o'; for v=0, E_o' and E_1 coincide. Thus we expect the deepest minima of the diffraction patterns to occur, not at an energy E_o' but at an energy E_1, which happens to be closer to the free space resonance energy E_o when $E_o' < E_c$, as in our fits. Of course, when v is sufficiently large, namely $v \geq \frac{\gamma}{2}$, then α has no zeros and is always positive, as one sees for the example v=1 on Figure (4.3-VII)(b).

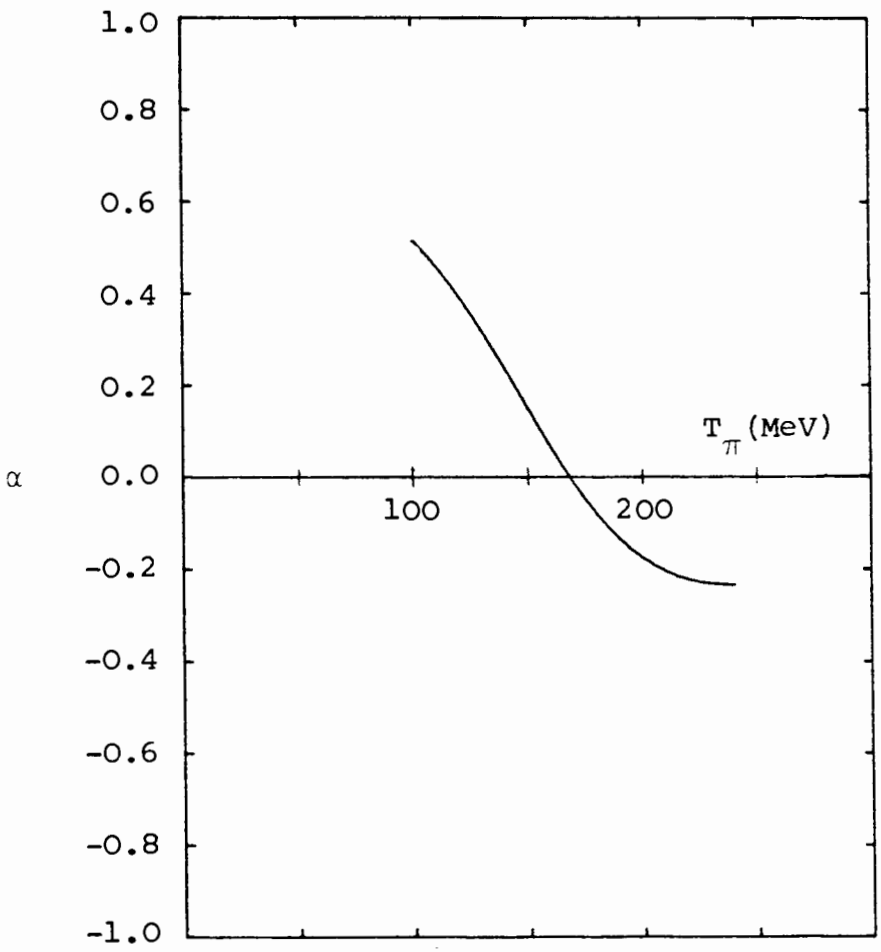

Figure (4.3 - VI) Real nuclear phase parameter α for $\pi - {}^{40}Ca$ as a function of pion kinetic energy; w = 0.6, v = 0.25.

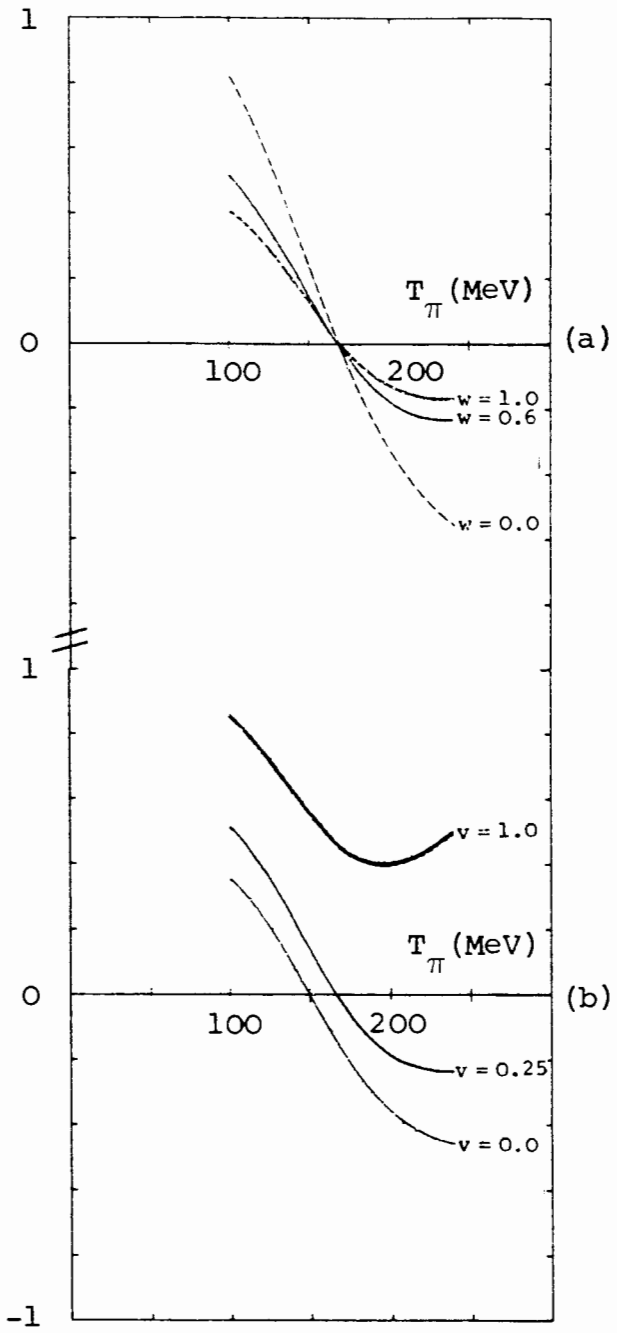

Figure (4.3 - VII)

Real nuclear phase shift parameter α for $\pi^{\pm}$ - ^{40}Ca scattering as a function of pion kinetic energy, illustrating the effect of varying (a) w and (b) v, the relative background imaginary and real potentials, from their fitted values of 0.6 and 0.25 respectively.

4.4 The total cross-section

Using our derived expression for the total cross-section for neutral particle scattering (3.4.14) with the critical impact parameter

$$\tilde{b}_o = R' + \tilde{a}\ln\left[\frac{v_o'}{v}\,\frac{1}{\gamma+w}\,\frac{(\gamma+w)(m_o'\Gamma)^2 + w(s-m_o'^2)^2}{(s-m_o'^2)^2 + (m_o'\Gamma)^2}\right] \qquad (4.4.1)$$

in which the isospin term γ is set equal to unity for π^o scattering, we have evaluated the total cross-section over an energy range from 100 MeV - 250 MeV, pion lab kinetic energy, which covers the resonance, for the $\pi^o - {}^{40,48}Ca$ scattering systems.

The results are presented in Figure (4.4-I). There are no available data to allow for a comparison to experiment; however, the general features of these predicted curves are consistent with other π-nucleus experimental total cross-section data[17,18].

The total cross-section is seen to display resonance characteristics and properties. The theoretical σ_T is peaked at $T_\pi = E_o' = 150$ MeV and falls off on either side of this energy. The peak is a direct consequence of the resonance. Compared with the πN total cross-section the π-nucleus σ_T possesses a distorted resonance shape and is 'flattened'.

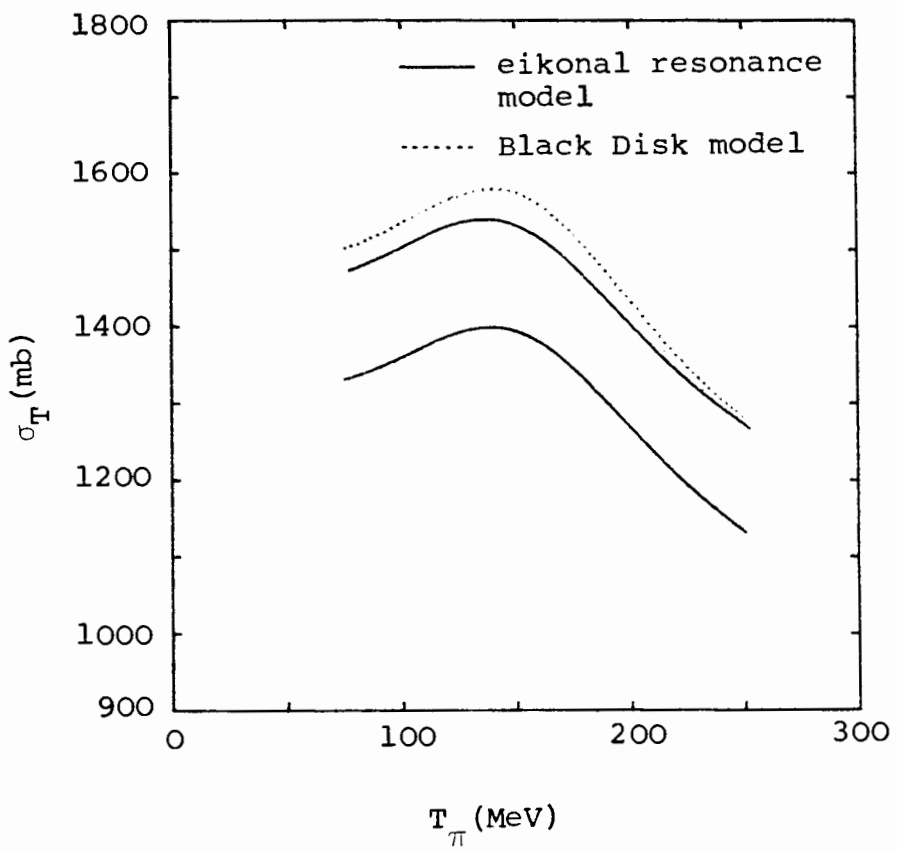

Figure (4.4 - I) Total cross-section eikonal resonance calculations for π^0 - ^{40,48}Ca. The Black Disk prediction for ^{48}Ca is superimposed for comparison.

Both π^o - ^{40,48}Ca curves show that the total cross-section peaks at 150 MeV, $\sim$ 30 MeV below the corresponding πN(3,3) resonance peak. In the framework of our formalism we do not provide a microscopic explanation of this downward shift in the position of the resonance for pion scattering by nuclei, but simply incorporate it into our theory as a phenomenological shift of the resonance energy of the πN system in a nuclear environment. This shift is believed to be due largely to multiple scattering effects[11].

Plotting Re($\overset{o}{f}$(o)), the real part of the π^o forward scattering amplitude, given by (3.4.12) against the π lab kinetic energy, Figure (4.4-II), we observe a shift in its zero. While Re(f_{π^oN}(o)) = 0 for T_π = 195 MeV[11] we find for π^o - ^{40}Ca scattering that Re($\overset{o}{f}$(o)) = 0 at an incident π kinetic energy of T_π = 168 MeV. This is not unexpected as we see from (3.4.12) that Re($\overset{o}{f}$(o)) is proportional to α and hence vanishes when α vanishes, i.e. at T_π = 168 MeV. This is a consequence of introducing the phenomenological energy shift into the formalism.

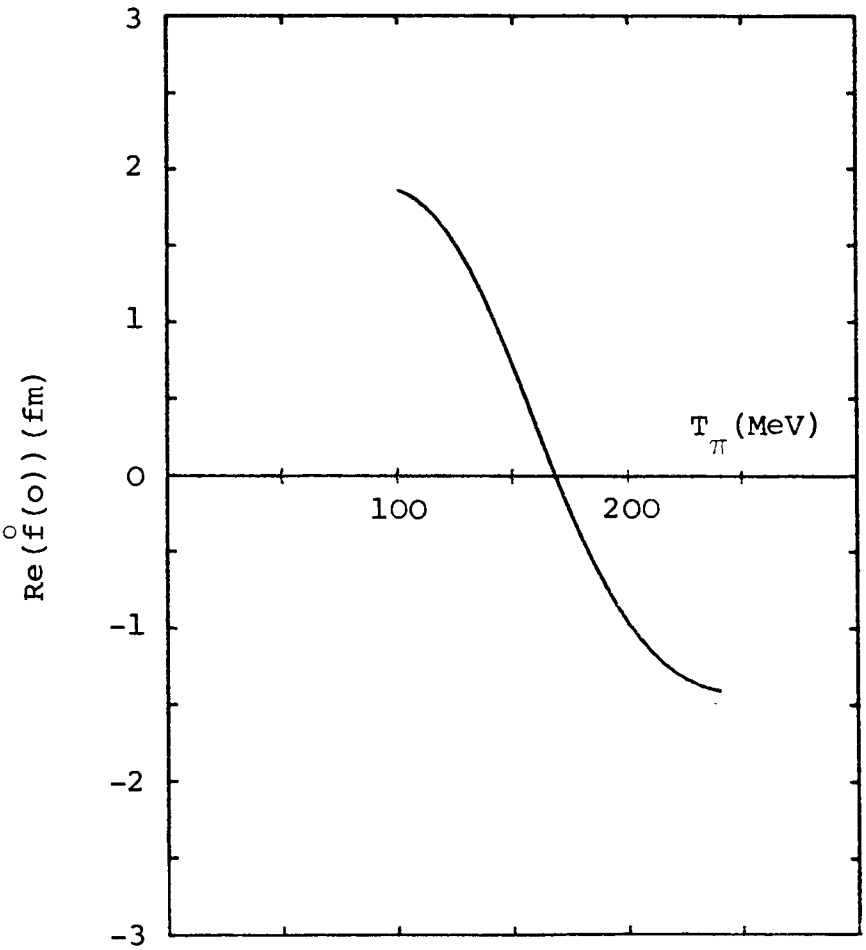

Figure (4.4 - II) Plot of the real part of the forward scattering amplitude for elastic scattering of neutral pions from $^{4\circ}Ca$ as a function of pion laboratory kinetic energy.

The total cross-section as measured in the Black Disk model:

The strong-absorptive nature of the scattering in the resonance region, due to the very strong πN interaction, yields an almost 'optically black' nucleus for π's.

For a constant nuclear density $R \propto A^{1/3}$ and hence, in the geometrical 'black disk' limit, $\sigma_T \propto A^{2/3}$. We observe a dependance of this Black Disk total cross-section on the number of nucleons. In addition, for a perfectly black nucleus, σ_T will be independent of energy.

The total cross-sections for π^0-^{48}Ca and π^0-^{40}Ca in the Black Disk model are related by the simple rule[11]

$$(\sigma_T)_{\pi^{48}Ca} = \left(\frac{R_{48}}{R_{40}}\right)^2 (\sigma_T)_{\pi^{40}Ca}$$

$$= \left(\frac{48}{40}\right)^{2/3} (\sigma_T)_{\pi^{40}Ca} \quad .$$

Taking the eikonal model predictions for the σ_T of ^{40}Ca, we apply the Black Disk relation given above to calculate the corresponding ^{48}Ca σ_T. We obtain the result shown by the dotted curve in Figure (4.4-I).

Comparing the predicted total cross-sections for π^0 - ^{48}Ca using the Black Disk scaling rule with our calculated values applying the eikonal formalism: the two predictions compare well with one another; the Black Disk prediction is slightly

larger than the eikonal results; which gives an idea of the deficiency of the Black Disk model. The fact that Black Disk scaling gives a slightly larger total cross-section than our eikonal prediction suggests that the disk is not totally black.

5. DISCUSSION

5.1 Comparative study of π^+ and π^- elastic scattering from the isotopes ^{40,48}Ca in the resonance region

In this energy regime elastic scattering of a π^- from a neutron is very much stronger than that from a proton (and vice versa for π^+). Thus we would expect $\pi^+\pi^-$ differences in ^{48}Ca, which has eight more neutrons than it has protons. In addition, Coulomb distortion should give rise to differences between the scattering of π^+ and π^- even on an isoscalar nucleus such as ^{40}Ca. However, we would expect the ^{48}Ca cross-section to differ more from the ^{40}Ca cross-section for π^- scattering than for π^+ scattering. Noting these points, we study the π-nucleus scattering data for evidence in support of these effects.

At an energy close to E_1 (i.e. at T_π = 180 MeV) the pion-nucleus interaction is very strong and absorptive, which produces the characteristic oscillatory diffraction pattern in the angular distributions. At energies further from the value of E_1 (i.e. at T_π = 130 , 230 MeV) the measured angular distributions are observed to be much smoother.

Further, the diffractive minima for π^- scattering are deeper above resonance than below it. On the contrary for π^+ scattering, the minima are deeper below resonance than above. At T_π = 180 MeV the minima of the diffraction oscillations are still deeper, the peak-to-valley ratios for π^+ and π^- scattering from each of the targets being relatively constant. This feature of the angular distributions can be explained in terms of the differences in the relative phase of the Coulomb and nuclear amplitudes at these energies. The subject of Coulomb-nuclear interference will be dealt with in detail in the next section.

Large $\pi^+\pi^-$ cross-section differences are observed for ^{48}Ca at the minima of the angular distributions, in particular, at incident pion kinetic energies T_π = 130 , 230 MeV; however the corresponding $\pi^+\pi^-$ differences in ^{40}Ca are less pronounced.

The differences noted between the cross-sections for the elastic scattering of positive and negative pions by the isoscalar nucleus ^{40}Ca can be explained in terms of the

distortion by a static Coulomb potential. The remaining discrepancies between the π^+ and π^- scattering off ^{48}Ca are thus presumably due to the neutron excess.

Close inspection of the 130 MeV data, presented in Figure (5.1-I), reveals that the ^{48}Ca $\pi^+\pi^-$ cross-sections near the minima of the angular distributions differ up to a factor of 4; this is in contrast to the ^{40}Ca data where the effect is less pronounced. In addition, the π^- minima are observed to be systematically at slightly smaller angles than those of π^+, due to the Coulomb shift between π^+ and π^-. In the ^{48}Ca data the position of the first minimum is shifted by 4° towards smaller angles for π^-; the shift is 5° for the position of the second minimum. A smaller shift of the minima are observed in the ^{40}Ca angular distributions (2° for the first minimum and $\sim 2^\circ$ for the second minimum)[24].

Similar comments to these can be made about the behaviour of the angular distributions measured at 230 MeV.

We introduce the relative difference function

$$PI(q) = \left(\frac{\sigma_{\pi^-}(q) - \sigma_{\pi^+}(q)}{\sigma_{\pi^-}(q) + \sigma_{\pi^+}(q)} \right) \qquad (5.1.1)$$

which magnifies the effects of the Coulomb distortion - evaluated for both isotopes $^{40,48}Ca$.

Calculations for PI(q) for both calcium isotopes at the three

incident pion kinetic energies are presented in Figure (5.1-II). This theoretical difference function was evaluated in the eikonal approximation, the parameters of the eikonal parametric model as given in section 4.3, Table (4.3-I). The plots using PI(q) have the advantage of smearing out many of the uncertainties in the reaction mechanism while it enhances the effects of isotope differences and Coulomb-nuclear interference. They display very clearly the differences in the diffraction pattern of π^+ and π^- scattering. The variations in PI(q) are observed to be very much larger in amplitude in the region of the diffraction minima, as expected, and the corresponding shift $\delta\theta = (\theta_{\pi^+}^{min} - \theta_{\pi^-}^{min})$ in the case of ^{48}Ca is increased, which is related to the presence of the eight extra neutrons.

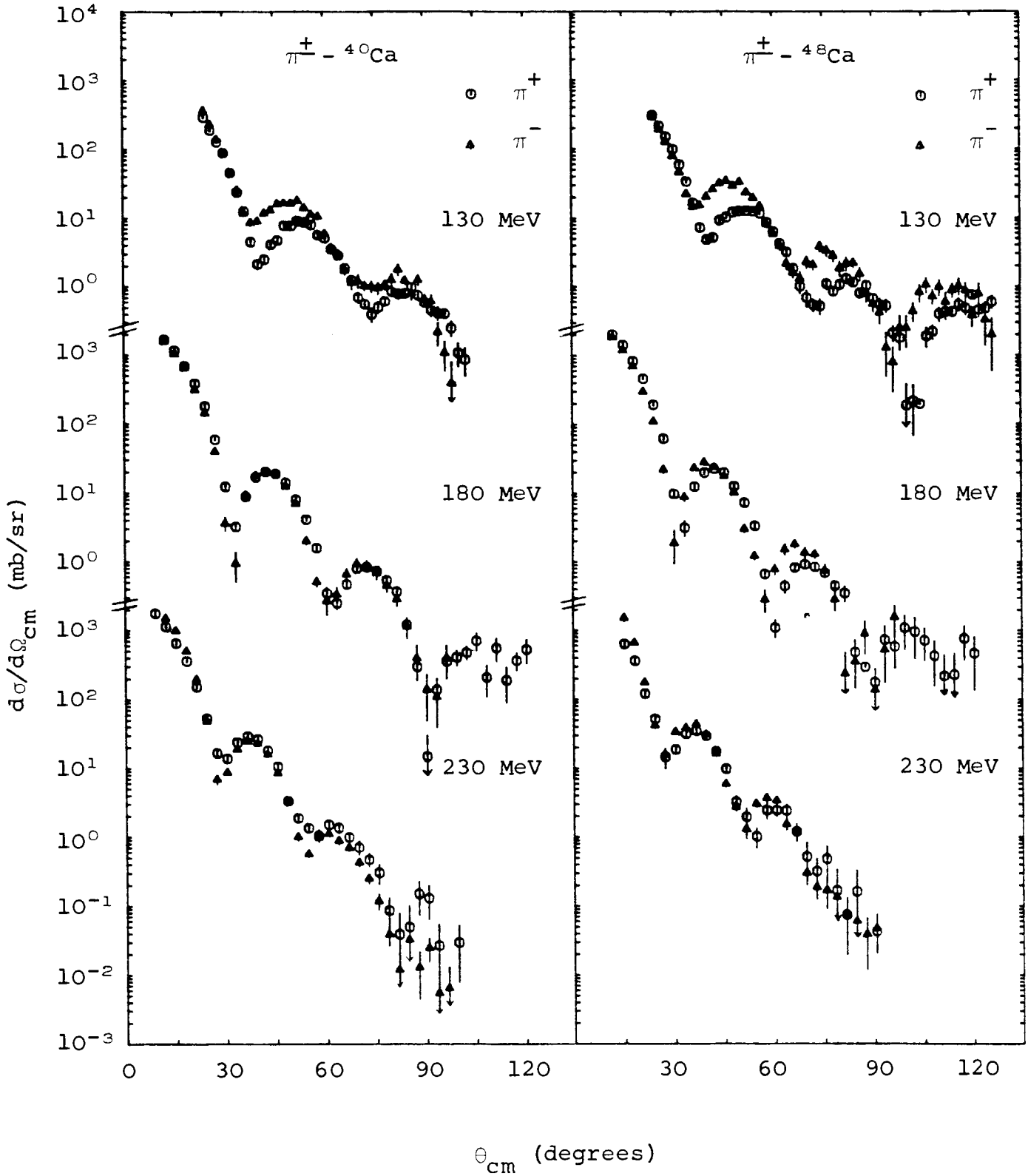

Figure (5.1 - I) $\pi^+\pi^-$ scattering, plotted for ^{40}Ca and ^{48}Ca at T_π = 130, 180 and 230 MeV [16].

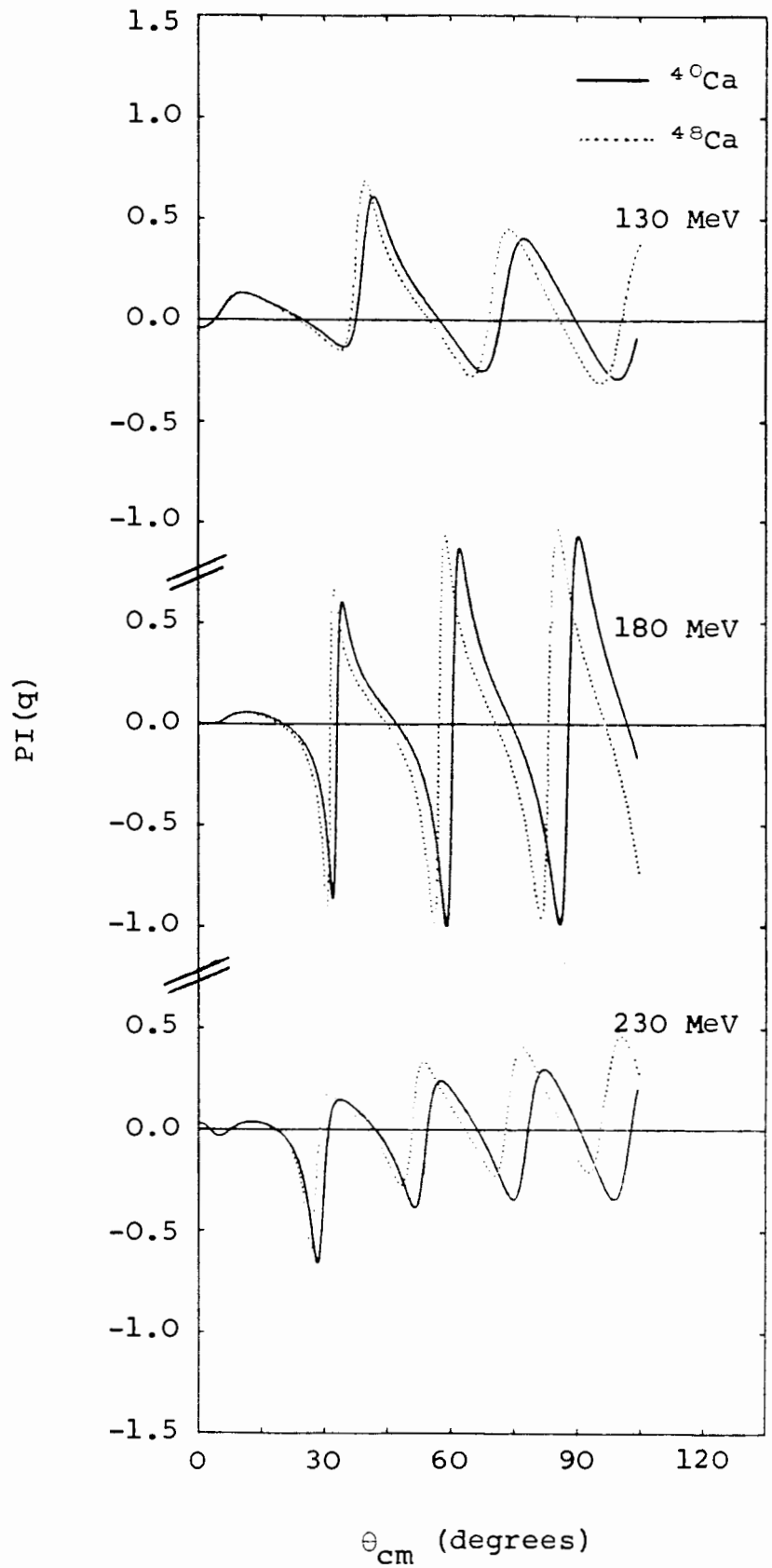

Figure (5.1 - II) Relative π^-/π^+ differential cross-sections for pion scattering from ^{40}Ca and ^{48}Ca.

Having studied separately the elastic scattering of charged pions by ^{40}Ca and ^{48}Ca, we now compare the differential cross-sections for both isotopes either for π^+ or π^-.

The marked feature of the data, presented in Figure (5.1-III), is that the variations of the isotopic shift are larger for π^- than for π^+ scattering. Compared with the π^- ^{40}Ca data, the π^- ^{48}Ca differential cross-section is characterised by a much steeper forward peak, a large shift in the position of the first minimum towards smaller angles ($\sim 2^\circ$ in the T_π = 180 MeV data) and an overall more diffractive structure. On the other hand, the π^+ ^{48}Ca angular distribution is very similar to the π^+ ^{40}Ca one but for a slightly steeper forward slope and a small shift towards smaller angles ($\sim \frac{1}{2}^\circ$ at the first minimum).

This observation is a clear indication of the sensitivity of the angular distributions to the neutron excess in the ^{48}Ca nucleus.

We study the isotopic shift for differential cross-sections using the quantity

$$CA(q) = \left(\frac{\sigma_{48}(q) - \sigma_{40}(q)}{\sigma_{48}(q) + \sigma_{40}(q)} \right) \qquad (5.1.2)$$

which magnifies the effect of the neutron excess in ^{48}Ca - evaluated for both π^+ and π^-.

Calculations for the isotopic shift of the angular distributions are given in Figure (5.1-IV). A study of the behaviour of CA(q) reveals the effect of adding eight extra neutrons to the ^{40}Ca nucleus.

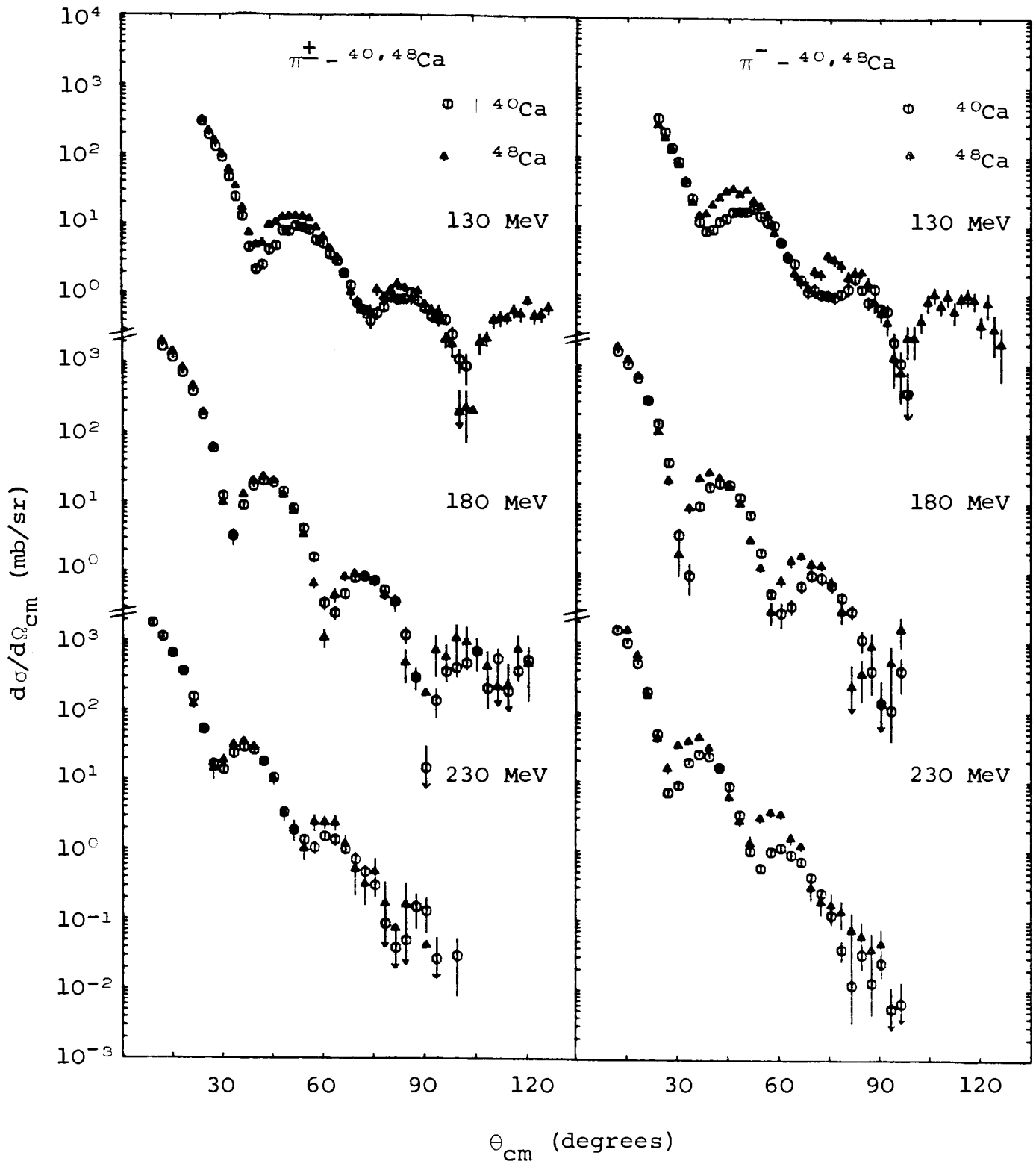

Figure (5.1 - III) ^{40,48}Ca scattering, plotted for π^{+} and π^{-}, at T_{π} = 130, 180 and 230 MeV [16].

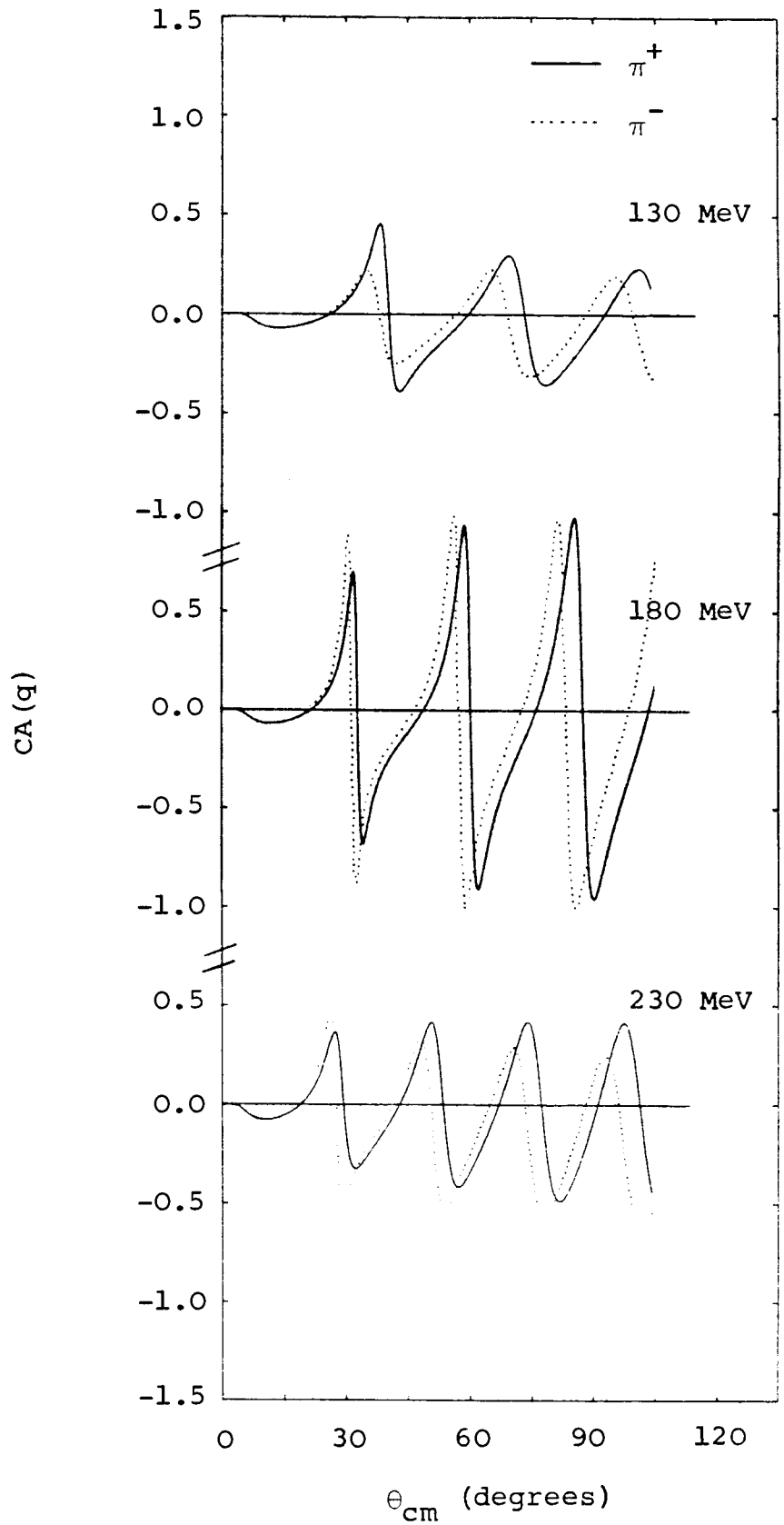

Figure (5.1 - IV) The isotopic shift, evaluated for both π^+ and π^- scattering.

5.2 The Coulomb-nuclear interference phenomenon

In this section we investigate the Coulomb-nuclear interference effects.

Much effort has been put into attempting to formulate the scattering problem in such a manner as to provide insight into the observed Coulomb-nuclear interference phenomenon. Since the Coulomb and nuclear interactions possess very different physical properties they should obviously be treated separately in the formalism.

We have expressed our scattering function in factored form, containing separate nuclear and Coulomb terms. The effect of the nuclear interaction on the scattering amplitude has been shown to enter through the Fourier transform of the derivative of the nuclear part of the scattering function, while that of the relatively weak Coulomb interaction via the Rutherford point-charge phase shifts.

We write our expression for the eikonal elastic scattering amplitude (2.2.18) in terms of contributions to the far- and near-side branches of the scattering amplitude. Using the asymptotic forms of our functions our expression for the scattering amplitude is obtained in which the competitive effects of nuclear refraction and residual Coulomb deflection can clearly be seen.

Returning to our evaluation of the eikonal elastic scattering amplitude, dealt with in section 2:

Substitution of the quantities given by (2.2.17) into (2.2.18) yields this expression for the eikonal elastic amplitude

$$f(q) = \frac{ik}{2q}\left\{\left(\tilde{F}_N[a(q_o+q)]\left[J_1(b_oq) + iJ_2(b_oq)\right]\right.\right.$$
$$+ \left.\tilde{F}_N[a(q_o-q)]\left[J_1(b_oq) - iJ_2(b_oq)\right]\right)$$
$$+ \frac{i2nb_o}{q}\left(\tilde{F}_N[a(q_o+q)]\left[J_o(b_oq) + iJ_1(b_oq)\right]\right.$$
$$\left.\left. + \tilde{F}_N[a(q_o-q)]\left[J_o(b_oq) - iJ_1(b_oq)\right]\right)\right\} . \qquad (5.2.1)$$

Replacing the Bessel functions in the above with their asymptotic forms yields the asymptotic expression

$$f(q) = \left(\frac{k^2b_o}{2\pi q^3}\right)^{\frac{1}{2}} e^{i2\sigma_p(b_o)}\left\{e^{i(b_oq-\frac{\pi}{4})}\left(\tilde{F}_N[a(q_o+q)] - \left(\frac{q_o}{q}\right)F_N[a(q_o+q)]\right)\right.$$
$$\left. - e^{-i(b_oq-\frac{\pi}{4})}\left(\tilde{F}_N[a(q_o-q)] + \left(\frac{q_o}{q}\right)F_N[a(q_o-q)]\right)\right\} \qquad (5.2.2)$$

which we can approximate, for asymptotic q and small Coulomb interaction, by

$$f(q) = \left(\frac{k^2b_o}{2\pi q^3}\right)^{\frac{1}{2}} e^{i2\sigma_p(b_o)}\left\{e^{i(b_oq-\frac{\pi}{4})}\,\tilde{F}_N[a(q_o+q)] - e^{-i(b_oq-\frac{\pi}{4})}\,\tilde{F}_N[a(q_o-q)]\right\} \qquad (5.2.3)$$

Setting

$$\phi_{\pm}(b_o,q) = \left(\frac{\pi}{4} - b_o q \pm 2\sigma_p(b_o)\right) \tag{5.2.4}$$

in the above we arrive at

$$f(q) = \left(\frac{k^2 b_o}{2\pi q^3}\right)^{\frac{1}{2}} \left\{ e^{-i\phi_-(b_o,q)} \tilde{F}_N[a(q_o+q)] - e^{i\phi_+(b_o,q)} \tilde{F}_N[a(q_o-q)] \right\} \tag{5.2.5}$$

In the eikonal approximation, scattering by a nuclear potential in the presence of strong-absorption can be expressed in terms of the Fraunhofer diffraction scattering amplitude.

Pure Fraunhofer scattering is realised in the neutral limit (limit $n \to o$)[25], the angular distributions corresponding to scattering by a perfectly absorbing sharp-edged sphere.

For pure Fraunhofer scattering in the sharp cut-off absorption model the amplitude can be expressed as a sum of the contributions from the far- and near-side branches of the Fraunhofer scattering amplitude[4]

$$f_{FRA}(q) = \left(\frac{k^2 b_o}{2\pi q^3}\right)^{\frac{1}{2}} e^{i2\sigma_p(b_o)} \left\{ e^{i(b_o q - \frac{\pi}{4})} - e^{-i(b_o q - \frac{\pi}{4})} \right\} \tag{5.2.6}$$

$$= f^{(-)}_{FRA}(q) + f^{(+)}_{FRA}(q) \tag{5.2.7}$$

where

$$f^{(-)}_{FRA}(q) = \left(\frac{k^2 b_o}{2\pi q^3}\right)^{\frac{1}{2}} e^{-i\phi_-(b_o, q)} \tag{5.2.8}$$

is termed the contribution from the far-side and

$$f^{(+)}_{FRA}(q) = -\left(\frac{k^2 b_o}{2\pi q^3}\right)^{\frac{1}{2}} e^{i\phi_+(b_o, q)} \tag{5.2.9}$$

represents the near-side branch.

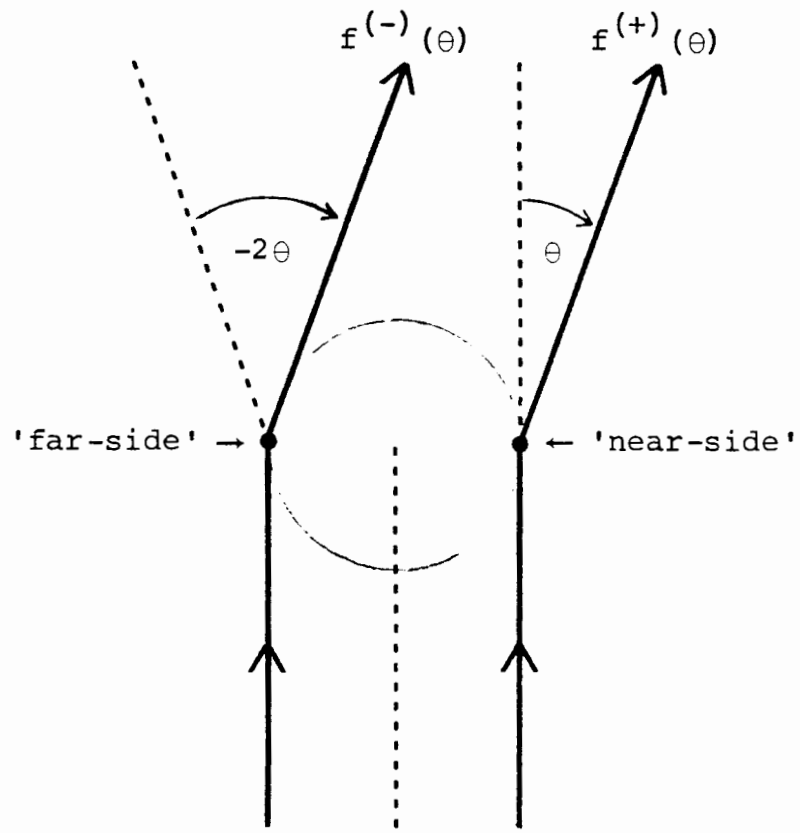

Figure (5.2 - I) 'Near-side' and 'far-side' scattering to forward angles.

On comparison with (5.2.8) and (5.2.9) our asymptotic expression for the eikonal elastic amplitude given by (5.2.5) can be rewritten as

$$f(q) = f^{(-)}_{FRA}(q)\,\tilde{F}_N[a(q_o+q)] + f^{(+)}_{FRA}(q)\,\tilde{F}_N[a(q_o-q)] \quad . \qquad (5.2.10)$$

The above expression illustrates how the two branches of the Fraunhofer scattering amplitude are modified - for smooth cut-off absorption (surface diffuseness) in the presence of the (weak) Coulomb interaction (represented by the quantity q_o) - in different ways by the modulation functions $\tilde{F}_N[a(q_o+q)]$ and $\tilde{F}_N[a(q_o-q)]$.

For $q_o > 0$ we observe that the Fraunhofer oscillations are damped by the function

$$D = \frac{\tilde{F}_N[a(q_o+q)]}{\tilde{F}_N[a(q_o-q)]} \quad . \qquad (5.2.11)$$

Adopting the Ericson parametric model in which the modulation functions are related to the Fourier transforms by

$$\tilde{F}_N(z) = \varepsilon F_N(z) \qquad (5.2.12)$$

with

$$F_N(z) = \frac{\pi z}{\sinh \pi z}\, e^{\alpha z} \qquad (5.2.13)$$

and

$$\varepsilon = \left(1 - i\left(\frac{2a}{b_o}\right)\alpha - \left(\frac{a}{b_o}\right)^2\left[\alpha^2 - \frac{\pi^2}{3}\right]\right) \qquad (5.2.14)$$

we obtain, asymptotically, the result

$$\tilde{F}_N[a(q_o \pm q)] = 2\pi a\varepsilon (q \pm q_o)\, e^{-\pi a(q \pm q_o)}\, e^{\pm \alpha a(q \pm q_o)} \,. \qquad (5.2.15)$$

We note here in passing that in the neutral limit the above expression further simplifies to

$$\tilde{F}_N[a(q_o \pm q)] \xrightarrow{n \to o} 2\pi aq\varepsilon\, e^{-\pi aq}\, e^{\pm \alpha aq} \,. \qquad (5.2.16)$$

Expression (5.2.10) in the Ericson model then reads as

$$f(q) = -(2\pi a\varepsilon)\left(\frac{k^2 b_o}{2\pi q}\right)^{\frac{1}{2}} e^{i2\sigma_p(b_o)}\, e^{\alpha a(q+q_o)}\, e^{-\pi a(q-q_o)}\, e^{i\frac{\pi}{4}}$$

$$\left\{ie^{ib_o q}\, e^{-2\pi aq_o} + e^{-ib_o q}\, e^{-2\alpha aq}\right\} \qquad (5.2.17)$$

and the asymptotic differential cross-section as

$$\sigma(q) = \left(\frac{2\pi a^2 b_o k^2}{q}\right) |\varepsilon|^2 e^{2\alpha a(q+q_o)}\, e^{-2\pi a(q-q_o)}$$

$$\left| ie^{ib_o q}\, e^{-2\pi aq_o} + e^{-ib_o q}\, e^{-2\alpha aq} \right|^2 \,. \qquad (5.2.18)$$

The differential cross-section is now expressed in a form in which the competitive effects of nuclear refraction and Coulomb deflection can clearly be seen. Through the exponential functions $e^{-2\pi aq_o}$ and $e^{-2\alpha aq}$ changes in the values of q_o and α will produce a relative enhancement of the

near- and far-side branches of the scattering amplitude. Further, $e^{-2\alpha aq}$ is dependant on q, hence the effectiveness of this term will change with angle.

Any net emphasis of one branch over the other tends to fill in the Fraunhofer minima - a feature we term damping: From inspection, we note that a repulsive Coulomb field (denoted by a positive q_o value) damps the far-side amplitude thus favouring the near-side branch; whereas an attractive nuclear field (denoted by a positive α) damps the near-side amplitude relative to the far-side branch. One can see that attraction generally favours the far-side branch, while repulsion favours the near-side. The Coulomb damping of one branch with respect to the other is fairly uniform over the angular range. On the other hand, the expected refractive damping of one branch relative to the other grows with angle - hence producing the observed effect of Fraunhofer minima being filled in at large angles.

We thus conclude:
If the nuclear and Coulomb interactions are acting together, that is, both attractive or both repulsive, then they both favour the same side and the observed diffraction pattern is damped relative to when the nuclear and Coulomb interactions are acting against one another; in which case they favour the opposite branches of the scattering amplitude causing enhanced interference between the far- and near-side branches, resulting in stronger oscillations with deeper minima.

In the neutral limit our asymptotic scattering amplitude in the Ericson model reduces to:

$$f(q) = \left(\frac{k^2 b_o}{2\pi q^3}\right)^{\frac{1}{2}} \left\{ e^{i\left(b_o q - \frac{\pi}{4}\right)} \tilde{F}_N(aq) - e^{-i\left(b_o q - \frac{\pi}{4}\right)} \tilde{F}_N(-aq) \right\}$$

$$\simeq -2\pi a\varepsilon \left(\frac{k^2 b_o}{2\pi q}\right)^{\frac{1}{2}} e^{\alpha aq} e^{-\pi aq} e^{\frac{i\pi}{4}} \left\{ ie^{ib_o q} + e^{-ib_o q} e^{-2\alpha aq} \right\} \tag{5.2.19}$$

and the corresponding neutral differential cross-section:

$$\sigma(q) \simeq \left(\frac{2\pi a^2 b_o k^2}{q}\right) e^{2\alpha aq} e^{-2\pi aq} |\varepsilon|^2 \left| ie^{ib_o q} + e^{-ib_o q} e^{-2\alpha aq} \right|^2 \tag{5.2.20}$$

which we can express in a form displaying the effect of the 'refractive damping' of the diffraction oscillations:

$$\sigma(q) \simeq \left(\frac{2\pi a^2 b_o k^2}{q}\right) e^{-2(\pi-\alpha)aq} |\varepsilon|^2 \left(1 + e^{-4\alpha aq} - e^{-2\alpha aq} \sin 2b_o q\right). \tag{5.2.21}$$

In terms of the above the following observed characteristics of our angular distributions, shown in Figure (5.2-II), can now be understood. From the deduced strength of α, the nuclear refraction parameter, it becomes clear, firstly, why the diffraction pattern observed at 180 MeV exhibits deeper minima than at the other two energies; and secondly, it offers an explanation as to why the minima of the diffraction oscillations for π^+ are deeper than for π^- scattering at 130 MeV, and vice versa at 230 MeV.

The small (negative) value for α at T_π = 180 MeV obtained from our fit, combined with the weak Coulomb interaction - denoted by $\pm q_o$ for $\pi^\pm$ scattering - will result in the far- and near-side branches being of similar strength. The two branches will beat against each other, producing the displayed strong oscillations. At large angles, damping of the diffraction pattern will be observed due to the relative enhancement of the near-side branch with increasing angle.

At an incident pion energy T_π = 130 MeV we note the following: For π^+ scattering the small repulsive Coulomb field favours the near-side, the attractive nuclear field the far-side; while for π^- scattering the attractive Coulomb and nuclear fields both favour the far-side branch of the scattering amplitude, which will be further enhanced with increasing angle. We would thus conclude that the π^+ scattering at 130 MeV displays deeper minima than the corresponding π^- scattering - a feature we do observe in the differential

cross-sections at this energy.

At T_π = 230 MeV our fit required a negative value for α, and we find that for π^+ scattering the near-side branch is favoured by both the repulsive Coulomb and nuclear fields, whereas for π^- scattering the far-side branch is favoured by the small attractive Coulomb field and the near-side by the repulsive nuclear field - the effectiveness of which will be enhanced with increasing angle. We would thus conclude that the π^- minima lie below those corresponding to π^+ scattering; however we would expect this feature to diminish with increasing angle - which we observe to be the case.

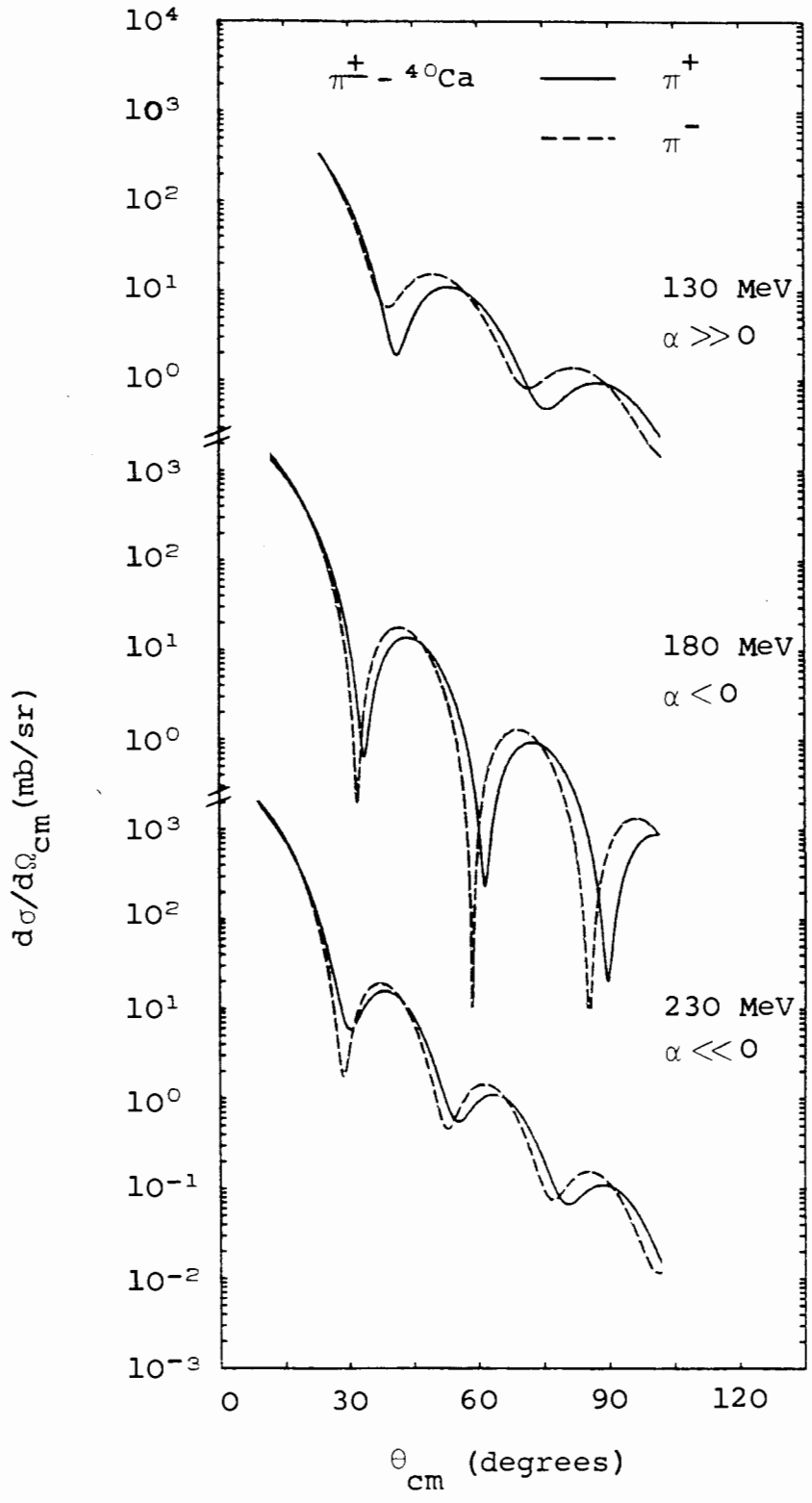

Figure (5.2 - II) $\pi^{\pm}$ - ^{40}Ca theoretically predicted differential cross-sections at T_π = 130, 180 and 230 MeV.

5.3 Discussion of the envelopes containing the diffraction oscillations and the Coulomb-nuclear damping of these oscillations

The angular distributions measured across the (3,3) resonance are seen to exhibit an interesting feature: below resonance the minima of the diffraction oscillations for π^+ are deeper than for π^- scattering, while at energies above resonance the opposite effect is observed - the minima of the π^- scattering cross-sections lie below those of π^+. This phenomenon has been observed in other examples of elastic π-nucleus scattering data measured across the (3,3) resonance .
We shall here relate it to the Coulomb-nuclear refractive damping of diffraction oscillations.

In this section we study the behaviour of the upper and lower envelopes of the π-nucleus cross-sections as functions of the pion charge and the sign of the nuclear interaction. We restrict our investigation to the N = Z target nucleus ^{40}Ca, which has no isospin dependence in its resonant optical potential.

The asymptotic elastic scattering cross-section:

$$\sigma(q) = |\varepsilon|^2\left(\frac{2\pi a^2 b_o k^2}{q}\right) e^{2\alpha a(q+q_o)}\, e^{-2\pi a(q-q_o)} \left| ie^{ib_o q}\, e^{-2\pi a q_o} + e^{-ib_o q}\, e^{-2\alpha a q}\right|^2 \qquad (5.3.1)$$

given in (5.2.18) is rewritten in the form:

$$\sigma(q) = |\varepsilon|^2\left(\frac{2\pi a^2 b_o k^2}{q}\right) e^{-2\pi aq}\left\{e^{-2\alpha aq}\, e^{2\alpha aq_o}\, e^{2\pi aq_o}\right.$$

$$+ e^{-2\pi aq_o}\, e^{2\alpha aq}\, e^{2\alpha aq_o}$$

$$\left. - 2e^{2\alpha aq_o} \sin 2b_o q\right\} \qquad (5.3.2)$$

the quantities in $\{\}$ brackets being those dependent on the signs of α and q_o; $|\varepsilon|^2$ is found to be an even function of α, hence insensitive to its sign.

The minima of $\sigma(q)$ occur at:

$$q_m = \frac{\pi}{b_o}(m+\tfrac{1}{4}) \qquad m = 0,1,2,... \qquad (5.3.3)$$

and:

$$\sigma(q_m) = |\varepsilon|^2\left(\frac{2\pi a^2 b_o k^2}{q_m}\right) e^{-2\pi a q_m}\left\{e^{-2\alpha a q_m} e^{2\alpha a q_o} e^{2\pi a q_o} + e^{-2\pi a q_o} e^{2\alpha a q_m} e^{2\alpha a q_o} - 2e^{2\alpha a q_o}\right\} . \qquad (5.3.4)$$

Hence the lower envelope of the cross-section, which passes through its minima, is:

$$\sigma_\ell(q) = g(\alpha^2,q)\left\{e^{-2\alpha a q} e^{2\alpha a q_o} e^{2\pi a q_o} + e^{-2\pi a q_o} e^{2\alpha a q} e^{2\alpha a q_o} - 2e^{2\alpha a q_o}\right\}$$

$$= 2g(\alpha^2,q)\left[\cosh(2\alpha a q_o) + \sinh(2\alpha a q_o)\right]\left[\cosh(2\alpha a q)\cosh(2\pi a q_o) - \sinh(2\alpha a q)\sinh(2\pi a q_o) - 1\right] \qquad (5.3.5)$$

where:

$$g(\alpha^2,q) = |\varepsilon|^2\left(\frac{2\pi a^2 b_o k^2}{q}\right) e^{-2\pi a q} . \qquad (5.3.6)$$

It is now convenient to define $q_o' = |q_o| > 0$. Then we can

write the $\pi^{\pm}$ cross-section lower envelopes as:

$$\sigma_{\ell}^{\pm}(q) = 2g(\alpha^2,q)\Big[\cosh(2\alpha aq_o') \pm \sinh(2\alpha aq_o')\Big]\Big[\cosh(2\alpha aq)\cosh(2\pi aq_o') \mp \sinh(2\alpha aq)\sinh(2\pi aq_o') - 1\Big] . \qquad (5.3.7)$$

We now form the difference between the π^+ and π^- lower envelopes:

$$\begin{aligned} f_{\ell}(\alpha) &\equiv \Big[\sigma_{\ell}^{+}(q) - \sigma_{\ell}^{-}(q)\Big] \\ &= 4g(\alpha^2,q)\Big[\cosh(2\alpha aq)\cosh(2\pi aq_o')\sinh(2\alpha aq_o') \\ &\qquad - \sinh(2\alpha aq)\sinh(2\pi aq_o')\cosh(2\alpha aq_o') \\ &\qquad - \sinh(2\alpha aq_o')\Big] \\ &= 4g(\alpha^2,q)\Big[\sqrt{1+\sinh^2(2\alpha aq)}\ \sqrt{1+\sinh^2(2\pi aq_o')}\sinh(2\alpha aq_o') \\ &\qquad - \sinh(2\alpha aq)\sinh(2\pi aq_o')\sqrt{1+\sinh^2(2\alpha aq_o')} \\ &\qquad - \sinh(2\alpha aq_o')\Big] . \end{aligned} \qquad (5.3.8)$$

Using the facts for $\alpha > o$, that:

$\sinh(2\alpha aq) > \sinh(2\alpha aq_o')$ $\qquad q > q_o'$ (Fraunhofer asymptotic region)

$\sinh(2\pi aq_o') > \sinh(2\alpha aq_o')$ $\qquad \alpha < \frac{\pi}{2}$

$\sinh(2\alpha aq_o') > 0$

we can show that $f_\ell(\alpha) < 0$ for $\alpha > 0$, and inspection of (5.3.8) shows that $f_\ell(\alpha)$ is an odd function of α, that is, $f_\ell(-\alpha) = - f_\ell(\alpha)$. It then follows that $f_\ell(\alpha) > 0$ for $\alpha < 0$.

For π-nucleus scattering at T_π = 130 MeV we obtained a positive value for α from fitting. It then follows that $f_\ell(\alpha) < 0$,

i.e. $\sigma^+_\ell(q) < \sigma^-_\ell(q) \rightarrow \sigma^+(q_m) < \sigma^-(q_m)$,

the minima of the π^+ diffraction oscillations lie below those corresponding to π^- scattering, which is found to be the case.

For T_π = 230 MeV, a negative α value was obtained in our fit. It is natural in our resonance model that α goes from a positive value (implying π-nuclear attraction) below resonance to a negative value (implying π-nuclear repulsion) somewhat above resonance. In this instance it follows that $f_\ell(\alpha) > 0$,

i.e. $\sigma^+_\ell(q) > \sigma^-_\ell(q) \rightarrow \sigma^+(q_m) > \sigma^-(q_m)$,

the minima of the π^- diffraction oscillations lie below those corresponding to π^+ scattering, which is also found to be the case.

Next, we look at the behaviour of the upper envelope.

The maxima of $\sigma(q)$ occur at:

$$q_M = \frac{\pi}{b_o}(M+\frac{3}{4}) \qquad M=0,1,2,... \qquad (5.3.9)$$

and:

$$\sigma(q_M) = |\varepsilon|^2\left(\frac{2\pi a^2 b_o k^2}{q_M}\right)e^{-2\pi a q_M}\left\{e^{-2\alpha a q_M}e^{2\alpha a q_o}e^{2\pi a q_o} + e^{-2\pi a q_o}e^{2\alpha a q_M}e^{2\alpha a q_o} + 2e^{2\alpha a q_o}\right\} \qquad (5.3.10)$$

when $q_M \gg |q_o|$ (Fraunhofer asymptotic region).

Hence the upper envelope of the cross-section, which passes through its maxima, is:

$$\sigma_u(q) = g(\alpha^2,q)\left\{e^{-2\alpha a q}e^{2\alpha a q_o}e^{2\pi a q_o} + e^{-2\pi a q_o}e^{2\alpha a q}e^{2\alpha a q_o} + 2e^{2\alpha a q_o}\right\}$$

$$= 2g(\alpha^2,q)\left[\cosh(2\alpha a q_o) + \sinh(2\alpha a q_o)\right]\left[\cosh(2\alpha a q)\cosh(2\pi a q_o) - \sinh(2\alpha a q)\sinh(2\pi a q_o) + 1\right] \qquad (5.3.11)$$

where:

$$g(\alpha^2,q) = |\varepsilon|^2\left(\frac{2\pi a^2 b_o k^2}{q}\right)e^{-2\pi aq} \quad . \tag{5.3.12}$$

Again, taking $q'_o = |q_o| > 0$, the $\pi^{\pm}$ upper envelopes are:

$$\sigma_u^{\pm}(q) = 2g(\alpha^2,q)\Big[\cosh(2\alpha aq'_o) \pm \sinh(2\alpha aq'_o)\Big]\Big[\cosh(2\alpha aq)\cosh(2\pi aq'_o)$$

$$\mp \sinh(2\alpha aq)\sinh(2\pi aq'_o) + 1\Big] \quad . \tag{5.3.13}$$

We form the difference between the π^+ and π^- upper envelopes:

$$f_u(\alpha) = \Big[\sigma_u^+(q) - \sigma_u^-(q)\Big]$$

$$= 4g(\alpha^2,q)\Big[\cosh(2\alpha aq)\cosh(2\pi aq'_o)\sinh(2\alpha aq'_o)$$

$$- \sinh(2\alpha aq)\sinh(2\pi aq'_o)\cosh(2\alpha aq'_o)$$

$$+ \sinh(2\alpha aq'_o)\Big]$$

$$= 4g(\alpha^2,q)\Big[\sqrt{1+\sinh^2(2\alpha aq)}\,\sqrt{1+\sinh^2(2\pi aq'_o)}\,\sinh(2\alpha aq'_o)$$

$$- \sinh(2\alpha aq)\sinh(2\pi aq'_o)\,\sqrt{1+\sinh^2(2\alpha aq'_o)}$$

$$+ \sinh(2\alpha aq'_o)\Big]$$

$$= f'_\ell(\alpha) + 8g(\alpha^2,q)\sinh(2\alpha aq'_o) \quad . \tag{5.3.14}$$

Hence:

$$\left\{f_u(\alpha) - f_\ell(\alpha)\right\} = 8g(\alpha^2,q)\sinh(2\alpha a q_o')$$

$$= \left\{\left[\sigma_u^+(q) - \sigma_u^-(q)\right] - \left[\sigma_\ell^+(q) - \sigma_\ell^-(q)\right]\right\}$$

$$= \left\{\left[\sigma_u^+(q) - \sigma_\ell^+(q)\right] - \left[\sigma_u^-(q) - \sigma_\ell^-(q)\right]\right\} \quad (5.3.15)$$

Noting that $\sinh(2\alpha a q_o') \gtreqless 0$ when $\alpha \gtreqless 0$, we see that the distance from min to max is greater for $\pi^+(\pi^-)$ than for $\pi^-(\pi^+)$ when $\alpha > o$ ($\alpha < o$). Thus, the diffraction oscillations are larger for $\pi^+(\pi^-)$ scattering when $\alpha > o$ ($\alpha < o$).

We now connect this result with Coulomb-nuclear refractive damping of the diffraction oscillations and the change in sign of the π-nuclear force as one goes through the resonance. The 'min-to-max' distance reflects the strength of the diffraction oscillations, and the relative signs of α and pion charge determine - via a combined Coulomb-nuclear effect - the magnitude of the refraction experienced by the pion. This concept of 'refractive damping' of the amplitudes of the diffraction oscillations was pointed out by Frahn[1], but the possibility of both an attractive and repulsive nuclear-force was not considered. However, as we have come to conclude from our resonance analysis and fitting procedure, both positive and negative values for α - corresponding to an attractive and repulsive nuclear interaction, respectively - have to be considered to explain the behaviour of the angular distributions across the resonance.

The diffraction oscillations are smaller (more damped) for an attractive (repulsive) nuclear interaction in the case of $\pi^-(\pi^+)$ scattering than in the case of $\pi^+(\pi^-)$ scattering. That is, the diffraction oscillations experience greater refractive damping when the nuclear and Coulomb refractive forces are acting in concert, i.e., both attractive or both repulsive, than when they are acting in opposition, i.e., one attractive and the other repulsive. Being able to switch the charge of the pion projectile provides us with a mechanism for probing the sign of the π-nuclear force via examination of these subtle diffractive effects. In Frahn's work on refractive damping[1], only the repulsive Coulomb force was considered, because both target and projectile were assumed to be nuclei. The existance of both the π^+ and π^- allows refractive damping to become a tool for probing the nuclear part of the π-nucleus force.

To be analogous with our results for $f_\ell(\alpha)$, we would have liked to be able to show $f_u(\alpha) \gtrless 0$ as well as our previous result $f_\ell(\alpha) \lesssim 0$, for $\alpha \gtrless 0$, but this is not always the case. In fact, it can be shown that $f_u(\alpha) \lesssim 0$ for $\alpha \gtrless 0$ when:

$$\sinh(2\alpha a q'_o) \lesssim \frac{\sinh(2\pi a q'_o)\sinh(2\alpha a q)}{\sqrt{1+\sinh^2(2\pi a q'_o)}\,\sqrt{1+\sinh^2(2\alpha a q)}} \quad . \qquad (5.3.16)$$

We should have liked the following picture at T_π = 130 MeV, where $\alpha > 0$,

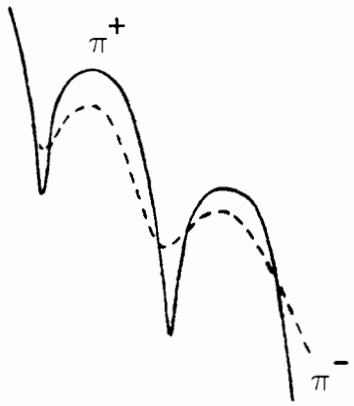

such that (1) $f_\ell(\alpha) < 0$ for all q, and (2) $f_u(\alpha) > 0$ for all q, to give the following situation:

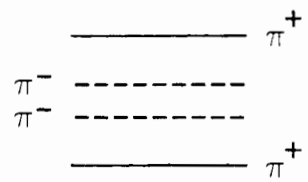

namely the π^- envelope lying inside the π^+ envelope.

However, what we have found is that (1) holds for all q but (2) does not always hold, that is, $f_u(\alpha) \not> 0$ for all q. In fact, $f_u(\alpha) < 0$ for q values such that:

$$\left(\frac{\sinh(2\pi a q_o')\sinh(2\alpha a q)}{\sqrt{1+\sinh^2(2\pi a q_o')}\sqrt{1+\sinh^2(2\alpha a q)}}\right) - \sinh(2\alpha a q_o') > 0 \quad . \tag{5.3.17}$$

Inserting the values of the parameters relevant at T_π = 130 MeV we find that this inequality is satisfied for $q > 0.2120$, corresponding to $\theta > 10.4^\circ$. As our scattering is measured at angles greater than $\theta = 10.4^\circ$ we have that $f_u(\alpha) < 0$ over our entire angular range. However, we still have that $f_u(\alpha) - f_\ell(\alpha) > 0$ for $\alpha > 0$, that is, the π^+ scattering exhibits the stronger oscillations.

Hence, what we observe at T_π = 130 MeV is the following:

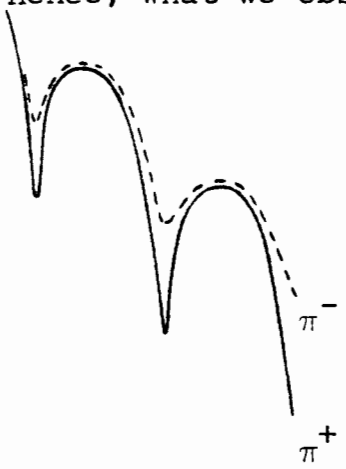

π^- ------- π^+ ——————— $\Big\}$ $f_u(\alpha) < 0$

π^- ------- $\Big\}$ $f_\ell(\alpha) < 0$

π^+ ——————— $\Big\}$

$\Big\}$ $f_u(\alpha) - f_\ell(\alpha) > 0$

At T_π = 230 MeV, where $\alpha < 0$, we should have liked the following situation:

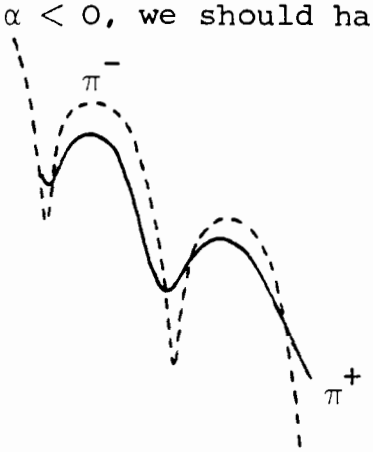

such that (1) $f_\ell(\alpha) > 0$ for all q, and (2) $f_u(\alpha) < 0$ for all q, yielding the following picture:

with the π^+ envelope lying inside the π^- envelope.

However, what we have found is that (1) holds for all q but (2) does not always hold, that is, $f_u(\alpha) \not< 0$ for all q. We find that $f_u(\alpha) \not< 0$ for $q > 0.2250$ corresponding to $\theta > 7.4^\circ$. As our scattering is measured at angles greater than $\theta = 7.4^\circ$ we have that $f_u(\alpha) > 0$ over our entire angular range. However, we still have that $f_u(\alpha) - f_\ell(\alpha) < 0$ for $\alpha < 0$, that is, the π^- scattering exhibits the stronger oscillations.

Hence, what we observe at T_π = 230 MeV is the following:

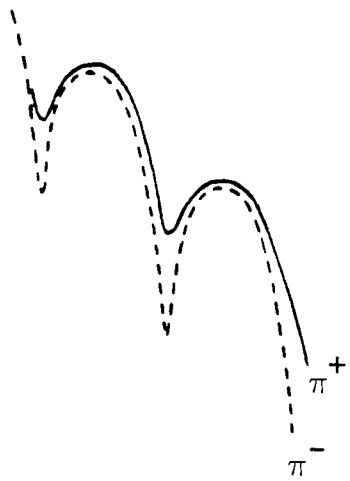

π^+ ——— $\}$ $f_u(\alpha) > 0$

π^- - - - - - $\}$

π^+ ——— $\}$ $f_\ell(\alpha) > 0$

π^- - - - - - $\}$

$\Big\}$ $f_u(\alpha) - f_\ell(\alpha) < 0$

Discussion of secondary effects:

In our immediately preceding discussion we have assumed that the values of $|q_o|$ and b_o are the same for both π^+ and π^- scattering. However, we know that this is not strictly the case.

Consider $b_o = \overset{o}{b}_o - \frac{n}{k}$. We recall that the sign of n is $\pm$ for $\pi^{\pm}$ scattering. The percentage change in b_o as one goes from π^+ to π^- at T_π = 130 MeV and 230 MeV is 7% and 5% respectively. Thus one need not worry unduly about the change in b_o with pion charge, and the previous discussion is not greatly affected. The cross-section $\sigma(q)$ contains a multiplicative factor of b_o, hence we find that $\sigma^+(q)$ and $\sigma^-(q)$ are in fact displaced from each other. However, on a log plot, this only alters their relative vertical positions, but not their individual vertical spreads from lower to upper envelope. Hence, for example, instead of:

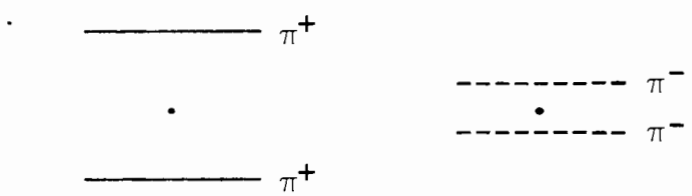

we will observe the following:

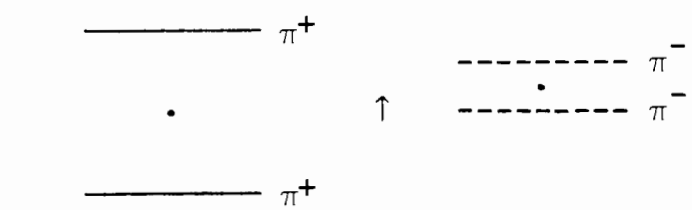

This effect, however, is sufficiently small not to materially alter our previous discussion.

Consider $q_o = \frac{2n}{b_o}$. From our above discussion of b_o we may conclude that the $|q_o|$'s are negligibly different for π^+ and π^- scattering. We therefore may expect that taking $|q_o|$ to be the same for both π^+ and π^- scattering will not have greatly affected our results.

Finally, we may note from (5.3.3) that the value of b_o affects the period of the diffraction oscillations. This period, of course, does not affect the upper and lower envelopes of those oscillations, but does affect the cross-section curve itself. Thus, the oscillations of the π^+ angular distributions will lag slightly behind those of the corresponding π^- angular distributions, an effect especially noticeable at the larger angles.

6. CLOSED FORM EVALUATION OF THE EIKONAL AMPLITUDE FOR STRONG-ABSORPTION SCATTERING - INELASTIC SCATTERING

In this section we present analytic expressions for the eikonal amplitude describing inelastic scattering at intermediate and high energies under strong-absorption conditions. We consider the direct excitation of low-lying collective states.

In a phenomenological approach it is expected that both elastic and direct inelastic scattering will be described in the same framework. Thus, we extend the method previously applied to obtaining a closed-form description of elastic scattering to the evaluation of the inelastic scattering amplitude. The Distorted-Wave theory for excitation of low-lying collective states lies at the basis of our approach.

The simple closed-form expressions derived for the inelastic scattering cross-sections are analogous to the strong-absorption formulae for elastic scattering. The close connection between inelastic and elastic scattering is made explicit.

6.1 The inelastic eikonal amplitude

In the eikonal approximation the Distorted-Wave amplitude for inelastic scattering of multipolarity L,M has been given in the form [1]:

$$f_{LM}(q) = -ik\delta_L \frac{[L:M]}{2\pi^{\frac{1}{2}}} \int_0^\infty db\, b\, D_N(b)\, e^{i2\sigma_p(b)}\, J_M(bq) \qquad (6.1.1)$$

in impact parameter space, where δ_L is referred to as the nuclear deformation length, the symbol [L:M] has the value:

$$[L:M] = \begin{cases} i^L \dfrac{[(L-M)!(L+M)!]^{\frac{1}{2}}}{(L-M)!!(L+M)!!} & \text{for } (L+M) \text{ even} \\ 0 & (L+M) \text{ odd}, \end{cases} \qquad (6.1.2)$$

and $D_N(b)$ is the elastic derivative nuclear scattering function which has been given previously in section 3.2.

In the derivation of the expression (6.1.1) which was given in Potgieter and Frahn[26], several assumptions were made: firstly that the collective model was applicable, in which case the inelastic scattering could be regarded as being induced by non-spherical deformations of the optical potential describing elastic scattering; secondly that, due to a relatively weak Coulomb interaction, the contribution from Coulomb excitation could be neglected, and thus only the Coulomb effects in the Distorted-Waves needed to be considered; and finally, that the Austern-Blair theory for describing the

nuclear interaction held[27], allowing the radial integrals of the Distorted-Wave theory to be expressed in terms of the derivatives of the nuclear part of the elastic scattering function.

For the same reasons as were given previously, we expand the point-charge phase shifts linearly about b_o, as given by (2.2.11).

Substitution of the expansion (2.2.11) into (6.1.1) gives:

$$f_{LM}(q) = -ik\delta_L \frac{[L:M]}{2\pi^{\frac{1}{2}}} e^{i2\sigma_p(b_o)} \int_o^\infty db\, b\, D_N(b)\, e^{i(b-b_o)q_o}\, J_M(bq) \tag{6.1.3}$$

which we express in terms of the general integral $I_M(q)$ as:

$$f_{LM}(q) = -ik\delta_L \frac{[L:M]}{2\pi^{\frac{1}{2}}} e^{i2\sigma_p(b_o)}\, I_M(q) \tag{6.1.4}$$

where:

$$I_M(q) = \int_o^\infty db\, b\, D_N(b)\, e^{i(b-b_o)q_o}\, J_M(bq) \quad . \tag{6.1.5}$$

Referring again to techniques described in reference [6] we evaluate (6.1.5) with the result:

$$I_M(q) = \frac{b_o}{2}\left\{\tilde{F}_N[a(q_o+q)]\left[J_M(b_oq) + iJ_{M+1}(b_oq)\right]\right.$$

$$\left. + \tilde{F}_N[a(q_o-q)]\left[J_M(b_oq) - iJ_{M+1}(b_oq)\right]\right\} \tag{6.1.6}$$

Using the relation (2.2.17) we express (6.1.6) as:

$$I_M(q) = b_o\left[\tilde{F}_+(q)\, J_M(b_o q) + \tilde{F}_-(q)\, J_{M+1}(b_o q)\right] \qquad (6.1.7)$$

to give the eikonal inelastic scattering amplitude in the form:

$$f(q) = -i\delta_L k b_o \frac{[L:M]}{2\pi^{\frac{1}{2}}}\left[\tilde{F}_+(q) J_M(b_o q) + i\tilde{F}_-(q) J_{M+1}(b_o q)\right] e^{i2\sigma_p(b_o)} \qquad (6.1.8)$$

and the differential cross-section for inelastic scattering of multipolarity L,M is given by:

$$\begin{aligned}\sigma_{LM}(q) &= |f_{LM}(q)|^2 \\ &= \frac{(\delta_L k b_o)^2}{4\pi}[L:M]^2\left|\tilde{F}_+(q) J_M(b_o q) + i\tilde{F}_-(q) J_{M+1}(b_o q)\right|^2 \\ &= \frac{(\delta_L k b_o)^2}{4\pi}[L:M]^2\Big\{|\tilde{F}_+(q)|^2 J_M(b_o q) + |\tilde{F}_-(q)|^2 J_{M+1}^2(b_o q) \\ &\qquad + 2\,\mathrm{Im}(\tilde{F}_+(q)\,\tilde{F}_-(q)) J_M(b_o q) J_{M+1}(b_o q)\Big\}.\end{aligned} \qquad (6.1.9)$$

The total inelastic cross-section is obtained from:

$$\sigma_L(q) = \sum_{M=-L}^{+L} \sigma_{LM}(q) \,. \qquad (6.1.10)$$

6.2 The eikonal amplitude in the Ericson parametric model

To aid in the interpretation of our formulae we again adopt the Ericson parametric model for the scattering function, given by (2.3.1).

Using the results of section 2.4, and noting that both $F_+(q)$ and $F_-(q)$ are real functions of the variable q, $\sigma_{LM}(q)$ reduces to:

$$\sigma_{LM}(q) = \frac{(\delta_L k b_o)^2}{4\pi} |\varepsilon|^2 [L:M]^2 \left\{ \left[F_+(q) J_M(b_o q) \right]^2 + \left[F_-(q) J_{M+1}(b_o q) \right]^2 \right\} \tag{6.2.1}$$

which, in the Ericson parametric model, is expressed as:

$$\sigma_{LM}(q) = \frac{(\delta_L k b_o)^2}{4\pi} [L:M]^2 |\varepsilon|^2 e^{2\alpha a q_o} \left(\frac{\pi a q}{\sinh(\pi a q)} \right)^2 \left\{ \left[1 + \sinh^2(\alpha a q) \right] \left[J_m(b_o q) \right]^2 + \left[\sinh^2(\alpha a q) \right] \left[J_{M+1}(b_o q) \right]^2 \right\} \tag{6.2.2}$$

and:

$$\sigma_L(q) = \sum_{\substack{L=-M \\ (L+M) \text{ even}}}^{+M} \sigma_{LM}(q) \quad . \tag{6.2.3}$$

6.3 The asymptotic differential cross-section

We proceed as before: replacing the Bessel functions in (6.2.2) by their asymptotic expressions given by (2.5.1), we find that in the asymptotic q region the inelastic angular distributions are described by:

$$\sigma_{LM}(q) = \frac{\delta_L{}^2 k^2 b_o}{4\pi^2 q} |\varepsilon|^2 [L:M]^2 e^{2\alpha a q_o} \left(\frac{\pi a q}{\sinh(\pi a q)}\right)^2 \cosh(2\alpha a q) \left[1 + (-)^M \operatorname{sech}(\alpha a q) \sin(2b_o q)\right] \quad (6.3.1)$$

in the Ericson model.

The corresponding inelastic cross-sections describing neutral and charged particle scattering are given by:

$$\sigma^o_{LM}(q) \simeq \overline{\sigma^o_{LM}}(q)\ \Omega^o_M(q)$$

$$\sigma^{\pm}_{LM}(q) \simeq \overline{\sigma^o_{LM}}(q)\left[1 - \frac{n}{kb_o}(1 - 4\alpha ka)\right] \Omega^{\pm}_M(q) \quad (6.3.2)$$

correct to first order in n, where we have defined a mean-inelastic cross-section (in analogy with the elastic scattering):

$$\overline{\sigma^o_{LM}}(q) = \frac{\delta_L{}^2 k^2 b_o}{4\pi^2 q} [L:M]^2 |\varepsilon|^2 \left(\frac{\pi a q}{\sinh(\pi a q)}\right)^2 \cosh(2\alpha a q) \quad (6.3.3)$$

and the diffraction oscillations are given by:

$$\Omega_M^{o}(q) = \left[1 + (-)^M \operatorname{sech}(2\alpha aq)\ \sin(2b_o q)\right]$$

$$\Omega_M^{\pm}(q) = \left[1 + (-)^M \operatorname{sech}(2\alpha aq) \sin\left[2(b_o - \tfrac{n}{k})q\right]\right] . \qquad (6.3.4)$$

Inspection of the neutral asymptotic elastic scattering cross-section:

$$\sigma(q) \simeq \frac{k^2 b_o}{\pi q^3} |\varepsilon|^2 \left(\frac{\pi aq}{\sinh(\pi aq)}\right)^2 \cosh(2\alpha aq)\left[1 - \operatorname{sech}(2\alpha aq)\ \sin(2b_o q)\right] \qquad (6.3.5)$$

and the corresponding inelastic expression:

$$\sigma_{LM}(q) \simeq \frac{\delta_L{}^2 k^2 b_o}{4\pi^2 q} [L:M]^2 |\varepsilon|^2 \left(\frac{\pi aq}{\sinh(\pi aq)}\right)^2 \cosh(2\alpha aq)$$

$$\left[1 + (-)^M \operatorname{sech}(2\alpha aq)\ \sin(2b_o q)\right] \qquad (6.3.6)$$

for [L+M] even, highlights the 'Blair phase rule'[28]. We observe that for even L, the inelastic diffraction oscillations are out of phase with those of odd L and with the elastic one by 180^o, that is, the locations of the maxima and minima are interchanged.

For completeness, we rewrite expressions (6.3.3) and (6.3.4) in terms of an impact parameter describing both neutral and charged particle inelastic scattering, as was done for the elastic scattering case.

Strictly to first order in n, we find that the asymptotic inelastic cross-sections describing neutral and charged particle scattering are given by:

$$\sigma^{\circ}_{LM}(q) \simeq \overline{\sigma^{\circ}_{LM}}(q)\ \Omega_M(q)$$

$$\sigma^{\pm}_{LM}(q) \simeq \overline{\sigma^{\circ}_{LM}}(q)\left[1 - \frac{n}{\overset{\circ}{b}_o k}\ (1 - 4\alpha ka)\right]\Omega_M(q) \qquad (6.3.7)$$

where:

$$\overline{\sigma^{\circ}_{LM}}(q) = \frac{\delta_L{}^2 k^2 \overset{\circ}{b}_o}{4\pi^2 q}\ [L:M]^2\ |\varepsilon|^2 \left(\frac{\pi aq}{\sinh(\pi aq)}\right)^2 \cosh(2\alpha aq)$$

$$\Omega_M(q) = \left[1 + (-)^M \operatorname{sech}(2\alpha aq)\sin(2b_o q)\right] \qquad (6.3.8)$$

with b_o defined as:

$$b_o = \overset{\circ}{b}_o - \frac{n}{k} \quad . \qquad (6.3.9)$$

6.4 The eikonal amplitude in the eikonal parametric model

For purposes of calculation we restate the results of section 6.1, evaluated this time in the eikonal parametric model.

The eikonal parameterization of the nuclear scattering function is given by (3.3.5).

Using the results of section 3.4 and reference[1], we write down the expression for the differential cross-section describing inelastic scattering of multipolarity L,M in the eikonal parametric model:

$$\sigma_{LM}(q) = \frac{(\delta_L k\tilde{b}_o)^2}{4\pi}\,[L:M]^2\left(\frac{\pi\tilde{a}q}{\sinh(\pi\tilde{a}q)}\right)e^{2\alpha\tilde{a}q_o}\,|\tilde{\varepsilon}|^2$$

$$\left\{\left[1+\sinh^2(\alpha\tilde{a}q)-\sin^2(\beta\tilde{a}q)\right]\left[J_M(\tilde{b}_o q)\right]^2\right.$$

$$+\left[\sinh^2(\alpha\tilde{a}q)+\sin^2(\beta\tilde{a}q)\right]\left[J_{M+1}(\tilde{b}_o q)\right]^2$$

$$\left.-\left[\sin(2\beta\tilde{a}q)\right]\left[J_M(\tilde{b}_o q)J_{M+1}(\tilde{b}_o q)\right]\right\} \qquad (6.4.1)$$

where the parameters have the same meaning as in the elastic scattering expression:

$$\tilde{b}_o = R - \frac{n}{k} + \tilde{a}\ln\left[\frac{W}{E}k\left(\frac{\pi\tilde{a}R}{2}\right)^{\frac{1}{2}}\right] \qquad (6.4.2)$$

$$\alpha = \arctan A = \arctan\frac{V}{W} \qquad (6.4.3)$$

$$\beta = \gamma + \tfrac{1}{2}\ln(1+A^2) \qquad (6.4.4)$$

and:

$$\tilde{\varepsilon} = \left[1 - i2(\alpha+i\beta)\left(\frac{\tilde{a}}{\tilde{b}_o}\right) + \left[\frac{\pi^2}{6} - (\alpha+i\beta)^2\right]\left(\frac{\tilde{a}}{\tilde{b}_o}\right)^2\right] \qquad (6.4.5)$$

as given previously.

We see that the effects of resonance are readily included in the eikonal parametric model of the eikonal inelastic scattering cross-section by using the resonant optical potential of section 3.

The total inelastic cross-section $\sigma_L(q)$ results, as before, from summing over all states M, for (L+M) even.

7. ANALYSIS OF EXPERIMENTAL DATA

We have shown that, in the eikonal approximation, the expressions describing the inelastic scattering of hadrons at intermediate energies under strong-absorption conditions can be manipulated into simple analytic formulae - the parameters of which can be largely determined from the corresponding elastic scattering cross-section fits. In this section we test these approximate analytic forms against experimental inelastic scattering data.

7.1 Eikonal resonance analysis

To test our formalism we analyse the recent data of 180 MeV pion inelastic scattering to the 'low-lying collective states' in ^{40}Ca and ^{48}Ca.

We choose the 2^+(3.908 MeV) and 3^-(3.736 MeV) states in ^{40}Ca, and the 2^+(3.832 MeV) and 3^-(4.507 MeV) states in ^{48}Ca on which to carry out our analysis.

The data for the reaction ^{40}Ca ($\pi^{\pm}$, $\pi^{\pm}$') were obtained from reference[19], taken in the angular range between 14° and 40° laboratory scattering angle for the transition to the 2^+ state, and between 14° and 80° for the case of the 3^- level. The data for the reaction ^{48}Ca ($\pi^{\pm}$, $\pi^{\pm}$') were obtained from reference[20], all data taken between laboratory scattering angles 21° and 76°.

Nuclear energy-level schemes obtained from shell-model potential theory predict that ^{40}Ca is a self-conjugate, N=Z doubly closed-shell nucleus. Similarly, ^{48}Ca is predicted to be a N≠Z doubly closed-shell nucleus. Both ^{40}Ca and ^{48}Ca are examples of even-even nuclei. The pairing interaction, acting between opposed spin pairs of nucleons, together with the closed-shell ground state configuration causes these nuclei to be particularly tightly bound. Thus the nature of their low-lying excited states is one of collective behaviour, in particular, collective vibrations of the nucleus.

Inelastic scattering in these two nuclei can thus be regarded as an excitation of a collective state, the ^{40,48}Ca nuclei being regarded as highly collective.

Using formulae (6.2.2) and (6.2.3) we can write down explicit expressions for the eikonal differential cross-section describing π^+ and π^- inelastic scattering to the 2^+ and 3^- states in the ^{40,48}Ca nuclei.

We find that the differential cross-section for the excitation of the 2^+ state is given by:

$$\sigma_2(q) = |\tilde{\varepsilon}|^2 \frac{(\delta_2 k\tilde{b}_o)^2}{4\pi} \left(\frac{\pi\tilde{a}q}{\sinh(\pi\tilde{a}q)}\right) e^{2\alpha\tilde{a}q_o} \times$$

$$\left\{[1 + \sinh^2(\alpha\tilde{a}q) - \sin^2(\beta\tilde{a}q)]\left[\frac{1}{4}J_o^2(\tilde{b}_o q) + \frac{3}{4}J_2^2(\tilde{b}_o q)\right]\right.$$

$$+ [\sinh^2(\alpha\tilde{a}q) + \sin^2(\beta\tilde{a}q)]\left[\frac{5}{8}J_1^2(\tilde{b}_o q) + \frac{3}{8}J_3^2(\tilde{b}_o q)\right]$$

$$- \sin(2\beta\tilde{a}q)\left[\frac{1}{4}J_o(\tilde{b}_o q)J_1(\tilde{b}_o q) - \frac{3}{8}J_1(\tilde{b}_o q)J_2(\tilde{b}_o q)\right.$$

$$\left.\left. - \frac{3}{8}J_2(\tilde{b}_o q)J_3(\tilde{b}_o q)\right]\right\} \qquad (7.1.1)$$

and for excitation of the 3^- state:

$$\sigma_3(q) = |\tilde{\varepsilon}|^2 \frac{(\delta_3 k\tilde{b}_0)^2}{4\pi}\left(\frac{\pi\tilde{a}q}{\sinh(\alpha\tilde{a}q)}\right) e^{2\alpha\tilde{a}q_0} \times$$

$$\left\{[1 + \sinh^2(\alpha\tilde{a}q) - \sin^2(\beta\tilde{a}q)]\left[\frac{3}{8}J_1^2(\tilde{b}_0 q) + \frac{5}{8}J_3^2(\tilde{b}_0 q)\right]\right.$$

$$+ [\sinh^2(\alpha\tilde{a}q) + \sin^2(\beta\tilde{a}q)]\left[\frac{3}{16}J_0^2(\tilde{b}_0 q) + \frac{1}{2}J_2^2(\tilde{b}_0 q) + \frac{5}{16}J_4^2(\tilde{b}_0 q)\right]$$

$$- \sin(2\beta\tilde{a}q)\left[-\frac{3}{16}J_0(\tilde{b}_0 q)J_1(\tilde{b}_0 q) + \frac{3}{16}J_1(\tilde{b}_0 q)J_2(\tilde{b}_0 q)\right.$$

$$\left.\left. - \frac{5}{16}J_2(\tilde{b}_0 q)J_3(\tilde{b}_0 q) + \frac{5}{16}J_3(\tilde{b}_0 q)J_4(\tilde{b}_0 q)\right]\right\} \qquad (7.1.2)$$

The shapes, though not the normalizations, of these theoretical cross-sections are completely specified within this model by the parameterization of the scattering function used in describing the elastic scattering cross-sections. Nuclear structure information is obtained from normalization to the experimental inelastic cross-sections. The normalization factor characterising the transition to a state L is given by δ_L, such that $\sigma_{inel} \propto (\delta_L)^2$.

δ_L in turn is proportional to the sum of the elementary πN amplitudes over the N neutrons and Z protons in the nucleus. We have already noted that for (3,3) resonance dominance, the isospin properties of the πN system results in the resonant amplitude for $\pi^+ p$ ($\pi^- n$) elastic scattering being three times that for $\pi^- p$ ($\pi^+ n$) elastic scattering. Describing π-nucleus scattering in terms of the amplitude for πN scattering by use of an Impulse Approximation, this 3 : 1 enhancement should also be observed in π-nucleus inelastic scattering. This should give rise to differential effects in π^+ and π^- interactions with nuclei having different neutron and proton numbers.

Hence, neglecting non-resonant amplitudes in the resonance region and assuming $\pi^{\pm}$ inelastic scattering to be a direct process,

$$\delta_L(\pi^{\pm}) = \gamma(\pi^{\pm}, N, Z)\, \delta_L{}^R \qquad (7.1.3)$$

where:

$$\gamma(\pi^{\pm},N,Z) = \begin{cases} (3Z+N)/2A & \text{for } \pi^{+} \\ (Z+3N)/2A & \text{for } \pi^{-} \end{cases} \qquad (7.1.4)$$

as in section 3.2, from which an expression for the ratio of the π^{-}/π^{+} deformation lengths can be found:

$$\left(\frac{\delta_L(\pi^{-})}{\delta_L(\pi^{+})}\right)^2 = \left(\frac{Z+3N}{3Z+N}\right)^2 . \qquad (7.1.5)$$

Equation (7.1.3) simply embodies the isospin reduction of the deformation length which was carried out in references[13,14]. $\delta_L{}^R$ is taken as independent of whether the π^{+} or π^{-} was involved. This agrees with our ideas of the collective picture in which these 2^{+} and 3^{-} states in the $^{40,48}Ca$ nuclei are viewed as equal amplitude proton and neutron deformations or vibrations of the nuclear surface, i.e. the collective proton and neutron structures undergo equal amplitudes of deformation in these particular states.

In the case of pion inelastic scattering off ^{40}Ca we simply get:

$$^{40}Ca\left(\frac{\delta_L(\pi^{-})}{\delta_L(\pi^{+})}\right)^2 = 1 \qquad (7.1.6)$$

because N = Z = 20, whereas our theoretically predicted value for pion inelastic scattering off ^{48}Ca is:

$$^{48}Ca\left(\frac{\delta_L(\pi^{-})}{\delta_L(\pi^{+})}\right)^2 = 1.40 \qquad (7.1.7)$$

because of its neutron excess.

Our fits to the pion inelastic scattering angular distributions using the eikonal parameterization of the scattering function are given in Figures (7.1-I) and (7.1-II). The parameters of the eikonal model as determined by fitting the elastic scattering angular distributions are given in Table (7.1-I). The values of δ_L, the nuclear deformation length, are chosen so as to bring the calculated cross-sections into agreement with the data. The values extracted for δ_L(exp) are summarized in Table (7.1-II).

The agreement between theory and experiment is generally good. The inelastic scattering data for the 2^+ and 3^- states are found to obey the Blair phase rule[28].

Figure (7.1-I)

Differential cross-sections for π^+ and π^- inelastic scattering to the 2^+, 3.908 and 3^-, 3.736 MeV states in ^{40}Ca at T_π = 180 MeV; data taken from reference[19].

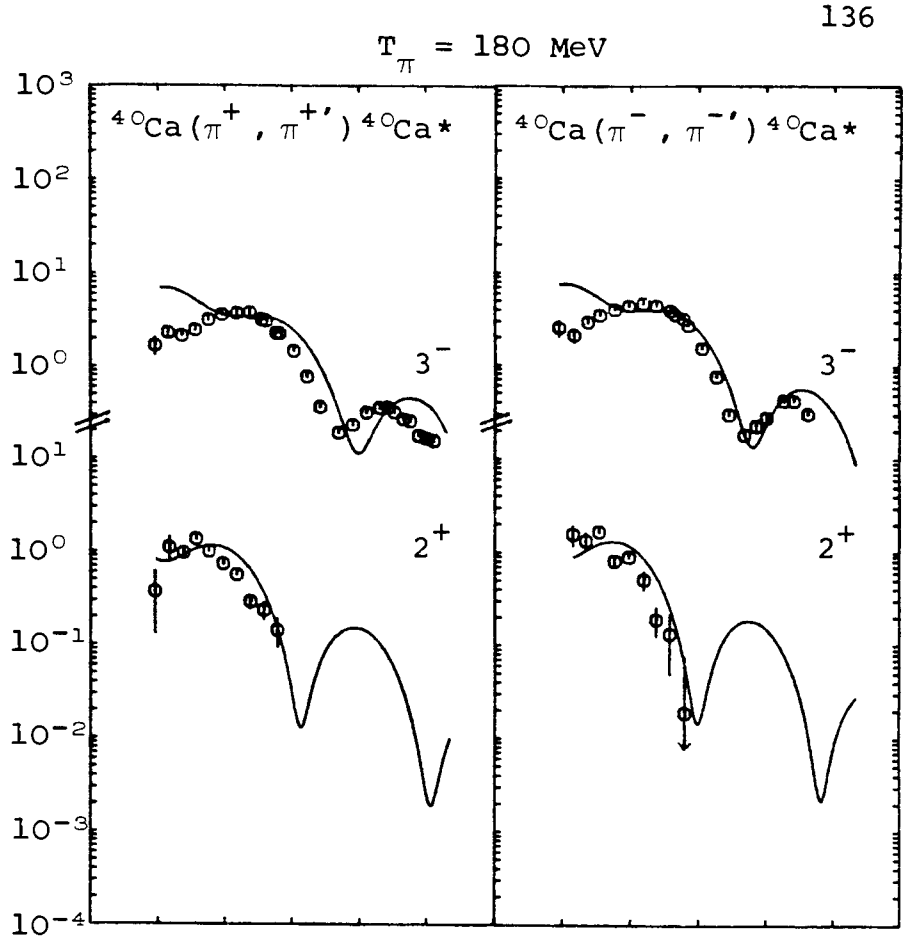

Figure (7.1-II)

Differential cross-sections for π^+ and π^- inelastic scattering to the 2^+, 3.832 and 3^-, 4.507 MeV states in ^{48}Ca at T_π = 180 MeV; data taken from reference[20].

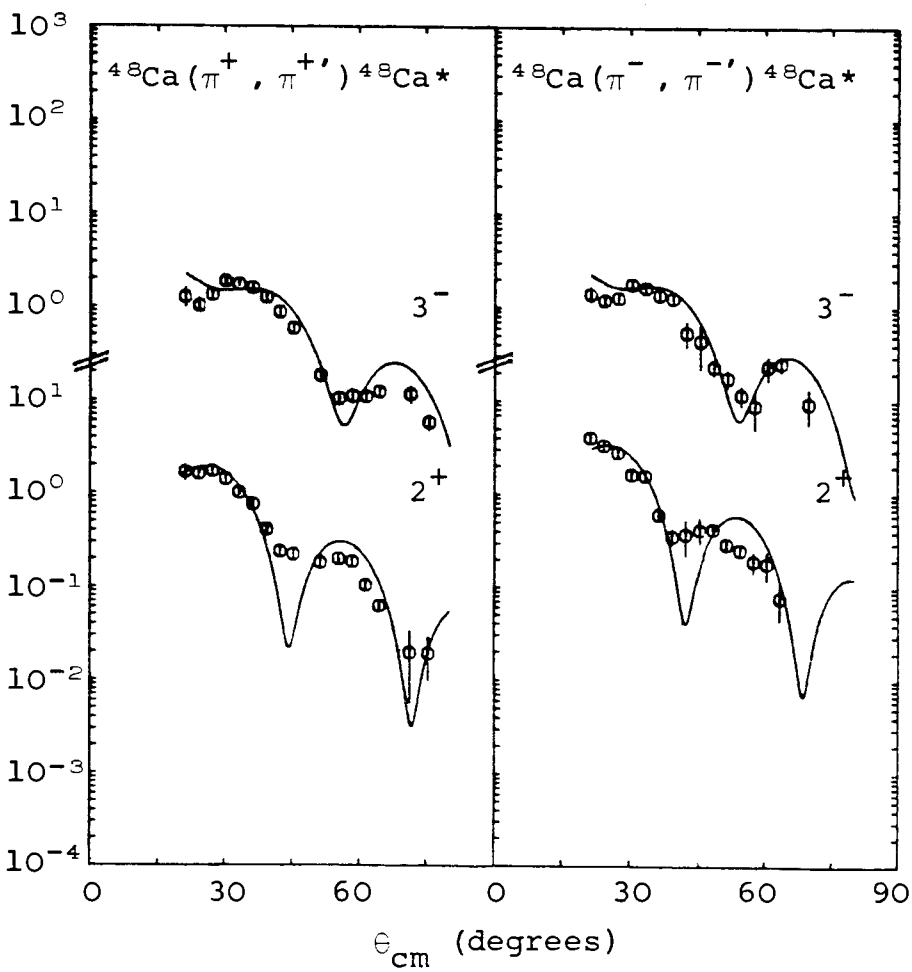

Table (5.1-I)

The parameters of the eikonal model as deduced by fitting the elastic scattering data at T_π = 180 MeV.

Target	beam	$\tilde{b}_o$(fm)	A
^{40}Ca	π^+	3.92	-0.03
	π^-	4.14	-0.03
^{48}Ca	π^+	4.20	-0.01
	π^-	4.42	-0.05

Table (5.1-II)

Deformation lengths for excited states from $\pi^{\pm}$ inelastic scattering.

Target	beam	E_L(MeV)	J^π	$\delta_L(\pi^{\pm})$ (fm)	$\left(\frac{\delta_L(\pi^-)}{\delta_L(\pi^+)}\right)^2 = R$
^{40}Ca	π^+	3.908	2^+	0.5	1.0
	π^-			0.5	
	π^+	3.736	3^-	1.3	1.0
	π^-			1.3	
^{48}Ca	π^+	3.832	2^+	0.60	1.56
	π^-			0.75	
	π^+	4.507	3^-	0.78	0.92
	π^-			0.75	

Comparison of our predicted value for the ratio of the π^-/π^+ deformation lengths, $\left(\frac{\delta_L(\pi^-)}{\delta_L(\pi^+)}\right)^2$, with the corresponding experimentally deduced quantity R turns out to be instructive.

Although the values for ^{40}Ca compare well, those obtained experimentally for ^{48}Ca do not agree with our prediction of 1.40. The value of R=1.40 is at least plausible for the 2^+ ^{48}Ca data but is completely out for the 3^- ^{48}Ca data.

This suggests that the isospin model given above may be oversimplified. When we made similar arguments for the optical potential, we found that the data forced us to also include a significant non-resonant background term (for example, w=0.6) in addition to the resonant term with its isospin factor of γ. This suggests that we also model our deformation length as the sum of non-resonant and resonant contributions:

$$\delta_L(\pi^{\pm}) = \delta_L^{NR} + \gamma(\pi^{\pm},N,Z)\,\delta_L^{R}(\pi^{\pm}) \qquad (7.1.8)$$

where we further permit the resonant $\delta_L^R(\pi^{\pm})$ to depend on the pion charge insofar as the inelastic channel L has unequal amplitude deformations of the neutron and proton structures. On the other hand we assume the non-resonant contribution δ_L^{NR} to be totally independent of isospin - even if the neutron and proton collective modes differ in amplitude, they are each excited to the same degree by either the π^- or π^+ acting via the background (non-resonant, isospin independent)

mechanisms. Note that we allow both the background δ_L^{NR} and the resonant $\delta_L^{R}(\pi^{\pm})$ to depend on the channel L. By permitting the background contribution to be channel dependent as well, that is, different for the 2^+ and 3^- transitions, we can hope to offer an explanation for the difference found between R and 1.40 for 3^- ^{48}Ca inelastic scattering. The discrepancy could be explained by assuming that 3^- ^{48}Ca inelastic scattering has a very strong background (non-resonant) contribution, giving $\left(\frac{\delta_3(\pi^-)}{\delta_3(\pi^+)}\right)^2$ a value ~ 1, that is, we may suppose that δ_L^{NR} completely overshadows the resonant part in certain channels.

An alternative assumption, also invoked by others[13,14], is to still neglect the background δ_L^{NR}, but to drop the idea of equal amplitude neutron and proton deformations in certain channels, for example, the 3^- channel, thus permitting $\delta_L^{R}(\pi^+) \neq \delta_L^{R}(\pi^-)$. This also leads to a channel dependent ratio of deformation lengths:

$$\left(\frac{\delta_L(\pi^-)}{\delta_L(\pi^+)}\right)^2 = \left(\frac{(Z+3N)\,\delta_L^{R}(\pi^-)}{(3Z+N)\,\delta_L^{R}(\pi^+)}\right)^2 . \qquad (7.1.9)$$

Further research is needed to clarify the extent to which both non-resonant and unequal-amplitude proton and neutron deformation effects influence the pion-nucleus deformation parameter $\delta_L(\pi^{\pm})$.

CONCLUSION

In this work, we have presented a detailed study of π^+ and π^- elastic scattering from the ^{40}Ca and ^{48}Ca nuclei in the resonance region, as well as of pionic inelastic excitation of some low-lying collective states of these nuclei. Model predictions for neutral pion total cross-section and real parts of the forward elastic scattering amplitude have also been made.

We conclude by stating that our proposed model - incorporating the resonance explicitly into the formalism describing the scattering - would seem to have been very successful. We have been able to reproduce the observed energy and angular dependence of the experimental differential cross-sections, which were measured at a range of energies across the resonance.

REFERENCES

1. W.E. Frahn, University of Paris, Orsay, Preprint IPNO/TH 80-44, September 1980

2. R.J. Glauber, High energy collision theory, Lectures in theoretical physics I (Interscience Publishers, New York, 1959)

3. W.E. Frahn and R.H. Venter, Ann. of Phys. 24 (1963) 243; R.H. Venter, Ann. of Phys. 25 (1963) 405

4. W.E. Frahn, Heavy-ion high-spin states and nuclear structure, vol 1 (IAEA, Vienna, 1975) 157

5. W.E. Frahn and D.H.E. Gross, Ann. of Phys. 101 (1976) 520

6. W.E. Frahn, Nucl. Phys. A337 (1980) 324

7. T.E.O. Ericson, in 'Preludes in Theoretical Physics' (A. de-Shalit, H. Feshbach, and L. van Hove, Eds.), page 321, North Holland, Amsterdam, 1965

8. Particle Properties Data Booklet, 'Review of Particle Properties', Phys. Lett. 75B (1978)

9. L.S. Kisslinger, Phys. Rev. 98 (1955) 761

10. W.B. Cottingame and D.B. Holtkamp, Phys. Rev. Lett. 45 (1980) 1828

11. S.C. Phatak, F. Tabakin and R.H. Landau, Phys. Rev. C7 (1973) 1803

12. L.S. Kisslinger and W.L. Wang, Ann. of Phys. 99 (1976) 374

13. S. Iversen et al., Phys. Rev. Lett. 40 (1978) 17

14. C. Lunke et al., Phys. Lett. 78B (1978) 201

15. S.K. Kauffmann, Z. Phys. A282 (1977) 163; University of Cape Town preprints (1976), unpublished

16. P. Gretillat et al., Nucl. Phys. A364 (1981) 270

17. C. Wilkin et al., Nucl. Phys. B62 (1973) 61

18. F. Binon et al., Nucl. Phys. B17 (1970) 168

19. C.L. Morris et al., Phys. Rev. C24 (1981) 231

20. K.G. Boyer et al., Phys. Rev. C24 (1981) 598

21. E. Segré, Nuclei and Particles, second edition (W.A. Benjamin, Inc.; 1977) page 748

22. S. Gasiorowicz, Elementary Particle Physics (Wiley 1966) page 294

23. T.F. Hill and W.E. Frahn, S.-Afr. Tydskr. Fis. 3 no. 1 (1980) 11

24. J-P. Egger et al., Phys. Rev. Lett. 39 (1977) 1608

25. W.E. Frahn, Ann. of Phys. 72 (1972) 524

26. J.M. Potgieter and W.E. Frahn, Nucl. Phys. 80 (1966) 434

27. N. Austern and J.S. Blair, Ann. of Phys. 33 (1965) 15

28. J.S. Blair, Phys. Rev. 115 (1959) 928